UNIVERSIDADE
BEIRA INTERIOR

Brain activity on encoding different textures
EEG signal acquisition with ExoAtlet®

Versão final após defesa

Júlia da Silva Ramos

Dissertação para obtenção do Grau de Mestre em
Bioengenharia
(2º ciclo de estudos)

Orientador: Prof. Doutor André Ferreira Costa Vieira
Co-orientador: Prof. Doutor Miguel Santos Pais-Vieira

Julho de 2023

Declaração de Integridade

Eu, Júlia da Silva Ramos, que abaixo assino, estudante com o número de inscrição M11867 de Bioengenharia da Faculdade de Engenharia, declaro ter desenvolvido o presente trabalho e elaborado o presente texto em total consonância com o **Código de Integridades da Universidade da Beira Interior**.

Mais concretamente afirmo não ter incorrido em qualquer das variedades de Fraude Académica, e que aqui declaro conhecer, que em particular atendi à exigida referenciação de frases, extratos, imagens e outras formas de trabalho intelectual, e assumindo assim na íntegra as responsabilidades da autoria.

Universidade da Beira Interior, Covilhã 27/07/2023

(assinatura conforme Cartão de Cidadão ou preferencialmente
assinatura digital no documento original se naquele mesmo formato)

Dedication

Para os meus pais e para a minha irmã.

Tenho Saudades

Quero fazer-te mais
Quero aplaudir o teu sucesso
Quero ser teu vapor
Estar nos teus poros, ar eterno
...
Quero morar no teu sorriso
Quero viver no teu sem fim
Quero morar no teu destino
Quero morar no teu jardim

Valter Lobo

Acknowledgements

Em primeiro lugar um obrigada aos meus melhores amigos, pais, Amélia Ramos e Pedro Magalhães. Por vezes o sentir que estavam perto mesmo estando longe, o sentir que acreditavam em mim quando eu não o fazia e as palavras de consolo quando eu não as dizia, foram o meu fôlego para continuar a fazer mais e melhor.
Em segundo lugar, agradecer ao meu orientador, o Dr. André Costa Vieira pelo acompanhamento e disponibilidade para trabalhar comigo. Um especial obrigado ao meu coorientador, o Dr. Miguel Pais-Vieira que embora não me conhecesse, nunca tivesse sido meu professor, e nem sequer fosse da mesma instituição de ensino, aceitou embarcar neste desafio comigo dando-me a oportunidade de sair da minha zona de conforto, de explorar novos conceitos e metendo à prova a minha capacidade de resiliência.
Como não poderia deixar de ser, um agradecimento ao professor João Lopes Fermeiro pela ajuda e incentivo de todas as vezes que entrei no laboratório com dúvidas, sem saber muito bem que fazer, e como conseguir alcançar o trabalho a que me propus.
Adicionalmente, um obrigada a todos os que ajudaram no decorrer das experiências e que se disponibilizaram para ir até ao porto, em especial, ao José Gabriel, à Mafalda Aguiar e à Inês Bruno.
Um obrigada às amizades que nasceram deste curso que são felizmente demasiadas para estar a citar o nome de todas. Contudo, um especial obrigada, à Carolina Salvador, à Beatriz Ferreira e à Lisana Moniz por estarem presentes nos bons momentos e, claro, nos menos bons. Por todos aqueles longos dias na sala de estudo, por todas as caminhadas coadjuvadas por longas conversas e por todos os jogos de tabuleiro, momentos que fomos colecionando e que permitiram respirar. Por fim, à Margarida Vilarinho e à Beatriz Resende que estiveram sempre disponíveis para longas conversas de café e passeios à beira-mar, obrigada.

Resumo

Os exoesqueletos motorizados desempenham um papel crucial no campo da reabilitação, melhorando a qualidade de vida das pessoas que deles necessitam. Deste modo, são um contributo importante para que os pacientes com condições físicas limitadas sejam mais facilmente integrados na sociedade, proporcionando-lhes mais autonomia e liberdade.
Embora esta tecnologia tenha os seus aspetos positivos, ainda existe a necessidade de descrever os correlatos cerebrais direcionados para o controlo do exoesqueleto. Por exemplo, a percepção de diferentes pavimentos quando se usa um exoesqueleto vai provavelmente causar alterações na actividade cerebral, o que pode ter impacto tanto na codificação sensorial como no controlo da interface cérebro-máquina (BCI).
Deste modo, o principal objetivo deste trabalho é descrever a atividade cerebral às diferentes texturas dos pavimentos, utilizando o exoesqueleto ExoAtlet ®. A fim de medir, processar, analisar e classificar o impacto de diferentes texturas em ritmos neurofisiológicos, foram registados sinais de 4 minutos atravês the Eletroencefalograma (EEG) com uma touca de 16 canais (actiCAP by Brain Products).
Cada um dos três voluntários foi instruído a dar passos no lugar em quatro tipos diferentes de pavimento (plano, alcatifa, espuma, e círculos de borracha) com e sem o exosqueleto, num total de oito condições experimentais diferentes. Foi aplicado um desenho contrabalançado e foi obtido o consentimento informado dos participantes (Comissão para as Ciências da Saúde da Universidade Católica Portuguesa - 99/2022). Adicionalmente, foram selecionados quatro classificadores: máquinas de vetores de suporte (SVM), k-vizinhos mais próximos (KNN), análise discriminante linear (LDA) e redes neuronais artificiais (ANN) para analisar três problemas de classificação distintos.
Os resultados obtidos por este estudo demonstraram que existiam alterações associadas à banda de frequência delta para os eléctrodos C3 e C4 e, ao comparar o desempenho dos classificadores, o LDA apresentou a melhor exatidão nos três problemas de classificação envolvendo todos os sujeitos.
Assim, estes resultados são consistentes com a hipótese de que o processamento sensorial dos pavimentos durante o controlo do exoesqueleto induz alterações neuronais.

Palavras-chave

Eletroencefalografia, Exoesqueleto, Textura do pavimento, Processamento, Classificação

Resumo alargado

Os exoesqueletos são dispositivos que melhoram a qualidade de vida das pessoas que apresentam condições motoras limitadas. Consequentemente, são um contributo importante para o campo da reabilitação física para que os pacientes se tornem mais facilmente integrados na sociedade, proporcionando-lhes mais autonomia.
Apesar de haver um grande número de aspetos positivos associados à utilização dos exoesqueletos, salientando-se de imediato a capacidade de locomoção, ainda não existe um conhecimento pleno de todas as suas implicações. Por exemplo, não se sabe se a utilização de um equipamento tão volumoso e rígido como o exoesqueleto para os membros inferiores, impede ou afeta a perceção tátil.
A literatura mostra que os seres humanos são significativamente sensíveis às propriedades de várias superfícies. Diferentes texturas são representadas pelo cérebro através de estímulos sensoriais provenientes de sensores na pele que geram, respetivamente, diferentes sinais elétricos posteriormente interpretados no córtex somatossensorial.
Consequentemente, torna-se relevante descrever os correlatos neuronais associados ao controlo do exoesqueleto que ainda não foram descritos em pormenor na literatura, existindo ainda, muitos desafios e fronteiras tecnológicas a ultrapassar para o desenvolvimento desta tecnologia.
Deste modo, o principal objetivo deste trabalho é descrever a resposta da atividade cerebral às diferentes texturas dos pavimentos, utilizando o exoesqueleto exoAtlet ®. A fim de medir, processar, analisar e classificar o impacto das diferentes texturas em ritmos neurofisiológicos, foram registados sinais de 4 minutos com uma touca de EEG de 16 canais (actiCAP by Brain Products). Foi obtido o consentimento informado dos participantes (Comissão para as Ciências da Saúde da Universidade Católica Portuguesa - 99/2022).
Cada voluntário foi instruído a dar passos no mesmo sítio em 4 tipos diferentes de pavimentos (regulares, alcatifa, espuma, e círculos de borracha) com e sem o exosqueleto, num total de 8 condições experimentais. Foi aplicado um desenho contrabalançado para se controlar potenciais efeitos associados à ordem de apresentação das diferentes condições experimentais, implicando que todos os sujeitos possuam uma ordem de pavimentos distinta.
As diferentes condições experimentais traduzem três problemas de classificação: i) um problema de duas classes que distingue os sinais com e sem exoesqueleto, ii) um problema de quatro classes que diferencia os 4 pavimentos e, iii) um problema de oito classes abrange todas as condições experimentais.
Consequentemente, os sinais foram classificados utilizando quatro algoritmos diferentes: máquinas de vetores de suporte (SVM), k-vizinhos mais próximos (KNN), análise discriminante linear (LDA) e redes neuronais artificiais (ANN).
Numa análise descritiva dos diferentes sinais de EEG obtidos pelos três voluntários, verificou-se que haviam alterações associadas à banda de frequência delta para os elétrodos C3 e C4 (que se encontram sobre as regiões associadas ao processamento sensoriomotor) dos

sujeitos com o exoesqueleto de acordo com a robustez das diferentes superfícies.
Comparando os desempenhos dos diferentes classificadores concluiu-se que o LDA apresentou o melhor desempenho perante os 3 problemas de classificação, envolvendo todos os sujeitos. O melhor desempenho com uma exatidão de 98.57% foi alcançada pelo problema binário.
Contudo, para as classificações de sujeito-dependente (dados de um único individuo) os resultados já indicaram que o melhor desempenho foi alcançado pelo modelo SVM, tendo este, em casos específicos, alcançado um desempenho perfeito com valores de exatidão de 100%.
Assim, este trabalho com foco no estudo de padrões neuronais induzidos por diferentes experiências sensoriais contribui para a compreensão do processo de codificação neural de texturas com um exoesqueleto, para subsequentemente se desenvolver sistemas BCI eficientes. Além disso, este estudo contribui para o desenvolvimento da área da reabilitação, mas também, de uma forma mais abrangente, para a evolução de interfaces cérebro-máquina com utilidade substancial em áreas militares e industriais.
Todavia, este trabalho apresenta limitações. Tendo em conta que os sinais de EEG foram recolhidos com uma impedância de 50kΩ, este valor pode afetar a qualidade dos dados [1][2]. Adicionalmente, o número de elétrodos do sistema de recolha de EEG impede a análise de zonas especificas do cérebro [3].
Por fim, em termos de trabalho futuro, as sugestões passam por aumentar o número de sujeitos em estudo, para construção de modelos de classificação mais robustos e de forma a validar os resultados obtidos por este estudo piloto. Paralelamente, seria interessante incluir recolhas noutros pavimentos irregulares com relevos acentuados de forma a compreender melhor o impacto de diversos pavimentos na atividade neuronal, em específico as alterações na potência das ondas delta.

Abstract

Powered exoskeletons play a crucial role in the rehabilitation field improving the quality of life for those who need them. Thus, being a major contribution for patients integration into society, providing them with more autonomy and freedom.
In spite of these positive outcomes, a thorough description of the brain correlates connected to exoskeleton control is still needed. For instance, the perception of different pavement textures when wearing an exoskeleton is probably going to cause changes in cerebral activity, which could impact both sensory encoding and Brain-Computer Interface (BCI) control.
Therefore, the main goal of this work is to describe the brain activity response to different textured pavements using ExoAtlet ® powered exoskeleton. In order to measure, process, analyze and classify the impact of different textures on neurophysiological rhythms, 4-minute signals were recorded by Electroencephalogram (EEG) with a 16-channel cap (actiCAP by Brain Products).
Each of the three experimental subjects was instructed to walk in place on four different types of pavement (flat, carpet, foam, and rubber circles) with and without the exoskeleton, for a total of eight different experimental conditions. A counterbalanced design was applied, and informed consent was obtained from participants (Committee for Health Sciences of the Universidade Católica Portuguesa - 99/2022). Additionally, four machine learning methods, Support Vector Machine (SVM), K-Nearest Neighbors (KNN), Linear Discriminant Analysis (LDA), and Artificial Neural Network (ANN), were selected in order to analyze three distinct classification problems.
This study found that there were changes associated with the delta frequency band for electrodes C3 and C4, and when comparing the classifiers performance, LDA presented the best accuracy across the three classification problems involving all subjects.
Thereby, this work concludes that the results are consistent with the hypothesis that sensory processing of pavement textures during exoskeleton control induces neural changes and delta variations of the C3 and C4 electrodes. Additionally, LDA demonstrated the best performance across the three classifications of subject-independent problems.

Keywords

Electroencephalography, Exoskeleton, Pavement texture, Processing, Classification

Contents

List of Figures

List of Tables

Acronyms and Abbreviations

AD	Alzheimer's Disease
ANOVA	Analysis of Variance
ANN	Artificial Neural Network
ANS	Autonomic Nervous System
AP	Action Potencial
BCI	Brain-Computer Interface
BSS	Blind Source Separation
CCA	Canonical Correlation Analysis
CE	Conformité Européen
CNS	Central Nervous System
CSF	Cebrospinal Fluid
CWT	Continuous Wavelet Transform
DL	Deep Learning
DWT	Discrete Wavelet Transform
ECoG	Electrocorticography
EEG	Electroencephalogram
EOG	Electrooculogram
FDA	Food and Drug Administration
FES	Functional Electrical Stimulation
FFT	Fast Fourier Transform
FIR	Finite Impulse Response
FN	False Negatives
FP	False Positives
fMRI	functional Magnetic Resonance Imaging
HMI	Human-Machine Interface

HPF	High-pass Filter
ICA	Independent Component Analysis
iEEG	Intracranial Electroencephalography
ITE	In-the-ear
KNN	K-Nearest Neighbors
LDA	Linear Discriminant Analysis
LFP	Local Field Potential
LPF	Low-pass Filter
LVO	Large Vessel Occlusion
MEG	Magnetoencephalography
MFNN	Multilayered Feed-forward Neural Network
ML	Machine Learning
MS	Multiple Sclerosis
NS	Nervous System
PD	Parkinson's Disease
PCA	Principal Component Analysis
PNS	Peripheral Nervous System
PSD	Power Spectral Density
PSG	Polysomnography
RMS	Root Mean Square
RNN	Recurrent Neural Networks
SCI	Spinal Cord Injury
SD	Standard Deviation
SE	Shannon Entropy
SFNN	Single-layered Feed-forward Neural Network
SNS	Somatic Nervous System
SVM	Support Vector Machine

TN	True Negatives
TP	True Positives
TTE	Temporary tattoo electrode
UV	Ultraviolet
WT	Wavelet Transform

Chapter 1

Introduction

In this chapter, the aspects that motivated the study of brain activity and the main goals intended to be achieved are presented. Consequently, an overview of the exoskeleton use and the correlation with the Electroencephalogram (EEG) signal analysis is given. The main objectives and contributions that this study aims to accomplish are also presented.

1.1 Outline

The document is organised in six different chapters. The current chapter 1 intends to describe the significance of this work and its relevance to the scientific community, along with some basic useful concepts of the brain to better comprehend the document's work. Chapter 2 provides a state–of–the–art on the exoskeleton robotic devices, the EEG recording technique, and the most crucial stages of analysing an EEG signal along with the most commonly used signal processing techniques.
Chapter 3 describes the framework conducted in this work in order to acquire and process the bio-signal. The applied process to acquired the EEG signal is described, the chosen pavements are characterised, and the selected models and methods for signal processing are justified. In the following chapter 4 the obtained results are accessed and chapter 5 discussed these results, taking into account the main goal of this work and some limitations are addressed.
The final chapter 6, presents the conclusions that can be drawn from the developed study. Furthermore, future improvements are proposed, in order to refine the quality of this study.

1.2 Context

When looking at a global scale, not only is there a rising trend in the occurrence of Spinal Cord Injury (SCI), but also an increase in average life expectancy each year. Society is not only living longer but also having more risk behaviours such as smoking, sedentary lifestyles, alcohol consumption, and bad eating habits that lead to the early onset of diseases such as hypertension, diabetes, and cholesterol that inevitably lead to an increase in the number of strokes [4][5][6].
As a result, it is imperative to address this looming social problem and develop new technologies to offer better medical services equal to all. Ultimately, wearable robotic devices enable mobility, independence, and a better quality of life for people with injuries or movement impairments.

Recent articles have shown that powered exoskeletons have benefits in the field of neurorehabilitation as they can intensify brain plasticity, making them a practical and valuable tool for the rehabilitation field [7]. This brain plasticity evaluation and monotorization is possible due to the acquisition of brain activity with, for example, an EEG during the experimental activities with exoskeletons.
Therefore, recent advances in EEG signal processing algorithms and analysis techniques have allowed patients with neurological disabilities and motor impairments to coordinate and control, with their thoughts, physical objects, such as, wheelchairs and exoskeletons. This communication pathway that interprets the brain signals and translates them to the desired physical motion is referred to as Brain-Computer Interface (BCI) [8].
In general, combining the two concepts of EEG and exoskeletons, will accelerate robotics and artificial intelligence research, resulting in more sophisticated robotic systems that can interact with humans and attend to their needs [7][9].
However, there are still many challenges and technological frontiers that need to be studied in order to develop more efficient exoskeletons with good levels of performance and, consequently, provide better health services to those who depend on these assisting devices to live better lives [7]. In addition, there are also impediments in the analysis of the EEG signal, as there is no pre-defined standard pipeline in the literature that allows an accurate pre-processing stage and analysis of the neuronal activity, meaning that there are numerous different approaches that can be considered when processing EEG data [10][11].
Initially, some basic concepts concerning the brain's anatomy are addressed in order to better comprehend how an EEG can measure and provide data about neural activity and how this bio-signal is formed and propagates across neurons. This information, described in the following subsections, helps to better understand the brain and facilitates the comprehension of the biological concepts and phenomena that are described and mentioned throughout the document.

1.2.1 Brain anatomy | Basics

When analyzing the human body and how cells are organized and communicate with one another, the brain is a complex part of the human system [12]. Looking even more closely, the brain's neural activity appears between the seventeenth and twenty-third weeks of gestation and, thereafter, those electrical signals never stop and are continuously giving information about the human body and interpreting the surrounding environment and its stimulus [12].
Neuroscience is responsible for studying the structure, function, and development of the Nervous System (NS), which plays a key role in our daily lives as the main control of our body, coordinating and regulating the communication of every human cell [13].
This complex network regulates various physiologic processes inside a human body by sending messages from the brain and spinal cord to every part of the body, and vice-versa. Therefore, it allows humans to think, move, say, and feel different emotions, presenting

also the ability of monitoring and coordinating physiological processes such as blinking and breathing without actively thinking about it [13]. When this communication pathway is compromised and unable to establish communication between the brain and the muscles, it leads to movement impairments that normally require physical therapy and assistive device interventions [12].

The NS is mainly segmented into two parts: the Central Nervous System (CNS) and the Peripheral Nervous System (PNS). The CNS is composed by the brain and the spinal cord, and the PNS consists of all the nerves that emerge from the brain or the spinal cord, meaning the nerve structures that are located outside of the CNS components. Therefore, this system is composed of spinal and cranial nerves [13], figure 1.1.

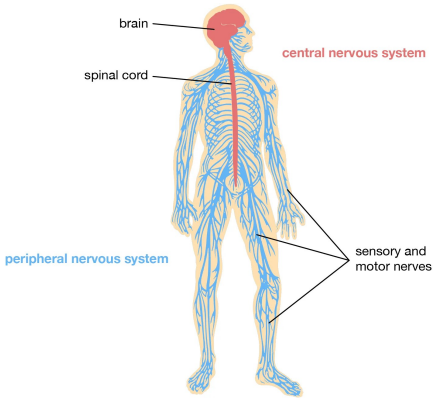

Figure 1.1: Central and Peripheral Nervous System (adapted from [14]).

In addition, the PNS is also divided into two distinct parts: the Somatic Nervous System (SNS) and the Autonomic Nervous System (ANS). The SNS controls voluntary movements and it is responsible for processing sensations, while the ANS controls in an automatic way functions such as blood pressure, heart rate, breathing, temperature regulation, appetite perception, water and electrolyte balance [13][15].

The brain is the central organ of the CNS and it is the main commander and leader of the human body. Is one of the more complex human organs, being physically protected by the skull, and it can be classified in many different ways. Therefore, from an embryological derivation point of view, the brain consists of three main areas: the forebrain, midbrain, and hindbrain [15].

Each one of these three main areas is composed of different structures, so the brain can be structurally divided into 3 major components: the cerebrum, cerebellum, and brainstem [13], shown in figure 1.2.

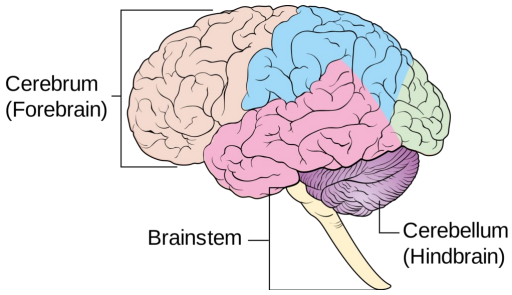

Figure 1.2: Three major brain components (retrieved from [16]).

1.2.1.1 Brainstem

The brainstem corresponds to the lower extension of the brain. Located in the midbrain in front of the cerebellum, it connects the cerebrum to the spinal cord. This anatomical structure plays an important role in controlling vital functions that are essential to human survival, such as, breathing, eye and facial movements, heartbeat, or blood pressure [13][8].
Therefore, this is the area where relies the autonomic and subconscious control of simple mechanisms that normally humans are not aware, for example, sneezing, vomiting and coughing [13].

1.2.1.2 Cerebellum

The cerebellum, referred to as the “litle brain”, located in the hindbrain, is the second largest brain structure, prefacing about 10% when compared to the brain’s total volume, and is located at the lower back of the head. It’s mainly responsible for motor activity, movement and coordination. It is associated with fine motor skills, such as, performing a surgery or painting a picture and it helps on posture, balance maintenance and equilibrium [13].

1.2.1.3 Cerebrum

The cerebrum, located in the forebrain, represents the largest and dominant part of the human brain, consisting of more than three-quarters when compared to brain’s total volume. This part is associated with the coordination of movement, emotions, thought processes, and motor functions [13].
The cerebrum comprises grey and white matter. Grey matter is associated with a darker coloration, it is located on the outside of the white matter, surrounding it, and it is constituted by nerve-cell bodies. On the other hand, white matter is lighter in colour and located in the inner part of the cerebrum, and it is composed by axons (nerve fibers) that represent the communication channels between neurons [13].

The outer grey matter that surrounds the cerebrum with approximately 1 to 4 mm thick and organized in layers, it is described as cerebral cortex. It is divided into two hemispheres, left and right, due to the presence of a central sulcus. Each of the two hemispheres is also divided into four distinct lobes: frontal, parietal, occipital, and temporal [13][8], figure 1.3.

- Frontal Lobes

  The frontal lobe is the largest of the four lobes and its principal functional areas are: the prefrontal cortex, the primary motor cortex, the premotor cortex and the Broca's Area. This lobe is involved in many different functions related to motor movement, emotions, problem solving, personality, abstract thoughts among others [15][8].

- Parietal Lobes

  The parietal lobe is structurally composed by the primary somatosensory cortex and is responsible to process and recognise somatic sensations. This brain lobe is mainly related to sensations, involving sensory comprehension of taste, touch and pain [15][8].

- Occipital Lobes

  The occipital lobe is located on the back of the brain behind the parietal and temporal lobes and it contains the primary visual cortex responsible for receiving visual information. Therefore, this lobe is responsible for visual processing, allowing humans to determine colours, shapes and facial recognition [15][8].

- Temporal Lobes

  The temporal lobe includes several functions, namely the recognition of auditory stimulus as well as their processing. This anatomical structure features the auditory cortex and the Wernicke's area (speech cortex) that is responsible for verbal memory, allowing humans to understand and interpret a certain language [15][8].

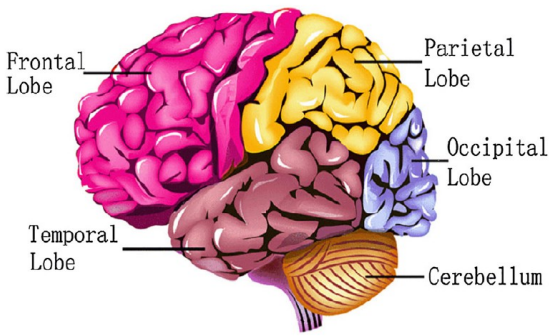

Figure 1.3: Four areas of the cerebral cortex and the cerebellum (retrieved from [8]).

Consequently, in order to understand the brain and its activity, the next subsection will focus on neuron communication, showcasing how the information is able to travel long distances and respond to external stimulus.

1.2.2 Brain Neural Activity

Looking more closely, at a histological level, our NS is composed by more than a thousand types of brain cells, but is mainly composed by two types: neurons (nerve cells) and supporting glial cells (neuroglia or glia) [13] [15].

Neurons are the basic unit of the NS and they are composed by a cell body (soma) and extensions of the cell body referred to as processes. Each neuron is composed by an axon (axonal process) that connects the neuron to its target and a variable number of dendrites (dendritic processes) responsible for receiving the messages from other neurons [13][15]. Therefore, nerve cells are capable to transmit electrical signals and communicate with each other via electrochemical messages [13].

All in all, neurons are divided into three sections: cell body, axon and dendrite, figure 1.4. The cell body contains the nucleus, where the genetic material is located. The dendrites resemble the branches of a tree and are the ones responsible for receiving signals. The axon resembles a long tail and sends the messages from the cell onward [13][15].

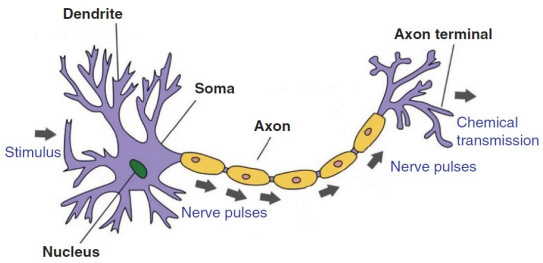

Figure 1.4: Structure of a neuron (adapted from [12]).

Neurons feature differences in size and shape between each other. Therefore, structural variations are classified according to the location of the cell body compared to the position of the axon and dendrites. Generally speaking, there are three main types of neuron forms: unipolar, bipolar, and multipolar, figure 1.5 [13].

Unipolar neurons are composed of a single axon that extends from the soma and segments itself into two or more branches. Bipolar neurons possess two extensions, the dendrites and the axon, extending from the cell body. This type of neuron is mainly found in the retina of the eye [13].

Finally, multipolar neurons possess a single main axon and various dendrites that extend from it. This type of neuron is the most commonly found in the CNS [13].

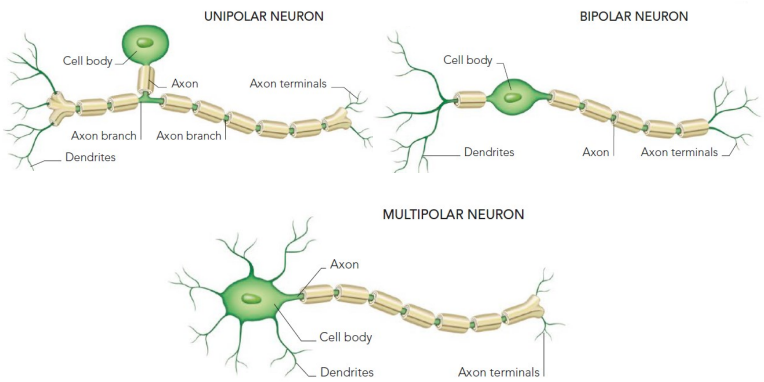

Figure 1.5: Types of neurons (adapted from [13]).

Although some brain regions can be identified and recognised by a specific type of neuron, making the distinction between neurons is a difficult task. Brain neurons form complex systems, mixing cells of different shapes and forms, making it difficult to distinguish them [13].

Additionally, these neurons are physically supported by glial cells[1]. Neuroglial cells play a crucial role in supporting, protecting and nurturing neurons, providing them with the required sugars and raw materials for their growth and repair. Although these cells are smaller in relation to the neurons size, they are up to fifty times more numerous when compared to the estimated brain's 86 billion neurons [13][15].

Glial cells are divided into six different types that perform different functions in the NS. The astrocytes, oligodendrocytes, microglial and ependymal cells are located in the CNS, while the Schwann cells (neurolemmocytes) and the satellite cells can be found in the PNS [15], figure 1.6.

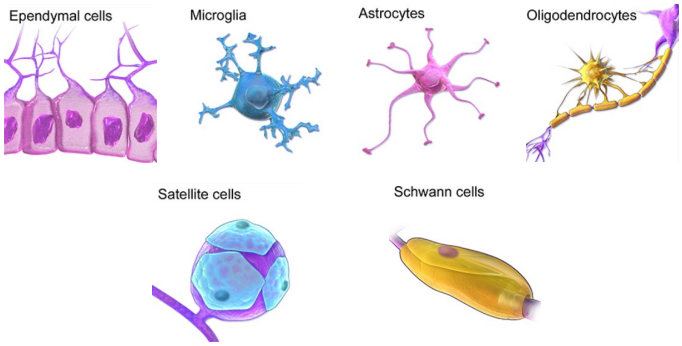

Figure 1.6: Types of glial cells (adapted from [17]).

Looking more closely into the CNS neuroglia, astrocytes are the most predominant type of glial cells in the CNS. They are responsible for monitoring and maintaining the composi-

[1]Glia translates to "glue" in Greek [13].

tion of the interstitial fluid of the CNS and also play a crucial part on neuronal behaviour, affecting memory and sleep patterns. The metabolism of neurotransmitters and the ionic potassium levels are also influenced and regulated by this type of glia [15][13].
Oligodendrocytes are responsible for producing myelin sheating along the axons. Therefore, by wrapping themselves around axons they provide support and insulation. This condition allows a faster propagation of the electrical impulse along the neurons [15].
On the other hand, microglial cells are the immune cells of the CNS, responsible for its protection. These phagocytic cells are a specialized population of macrophages that destroy microbial invaders and remove the debris from damaged and degenerating neurons. As a result, they are crucial to maintain and ensure the CNS health [15][13].
Finally, at the CNS level, the ependymal cells are relevant in Cebrospinal Fluid (CSF) production and homeostasis. They form a thin membrane that lines the ventricular system of the brain and the central canal of the spinal cord [15].
At the PNS neuroglia level, the Schwann cells perform the same function as the previously described oligodendrocytes but in the peripheral nerves, contributing to a faster saltatory conduction along the axon. Lastly, satellite cells provide nutrient support and regulate the electrical neuronal environment [15].

1.2.2.1 Action Potentials

A nerve impulse reflects the electrical signal that travels through a neuron. This information is typically referred to as Action Potencial (AP). Looking more closely, an AP corresponds to a temporary and sudden change in cation concentration on both sides of the cell membrane. This phenomenon reverses the polarity across the neuron membrane and triggers a variation of the potential along the length of the axon [12][13].
AP are discrete impulses that begin in the cell body and travel from there in one direction only. They take place due to various types of stimulus, such as, touch, light and chemical. Communication between the CNS neurons is established mainly by chemical activity synapses [12], described in sub-subsection 1.2.2.2.
The impulse corresponds mainly to the sodium (Na^+) and potassium (K^+) ions movement along a neuron, inducing the depolarisation and consequent repolarisation of the cell membrane [13]. Thus, an AP possesses three main phases, as presented in figure 1.7.

1. **Resting Potential -** At rest, neurons maintain a negative interior membrane potential around -60 and -70 mV. A negative concentration gradient implies that there are more positively charged particles on the outside than inside the neuron. Therefore, the outside of the membrane possesses more sodium (Na^+) and the inside more potassium (K^+) enabling the presence of a polarised membrane [13].

   An AP is triggered when the stimulus is large enough to bring the inside membrane potential up to its threshold value of -55mV, allowing the nerve pulse to travel along the axon [12].

2. **Depolarisation -** Refers to the change of membrane potential where the inside is now more positive than the outside. Neuronal excitability occurs due to the presence of Na^+ and K^+ channels with gates that are responsive to membrane potential. Designated by voltage-gated channels, they have the ability to open and close according to the potential's variation [12].

   Therefore, the Na^+ gates open and the sodium ions (positively charged) enter the cell's membrane through the channels, elevating the membrane potential, which means becoming less negative [13][12].

3. **Repolarisation -** An important step that allows to restore the balance between the ions on both sides of the membrane, meaning that the potassium ions are being transported into the inside of the neuron and the sodium in the opposite direction. This process is carried out by sodium-potassium pumps. Consequently the neuron restores it's resting potential [13].

   In this stage, the Na^+ channels close and the K^+ channels finally open. This mismatch occurs due to the fact that potassium channels take longer to open and close, allowing the previous phase (depolarisation) to occur. As the K^+ channels open the positive ions flow to the outside of the membrane, making the potential more negative and closer to the resting potential [12].

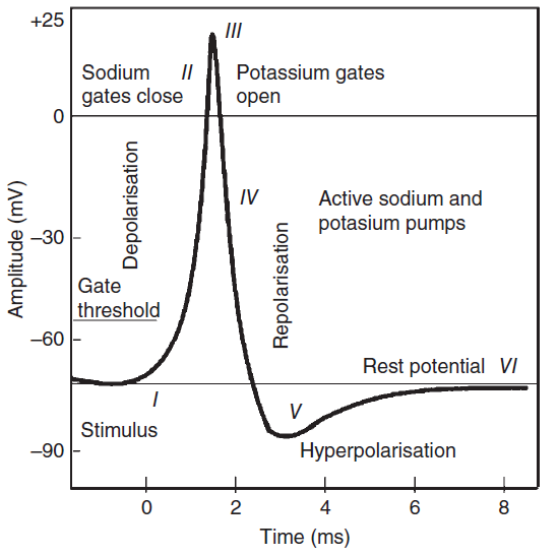

Figure 1.7: Action Potential (retrieved from [12]).

On the whole, for a human the process of conducting an AP along the axon, implies a potential range between -60 up to 10 mV [12]. By looking more closely, in figure 1.7, there is also an important phase designated by **hiperpolarization**, which is a crucial step in order to achieve the resting potential.
This stage of repolarisation means that the cell is more negative than its normal resting potential (-60 mV) reaching aproximaly -90 mV. This phenomenon occurs due to the

potassium channels that remain open, and, therefore, allow positive ions to abandon the inside of the cell membrane. Hiperpolarisation is responsible for guaranteeing that the signal travels in only one direction, preventing a new stimulus (another AP) to be triggered along the axon in the opposite direction [12].

1.2.2.2 Communication site | Synapses

As previously stated in the document, neurons are information messengers where dendrites receive the information and the axon sends the signal away from the cell body, therefore, excitability is a property inherent to all neurons [13].
Although neurons communicate to one another, they do not physically touch each other. Instead, there is a small gap between them known as the synaptic cleft that separates the presynaptic neuron (the one sending the signal) from the postsynaptic neuron (the one that is receiving the information) [13].
Consequently, in order for neurons to transmit information to one another despite the physical space, they send chemical signals at these junctions, also designated by synapses. At the synapse, when the previously described AP reaches the presynaptic cell, it unleashes the release of neurotransmitter molecules (chemical messengers) that diffuse[2] across the synaptic clef and bind to the postsynaptic cell. Within the different types of synapses, figure 1.8, axospinodendritic are the most prevalent type representing more than fifth percent of the brain total communication sites [13].
Hence, neurons use both electrical and chemical signals in order to establish communication [13].

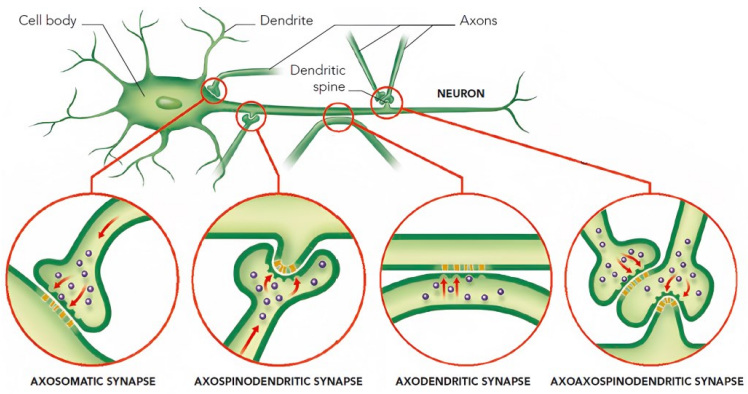

Figure 1.8: Communication between two neurons (adapted from [13]).

1.2.3 Neurological Disorders

Variations in normal brain activity can occur and they are usually translated into the origin of brain disorders, diseases and abnormalities. Certain neurological disorders are recog-

[2]Simple diffusion: neurotransmitters move across the gap from a higher concentration region to a lower concentration.

nised and diagnosed by implementing digital processing, feature extraction and classification methods to EEG signals [12].
Stroke is a clinical condition that is remarkably common in society, making an impact on a worldwide scale and being not only the second major cause of mortality but also the cause of patients physical disabilities. When the blood supply to a certain brain region is interrupted or very limited, this prevents oxygen to reach the tissues, leading to brain cell death, resulting in brain damage [18][19].
Mainly, strokes are segmented into ischemic and hemorrhagic, figure 1.9. The most prevalent one is the ischemic stroke, responsible for 85% of all cases. This specific type occurs when an artery, or more rarely, a vein, is blocked by a clot, and, consequently, the supply of O_2 and nutrients to the brain is not enough, causing the cell death. Right after, with 10-15% of the total cases, there is the hemorrhagic stroke, which, as the name itself suggests, takes place when a certain vessel ruptures and inevitably starts leaking. This type of incident is less common but more fatal than an ischemic stroke [18].

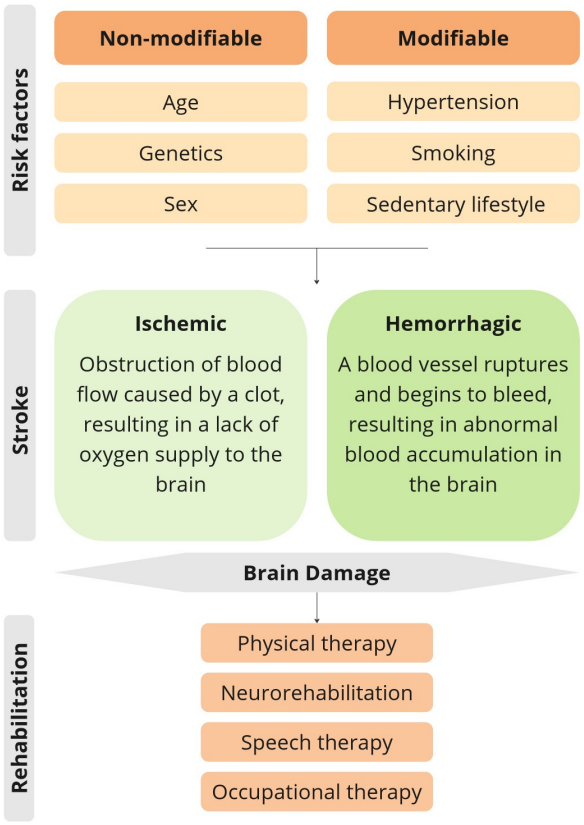

Figure 1.9: Stroke risk factors, types, and therapy approaches.

Consequently, since it has become more and more prevalent in developing countries, scientists have been focusing on studying and developing tools based on EEG analysis that can accurately diagnose and predict medical emergencies. An accurate prognosis for this condition enhances the medical treatments, making it possible to prevent severe repercussions and outcomes [18][19].
Certain correlations between the EEG signal and stroke condition have been demonstrated

in the literature. Articles have stated that cerebrovascular accidents, are characterised by higher brain asymmetry and certain brain rhythms: greater delta power and reduced alpha and beta power, which are also associated with Large Vessel Occlusion (LVO) strokes. Studies also present little information that highlights the capacity to distinguish ischemic from hemorrhagic strokes [19].

Despite the advances in the use of EEG as a prognostic and monitoring tool, the association of stroke with a power decrease in high-frequency wave rhythm and a power increase in low-frequency waves still faces challenges before it can become an accurate and clinically accepted diagnosis method. Therefore, it is crucial to better understand and comprehend what features of the EEG signal can be used to diagnose these occurrences [19].

SCI, along with strokes, is a leading cause of physical disability worldwide. Mainly, this condition is a consequence of traumatic experiences, such as violent falls and road accidents, that result in sudden lesions to the vertebrae. Non-traumatic SCI is a less prevalent condition that results from the patient itself when the body is suffering from infections or tumors [4].

Patients with SCI suffer alterations in the structural level of the spinal cord, a fundamental part of the CNS. The damaged neurons lose their ability to generate and grow. As a result, these cells cannot transmit signals, which implies a loss of sensory and motor information. Consequently, subjects lose partially or completely the capacity to perceive tactile sensations and to control their movements below the injury site [4].

Recently, studies have been focusing on finding the potential of using EEG to detect the neural changes induced by SCI. Studying the brain response to therapy and the alterations in the neural rhythms is a doorway to improve the performance of traditional treatments and therapies offered to these patients. According to [20], the ratio established between the alpha and theta waves can be potentially used as a biomarker to access the efficiency of the rehabilitation process and the ability of the brain to reorganise (plasticity) [20].

Dementia is a syndrome often used to describe the process that involves the loss of certain human abilities such as memory, social engagements, and relationships with close family members. This process is caused by the gradual loss of cognitive functions over time. The two most common types of dementia in society are Alzheimer's Disease (AD) and Parkinson's Disease (PD), figure 1.10 [12][21].

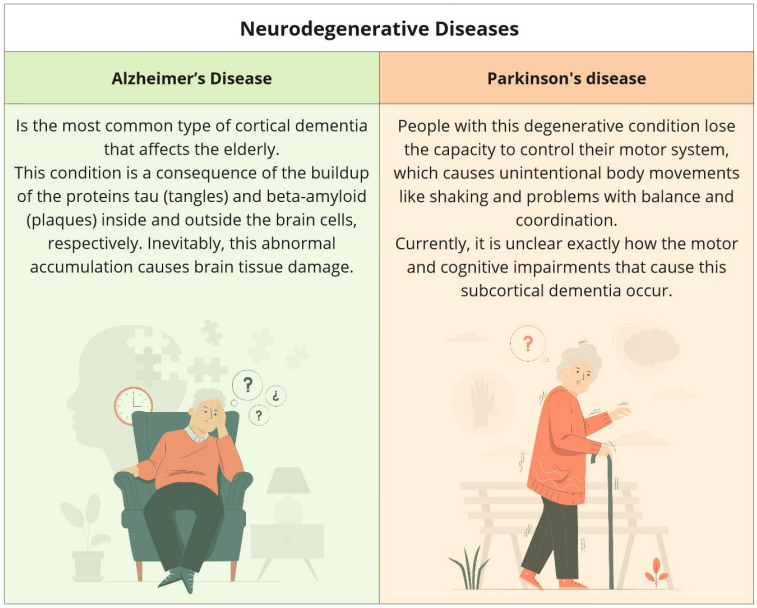

Figure 1.10: Neurodegenerative disease, AD and PD.

These neurodegenerative diseases can be studied and monitored by analysing EEG signals. When compared to healthy individuals, these neural activity traces show differences. Subcortical dementia, such as PD, is usually more difficult to identify in EEG data because it causes fewer irregularities than cortical dementias, such as AD [12][21].
Although EEG is not currently a commonly used method to diagnose these dementias, a recent review [21], emphasises the great potential of applying graph theory[3] to EEG patterns in order to study and diagnose AD and PD. Therefore, particular graph features may serve as biomarkers for these disorders, contributing to a deeper knowledge of the brain and improving the rehabilitation field [12][21][22].

1.3 Motivation and Objectives

To accurately and effectively retrieve information from the recorded signals, such as identifying specific frequency bands or patterns of activity, is still a big challenge for researchers. The growth, in the last years, of this research area that merges together two fundamental concepts, exoskeleton and electroencephalogram, is the starting point for the development of this work. The objective is to comprehend the behaviour of neural activity and its change according to different pavements, or if perchance the patient's concentration and focus required to control the robotic device makes these textural changes irrelevant and imperceptible at the neuronal level.
The main motivation for this research is: i) to determine whether exoskeletons themselves interfere with patients' ability to perceive and decode textures, ii) to establish the main differences between using and not using the exoskeleton by analysing the signal's

[3]Graph Theory: mathematical model that represents the brain and its complex network using a graph; consequently, several parameters can be used to measure specific graph qualities [21][22].

power, and iii) determining which frequency bands are able to characterise the different experimental conditions.
Since the EEG signal analysis and the information that can be retrieved from neural activity represent a substantial contribution to the field of neuroscience, this study, even in a early research stage, provides important information regarding this research area.

1.4 Contributions

This dissertation provides valuable knowledge and sheds light on a deeper understanding of the neurophysiological basis of tactile processing during exoskeleton control.
Therefore, this work provides more information about how external factors can affect neural signals. Although this study is not directly connected to BCI systems, it provides relevant data for the development of tactile sensation-based BCI systems that aim to provide sensory feedback to their users. This process allows a more immersive and real experience for the patients when using the exoskeleton, since the idea is to develop wearable devices that can give sensory feedback back to the patient according to the different surfaces.
This work also provides valuable information to the rehabilitation field when working with patients with physical impairments caused, for example, by SCI, since recognising the neural patterns in healthy individuals helps to assess the differences and monitor the evolution of the brain activity of patients with motor difficulties.
Furthermore, this knowledge is valuable for future works, since understanding how different pavements affect neural activity can result in a more accurate and reliable development of BCI systems.

1.5 Conferences and scientific work

Some of the work developed troughout this study provided the opportunity to attend Computational Intelligence and Intelligent Systems (CIIS) National Meeting 2023 for Interdisciplinary Health Care and VI iBiMED symposium:
1. J. Ramos, M. Pais-Vieira and C. Pais-Vieira, Neural correlates of pavement texture during exoskeleton control.
2. J. Ramos, C. Pais-Vieira and M. Pais-Vieira, Brain activity on encoding different pavement textures: a pilot study.

Chapter 2

State-of-the-Art

This chapter starts with a brief historical contextualisation about the evolution of exoskeleton over the years, and some of the most important robotic device features are addressed. Furthermore, this chapter describes the EEG exam. Thereafter, the techniques applied in signal processing are specified. Lastly, some articles, similar to the proposed theme in this dissertation, are presented.

2.1 Robotic Exoskeletons

In 2019, stroke was the fifth leading cause of death in the United States [6]. When these accidents are not fatal, people often suffer short or long-term repercussions, normally associated with lasting brain damage and disabilities that affect physical movement. This way, physical therapy is recommended for these individuals [6].
At a worldwide level, in 2019, there were 0.9 million new cases of SCI increasing the number to 20.6 million prevalent cases. Typically, this condition is clinically associated with paraplegia (lower body paralysis) or tetraplegia (upper and lower body paralysis), and along with the stroke survivors, these patients are also redirected to physical therapy [4]
Stroke and ischaemic heart disease were the two leading causes of death in Portugal prior to the COVID-19 pandemic, accounting for 9.9% and 6.4% of all causes of death, respectively. Along with the large number of stroke victims and survivors, the national life expectancy is higher than the European Union average [5]. Therefore, not only people who have daily physical limitations and rely on therapy are a concern to the health care system, but also the increase in life expectancy is an issue that needs to be taken into account. Since people are living longer and these diseases have a high prevalence, there is a need to address this social issue.
Consequently, these statistics highlight the importance of developing technologies to promote a more effective and less work-intensive rehabilitation, contributing to a better health care service. Neuromuscular diseases limit people's day-to-day life activities, increasing the likelihood of a sedentary and restricted lifestyle. Therefore, it is crucial to develop technologies, like rehabilitation robotic devices, that can counteract this trend [23].
Inevitably, exoskeleton robotic devices play an important role in assisting humans in performing certain activities that, without them, would be hard or maybe impossible to achieve [24]. The basic premise for the development of these mechanical wearable robots is the desire to replicate specific body parts functions by developing external structures that can either support and assist humans with joint and limb impairments, or enhance humans' biological potential [7].

Thus, the next subsections will provide a historical background. Since this dissertation works with a lower-limb exoskeleton, the most commonly used lower-limb exoskeletons in literature are described, as are the different types of classifications, areas of application, and challenges that this technology faces as it develops.

2.1.1 History

In reality, when looking at the timeline of human history, the first form of exoskeleton appears in 1890 with a Russian scientist, Nicholas Yagn, who created an apparatus[1], figure 2.1 to assist humans in walking, running and jumping activities [26].

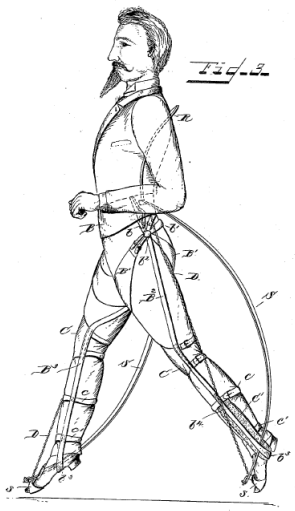

Figure 2.1: Apparatus (adapted from [27]).

Afterwards, in the late 1960s, the Hardiman I, figure 2.2, emerges as the first attempt in history to achieve a practical and ease to use full-body powered exoskeleton. The mechanical device built by General Electric Research alongside Cornell University and the U.S. Office of Naval Research was not successful [26]. Due to its large dimensions, weight and numerous physical layers, the exoskeleton produced uncontrolled movements that were dangerous for human subjects to wear them. In addition to having a poor walking speed, the device also required a long time to respond to commands in order to move [26].

[1]Apparatus: a set of equipment or tools or a machine that is used for a particular purpose [25]

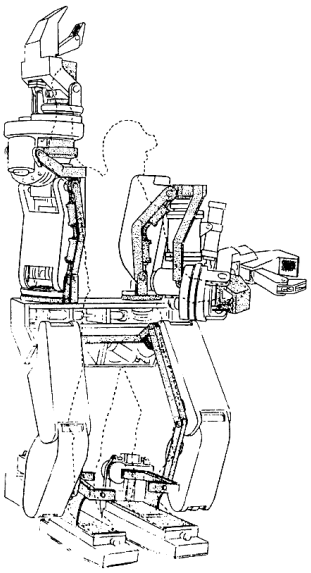

Figure 2.2: Hardiman I (adapted from [28]).

One of the history markers began in 1969 at the Mihailo Pupin Institute, where Prof. Miomir K. Vukobratovic oversaw the development of the first walking active exoskeleton [26].
This exoskeleton served as a precursor to the development of more sophisticated devices. It possessed seven pneumatic actuators and was electronically programmed. Although the exoskeleton was able to assist paraplegic patients, it did not provide them with support. Therefore, it did not prevent them from falling sideways. Later on, in 1972, a more advanced and improved version of the model was tested at the Belgrade Orthopedic Clinic [26].
Finally, in 1978, an active semi-soft mechanical device called Active Suit was a success in the field of rehabilitation and used in clinical studies [26]. This exoskeleton was controlled by a microprocessor and possessed rechargeable batteries of nickel oxide hydroxide and metallic cadmium (Ni–Cd batteries) [26].
Today's exoskeletons hold great promise for enhancing human performance, and in both the assistance and therapeutic fields, nonetheless, there is still much room for development and improvement [7].

2.1.2 Classification

In terms of exoskeleton's classification, there are many different categories according to various parameters in which they can be differentiate and classified [26].
Based on their intention, exoskeletons can be divided into three main categories these being, augmentation, assistive and therapeutic [24][7][26].
Augmentation exoskeletons are develop in order to maximise and enhance the biological characteristics of humans. Therefore, healthy human subjects are able to transport and handle heavy loads and work for several hours without severe physical strain. These

robotic structures are associated with industrial and military environments where they improve the manufacturing performance and provide soldiers with more strength and endurance [24][7].
Assistive exoskeletons support those with movement issues and impairments in carrying out daily chores, such as walking. Normally these situations arise from the presence of neurological diseases such as stroke, spinal cord injuries and muscle deterioration [24][7].
Therapeutic also refereed to as rehabilitation exoskeletons have an important role in the rehabilitation field, assisting patients in the physical recovery process. They support and guide the patient during body movement so that it is possible to reestablish their lost physical ability and natural movement [24][7].
In combination with the previous classification, exoskeletons can also be divided into to three categories according to the body part they are mimicking, figure 2.3. Thereby, exoskeletons are refereed to as upper limb, lower limb and specific joints, for instance, hip, knee and ankle [7]. In addition, there are some studies that consider yet another category referred to as full body exoskeletons that are mainly used to increase and amplify human strength [26].

a) b) c)

Figure 2.3: Exoskeletons types: a) Harmony exoskeleton produced by ReNeu Robotics Laboratory is an upper body exoskeleton (adapted from [29]); b) Ironhand produced by Bioservo Technologies is an active soft hand exoskeleton (retrieved from [30]); c) REX produced by Rex Bionics is a lower-limb exoskeleton (adapted from [31]).

In furtherance, taking into account the power source used by exoskeletons, they can be segmented in four categories, passive, pseudo-passive, powered and hybrid exoskeletons [26].
When referring to as passive exoskeletons, this category specifies the absence of external power sources to control the actuators, meaning that these devices only use mechanical forces represented, for example, by strings relying on the human muscle motion. Inevitably passive exoskeletons are lighter in weight when compared to the remaining types [26].
Pseudo-active devices incorporate characteristics from active and passive exoskeletons,

thereby they possess batteries, however these do not provide actuation [26].

Powered exoskeletons are actively controlled by sensors and actuators incorporated on them. These wearable device's can combine a series of different components responsible for moving and controlling the entire system. Therefore, they are able to convert electrical, hydraulic or pneumatic energy into mechanical forces [26].

Hybrid exoskeletons combine the characteristics of powered devices with the incorporation of Functional Electrical Stimulation (FES). This technique produces low-energy electrical pulses that are applied into the paralysed muscles, inducing body movement. The main goal is to restore the muscle's original and natural function by applying charges and stimulating the CNS. By combining electrical actuators with FES there is improvement of the rehabilitation process for patients with paralysis due to the electrical stimulation of the muscles [26][24][7].

2.1.3 Applications

The wide diversity of exoskeletons makes them useful in various fields with different purposes. There are four main areas of application for these devices: medical, military, industrial and civilian [26][24].

- Medical - Is one of the primary applications for these robotic devices since it plays an important role in helping health care professionals performing their job in an easier and more comfortable way. For instance, nurses and physiotherapists can move and handle patients without excessive physical effort and surgeons can perform long hours of surgery without jeopardising the precision of the medical intervention. Is an important field of study since it significantly improves the quality of life for individuals with neuromuscular illnesses, leading to more successful treatments and improved outcomes allowing the patients to regain their natural muscle gait [26].

- Military - In these military scenarios the application is based on two essential ideas: reducing soldier energy expenditure and at the same time increasing their productivity. Normally, the performed tasks involve long periods of time and are associated with running on uneven terrains and handling heavy weapons [26].

- Industrial - Developed to assist workers in performing physical labor-intensive tasks, boosting and augmenting human biological capacities in a way that generates less physical wear and tear. Therefore, industrial exoskeletons allow each worker to perform difficult job assignments for long periods of time without endangering their health. Normally they can be found in factory production lines [26][24].

- Civilian - Associated with hazardous and dangerous environments, these exoskeletons are developed to assist and help people who work in these unsafe conditions, for example firefighters [26].

2.1.4 Lower-limb Exoskeletons

Lower-limb exoskeletons for physical rehabilitation have shown their potential, not only in assisting and easing the work of health professionals, but also by helping patients gain leg mobility and counteracting the effects of a sedentary life and the secondary diseases that can result from it [23][7].

According to literature, Ekso, HAL and Rewalk are the most frequently used exoskeletons in clinical research studies and they possess Food and Drug Administration (FDA) approval and/or Conformité Européen (CE) mark [23].

Wearable lower-limb exoskeletons, such as Ekso, have demonstrated to be effective in treating and achieving better results during the rehabilitation process of a patient. When compared to conventional physical therapy, these devices demonstrate notable results in improving gait speed tests and the muscular system's ability to contract in a more efficient way [32][23].

Promoting neuroplasticity is a crucial aspect because it demonstrates the potential of exoskeletons in the process of physical rehabilitation, which could increase the effectiveness of the care system for those with physical disabilities [32].

2.1.4.1 EksoNR

EksoNR, figure 2.4, is a robotic lower-limb exoskeleton, created by Ekso Bionics, USA and is directed towards the field of rehabilitation. This exoskeleton was the first to be approved by the FDA in order to assist patients with neuromuscular diseases such as stroke, SCI and Multiple Sclerosis (MS). During the exercises, it collects data regarding the duration of the session, the walking velocity and the covered distance [33][23][7].

Figure 2.4: EksoNR exoskeleton (retrieved from [33]).

2.1.4.2 HAL

HAL, figure 2.5, is a medical device developed by CYBERDYNE in Japan to treat people with lower-limb impairments, providing them with autonomy to perform simple daily activities. A study published in 2009 made HAL the first exoskeleton to participate in human clinical trials. The main goal of this technology is to allow patients to improve and regain their natural ability to walk [34][23].

Figure 2.5: HAL exoskeleton (adapted from [34]).

2.1.4.3 Rewalk

Rewalk, figure 2.6, facilitates and assist patients performing day-to-day body motions, such as, standing up, walking and going up and down the stairs. Together with the previous described Ekso, these two wearable exoskeletons cover the broadest variety of injuries. Therefore, can be applied in various situations with different clinical cases [35][23].

Figure 2.6: ReWalk exoskeleton (retrieved from [35]).

2.1.5 Challenges and Future perspectives

When reviewing the literature, it is noticeable that this research area in the last years has rapidly evolved, showcasing it's numerous potential in diverse sectors of society. However, there are still many challenges when addressing exoskeletons and the technology involved. Therefore, one of the crucial points that needs to be improved in the near future relies on the structure it self. Being a heavy and robust device makes it more challenging for patients to wear it, and in some cases, the friction developed between patient and machine may cause unwanted discomfort and wounds [26][24].
Inevitably, the dimensions and the weight are parameters of an exoskeleton that need to be taken into account and reduced in order to obtain more practical devices that look less foreign to the general public [26][24].
Another problem arises with the actuators, since they are not prepared to be embedded in these robotic structures and can produce unpleasant sounds. Regarding accessibility, this technology is associated with high expenses, making it difficult for people to access these assistive devices [26].

2.2 Electroencephalogram | EEG

Electroencephalogram is a non-invasive technique applied to monitor the neural activity and is widely used in the biomedical engineering field, thus being an important tool in the neuroscience research area.

2.2.1 History

Prior to creating the EEG, it is essential to comprehend the idea of electricity and, subsequently, relate it to how the human body's organs work. Hence, the first step towards the birth of the EEG began with William Gilbert (1544-1603), Galileo Galilei (1564-1642), and Thomas Willis (1621-1675), who studied the electricity and electrical properties of certain materials [36].
A few decades later, there were more advances regarding the functioning and anatomy of the nervous systems and how their cells communicate. From the University of Pisa in Italy, Carlo Matteucci (1818-1868) was a neurophysiologist who developed important work and paved the way for modern electrophysiology by studying animal electricity. In Berlin, Germany, Emil Du Bois-Reymond (1818–1896) was an electrophysiologist who uncovered and established the concept of the AP, introducing the idea that current impulses activated the nerves and were flowed by electrical releases [36][12].
Despite the fact that Reymond and Matteucci's theories and ideas clashed, they were pivotal and are regarded as the founders and fathers of modern electrophysiology because they were the first to record and interpret the biological process of electrical signals sent by frog muscle nerves. However, in 1849, the German physician and physicist, Hermann

Von Helmholtz (1821–1894), was able to verify and accurately acquire the velocity of the electrical impulses during nerve activation [36][12].

A couple of years later, in 1875, a British physiologist named Richard Caton (1842–1926) was the first to observe, with a galvanometer[2], the electrical brain activity of rabbits and monkeys [36][12][37].

In 1890, a polish physiologist from Kraków named Adolf Beck (1863-1942), discovered, with Hermann's galvanometer, that the brain activity from the cerebral cortex of immobilised dogs and rabbits upon sensory stimulation is characterised by desynchronization. Consequently, this was the first study that provided information about evoked potentials since he discovered that the amplitude of the electrical responses to stimulus decreased. In addition, he also concluded that the recorded oscillations were independent of heart and respiration rhythms [37][36].

The findings discovered by Richard Caton became the starting point for the work developed by Berger. Hans Berger (1873-1941), figure 2.7 right side, was the first scientist to report, in 1929, the results of recording the human brain's electrical activity, elektrenkephalogramm[3], using electrodes placed on his own daughter's scalp, figure 2.7 left side [36][12][37].

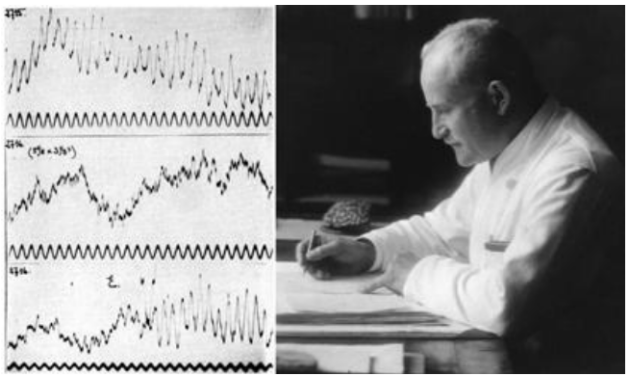

Figure 2.7: Elektrenkephalogramm: the upper trace represents alpha waves, the middle trace represents beta waves, and lower trace represents the sum of the waves (left). Hans Berger (right) (retrieved from [37]).

His research started in 1920, and his findings showed that it was possible to, in a non-invasive way, record the brain activity of humans and study the neural oscillations that describe that signal. He also discovered that the signals varied in amplitude and frequency. Consequently, he characterised the signal with beta and alpha waves and stated that these waves were associated with different mental activities [36][12][37].

Consequently, the contributions provided by Caton, Beck and Berger make them the co-founders of the EEG technique as we know it today, providing crucial information and knowledge used to develop more efficient and accurate brain imaging techniques [37].

[2]Galvometer: device that measure electrical currents [36]

[3]Elektrenkephalogramm: designated by Berger and was then translated to English as Electroencephalogram [37]

2.2.2 Neuroimaging techniques

Monitoring and detecting brain activity abnormalities is crucial for enhancing human life quality since it enables the early diagnosis of various types of diseases [12]. Our brain provides information about the overall functioning and state of the human body, and therefore it is important to access the pros and cons of the different methods used in the medical field to acquire brain data [12].

Although this dissertation focuses on EEG to exam and study brain activity, there are other methods and exams to monitor and detect abnormalities in the brain functioning and structure. For example, Magnetoencephalography (MEG) and functional Magnetic Resonance Imaging (fMRI) are other ways to record brain activity beyond the traditional EEG systems [12].

In terms of clinical exam and how it is performed, EEG showcases various practical advantages over MEG and fMRI. Portability is one of the reasons, as it can be easily transported in a suitcase to different places, such as hospitals and patients homes [22].

Both EEG and MEG present high temporal resolution. However, MEG stands out by combining it with a high spatial resolution. This technique measures the magnetic fields generated by brain electrical activity, and in terms of high frequency brain activity, MEG also performs better results than EEG at detecting frequencies above 60 Hz. Despite the cons, this exam is only performed in specialised rooms, making it stationary and expensive to maintain [22].

At last, fMRI presents poor time resolution and the overall system is expensive. Therefore, is limited in terms of availability and since the basic principle consists in the relation between the blood flow and neural activity, brain abnormalities cannot be detected due to low interference on the amount of oxygenated blood [12][22].

Along with these methods, there is also the Electrocorticography (ECoG) that provides accurate measures of brain activity involving direct electrode placement on the patient's brain (invasive method), described in more detailed in subsubsection 2.2.4.1.

2.2.3 EEG Signal

The voltage fluctuations detected by an EEG are direct reflections of the electrical phenomena of populations of neurons rather than just representing the electrical activity of a single neuron. Therefore, the electrode positioned in the scalp is able to detect relevant information about cortical neural fluctuations of a group of neurons [22][8].

The EEG signal translates the synaptic stimulation during neural activation. The information is propagated along the neuron and when it arrives to the neural junction, this impulse generates synaptic currents responsible for creating a magnetic field that, consequently, generates a secondary electrical field recorded by EEG [12]. Therefore, it translates the sum of the excitatory and inhibitory postsynaptic potentials of populations of neurons firing synchronously with parallel geometric orientation [22].

EEG data is classified as a rhythmic signal, figure 2.8, with consecutive oscillations that

can be described in three main features: frequency, power or phase [22].

Figure 2.8: Main oscillations features (adapted from [22]).

The wave frequency is presented in hertz (Hz) and consists on the number of cycles per second, meaning that a signal with a frequency of 0.2 Hz represents two cycles per 10 seconds. The power corresponds to the square of the oscillation amplitude and it translates the energy of a specific frequency band. Finally, the phase is expressed in radians or degrees and gives information about the location of a certain point in the wave cycle [22]. In order to describe an EEG signal, the waveforms are classified by frequency and, therefore, commonly divided into five major categories ranging from 0.5 Hz to frequencies above 30 Hz. Delta (δ), theta (θ), alpha (α), beta (β) and gamma (γ), are the dominant five brain rhythms, respectively from the lower to the higher frequency band, figure 2.9 [12][8].

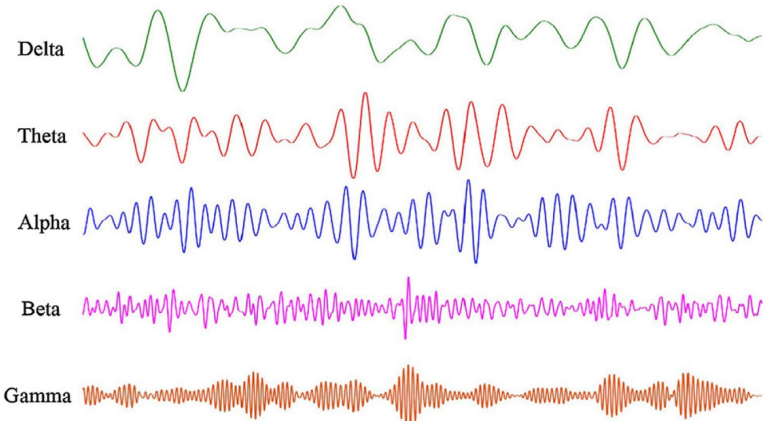

Figure 2.9: Waveforms of five major EEG bands (retrieved from [8]).

The following description of each frequency band is related to general states repeatedly found in multiple studies [12][8], however it should be noted that detailed studies in specific experimental paradigms will often find some of these frequency bands associated with other mental processes [3][38][39].

Delta waves have the lowest frequency range, 0.5 to 4 Hz. Literature correlates this rhythm with deep sleep or waking stages, where the brain is still transitioning to an active and alert level, and also it correlates with anaesthetised patients [12][8].
Theta is located in the frequency range of 4 to 8Hz and is normally associated with relaxation and spiritual stages of deep meditation and is also linked to human creativity [12][8]. When abnormal activity of this brain rhythm is found, it can often be associated with the presence of physical or mental issues [12].
Alpha corresponds to a frequency range of 8–13 Hz. It is noticeable when people are in a relaxed state without being actively concerned and focusing on something, and it is detectable when people are at rest with their eyes closed [12][8].
Beta is characterised by frequencies between 14–26 Hz [12], although it can be also considered in the frequency range of 13 to 30 Hz [8]. This brain rhythm is directly linked to a state where a person is alert and concentrated, meaning that is linked to solving problems and actively being aware of external stimulus. A high-level frequency of this wave is also interconnected to human panic states [12][8].
Therefore, when a person is calm, alpha waves predominate in the cerebral cortex, while beta rhythm gradually decreases as emotional activity rises [8].
Finally, gamma wave corresponds to frequencies above 30 Hz and presents low amplitude, normally lower than 2 μV [8]. This wave appears when a person is in a high alert and actively processing information, normally correlated with tasks that demand high levels of concentration. The presence of low levels of gamma wave patterns is related to brain diseases and dysfunctions [12][8].
Although there have been established intervals that restrict the range of each frequency, it is crucial to emphasise that there are no boundaries that restrict and determines precisely brain rhythms. In literature theta can also be associated with different frequency intervals such as, 3 to 9 Hz or 3 to 7 Hz [22].

2.2.4 EEG Recording System

As aforementioned, EEG presents low spatial resolution and this feature is defined by the low number of electrodes used in data acquisition and the signal attenuation effects caused by the skull and the scalp. Therefore, the number of required electrodes to perform a study is directly affected by the type of analysis intended to be developed [22][10].
Most modern EEG devices have between 24, 32 up to 128 channels. Although more electrodes provide more detailed information, it is important to take into account that when increasing the number of channels, the cost and time also increases with it. Meaning that for quotidian activities, it is often better to have a small number of electrodes. [10].
EEG electrodes can be classified in terms of the selected recording technique. Thus, in literature, there are invasive and non-invasive electrodes. When referring to non-invasive techniques, no surgery is required and, therefore, the electrodes are positioned at the subject's scalp. On the other hand, invasive screening of brain activity implies surgery where the electrodes are placed directly on the patient's brain. The main advantage of this tech-

nique relies on the proximity to the electrical source and the reduction of signal noise [12][22].

Since technology is continuously evolving, scientists are constantly developing and improving traditional methods and devices in order to better comprehend and understand the brain. Some of these innovative methods, including glasses and ear EEG and tattoo electrodes, are described below [40] [41] [42][43].

E-glasses, figure 2.10, are eye glasses with incorporated sensors and electrodes that allow a continuous motorisation of valuable biological, physical and optical human signals and parameters. By recording brain activity, this device can obtain information about the subject's cognitive state. Therefore, this technology can also be used as an application for Human-Machine Interface (HMI) allowing the subject to interact with machines, computer programs (game playing) or other systems [40].

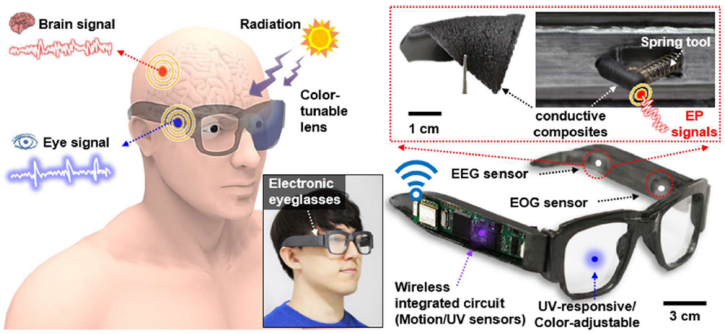

Figure 2.10: 3D printed E-glasses and detailed schematic illustration of the incorporated sensors for monitoring brain activity, eye movement, body movement and UV radiation (adapted from [40]).

These glasses integrate into their frame sensors for EEG and Electrooculogram (EOG) recordings (brain activity and eye movement), for Ultraviolet (UV) radiation, which enables the glasses lenses to change and adapt their color according to the radiation intensity (sunglasses or eyeglasses), accelerometers to track body motions, and a wireless module. Although this innovation has significant potential in a variety of societal sectors, including health, sports, entertainment, and education, there are still many challenges and boundaries that need to be overcome in order to obtain a device that is accurate, comfortable, and at an affordable price [40].

An ear EEG, is a small wearable device placed within the ear canal that records the neural signals from the user's brain. More specifically the In-the-ear (ITE) recording system, figure 2.11, is a earplug for hearing aid with dry electrodes that enable the signal acquisition of the subject's brain activity. This innovative approach proposed in the study [41], when compared to the classic scalp EEG presents various advantages since it is easier, faster, cleaner, and more comfortable for the patient.

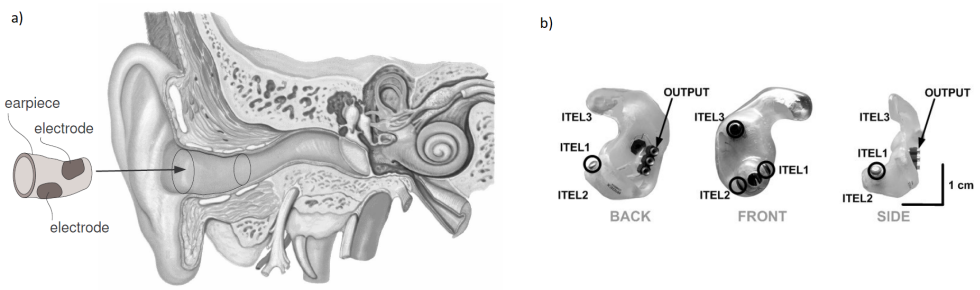

Figure 2.11: ITE system: a) Placement of the earpiece in the right ear; b) Three different perspectives of the left ITE earpiece (ITRL) (adapted from [41]).

Most recent studies on ear EEG systems have focused on enhancing the electrode architecture, on implementing a wireless system to eliminate the need for cables, and assessing the potential of this device in diverse applications such as BCI and sleep monitoring. Therefore, in the study by Tabar and colleagues, the main focus relies on developing an ear EEG recording system that is comfortable for the patient and provides accurate data that leads to reliable diagnosis of sleep disorders [44].

The proposed ear system, figure 2.12, was built with soft silicone and with a custom-made specific EEG amplifier. The results showcase the possibility of it being a good alternative to the Polysomnography (PSG) for sleep studies [44].

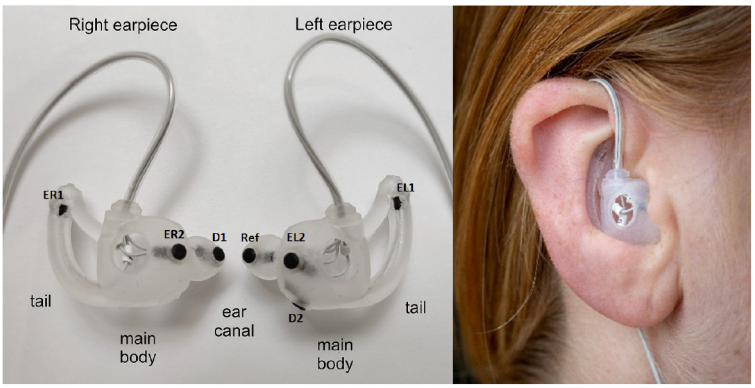

Figure 2.12: Ear EEG, earpieces with the electrodes and the three main parts of the recording system: ear canal, tail, and main body (Electrodes - EL1, EL2, ER1, and Er2: data, D1 and D2 ground, ref: reference) (retrieved from [44]).

The Temporary tattoo electrode (TTE), figure 2.13, consists of a dry cutaneous wearable electrode that is temporarily placed into the patient's scalp. These electrodes are made of conductive materials, such as metals and graphene, that ultimately enable the electrical signals to be detected. When developing these wearable epidermal devices, there are two crucial factors in order to create a compatible skin-tattoo interface: the thickness and the modulus of elasticity. Therefore, the tattoo itself should be thin, and the elasticity should be as close to the skin as possible [43].

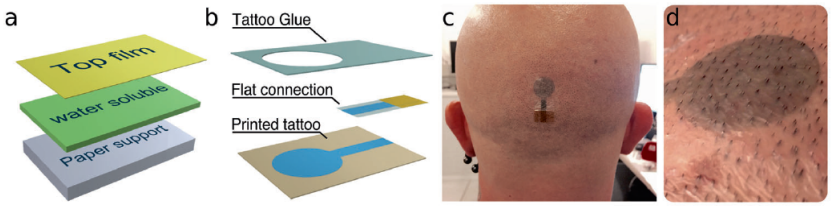

Figure 2.13: Temporary tattoo electrodes: a) layered structure of the TTEs; b) detailed perspective of the fabricated TTEs; c) placement of a tattoo electrode on the scalp (Oz position); d) TTEs after 12h from placement onto patient's scalp (adapted from [43]).

When comparing the signals recorded with the TTE and an Ag/AgCl medical electrode, the results indicated that the tattooed electrode performed better, presenting higher sensitivity. This pioneering approach for measuring brain activity translates into a more comfortable and cleaner way to perform the exam. The probability of causing skin irritation is also smaller, and placing or retrieving them is faster then the scalp EEG. Although this is a new technology, the results are promising and could be used in a variety of ways in the future [43].

2.2.4.1 EEG Electrodes

EEG electrodes are characterised as small metal discs with a conducting surface able to measure the electrical potential difference between each electrode in the recording system and a reference electrode also placed in the subject's scalp [22].
In EEG recordings, impedance refers to the electrical resistance between the electrode and the scalp. Therefore, the presence of high levels of impedance leads to distortions and negatively affects signal analysis. It is commonly measured in ohms (Ω) [12][22].
Consequently, low impedance levels are desired when recording EEG signals. Some of the approaches to minimise these effects are associated with scalp cleanliness, and skin hydration. Ensuring that the surface is hydrated decreases the friction between the two surfaces, minimizing the effects of the electrode-skin impedance [12][22].
The application of a conductive gel between the electrode and the scalp reduces the impedance value, providing better electrical contact. The EEG recording system is responsible for detecting the brain's electrical potential difference between two locations, each electrode and the reference one [22].
The EEG signal is described as multidimensional. Although it can be conceptualized as a two-dimensional signal since the electrical potential changes over time and space, the space feature is measured by each electrode distributed in the scalp. Further analysis can provide more information not only about time and space but also about frequency, power (specific EEG band frequency strength), and phase (position within the wave). This multidimensionality offers numerous and various ways to describe and evaluate the EEG signal [22].
Electrodes, as described above, can record neural activity either at the cerebral cortex level (invasive) or at the patient's scalp (non-invasive). When addressing the invasive mea-

surement of neural activity, the exam is designated by Intracranial Electroencephalography (iEEG) which allow a more in-depth knowledge of the neural activity, specifying the neurons' firing times and locations [12][45].

Consequently, iEEG is a neural activity recording technique performed by electrodes placed directly on the surface of the cortex or more in depth into the cortex tissue with penetrating electrodes. Thus, the difference between the different invasive exams is established by the location of the electrodes [45].

ECoG is classified as a specific type of iEEG were the electrodes are positioned at a more superficial level, directly on the cortex surface. This technique implants strips or grids of circular plate shaped electrodes in the subdural space covering a substantial portion of the cerebral cortex without penetrating it [46][45], figure 2.14.

Furthermore, penetrating or depth electrodes (microelectrodes), characterized by their cylinder shape, are also a specific type of iEEG were the implant occurs in a deeper region of the cerebral cortex, allowing a more in depth knowledge about the spikes or AP (firing of individual neurons) and the Local Field Potential (LFP) (activity of a population of neurons) [46][45], figure 2.14.

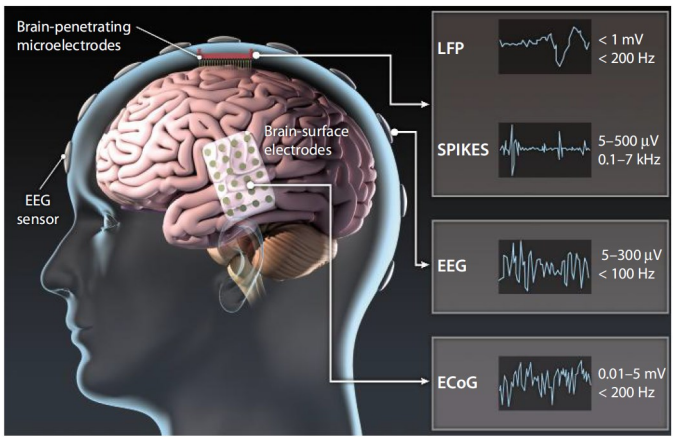

Figure 2.14: Neural measurements techniques and signal properties of EEG, ECoG and penetrating electrodes (retrieved from [46]).

Compared to the non-invasive EEG, both ECoG and depth electrodes have higher temporal and spatial resolutions. However, there are slight differences between them. Since the microelectrodes are located more deeply in the cortex, this technique possesses higher temporal resolution when compared to the ECoG. In contrast, the ECoG has higher spatial resolution, since the electrodes located in the cortex cover a larger surface area, allowing more detailed and accurate information about the localization of neural activity [46][45].

Normally, the non-invasive electrodes can be segmented into 3 categories: dry, wet, and semi-wet [1][2], figure 2.15.

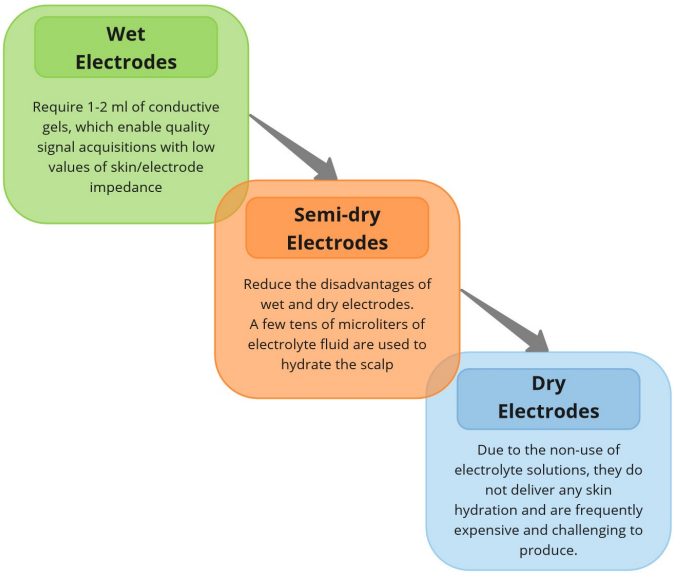

Figure 2.15: Type of electrodes: wet, semi-dry and dry.

To some extent, semi-dry electrodes are considered a new generation, with the primary goal of filling the gap between conventional wet and dry electrodes, preserving their benefits while minimising their disadvantages. These rely on a few tens of microliters of electrolyte fluid to hydrate the scalp, which is significantly less than the volume of conductive gel, 1-2 ml, utilised for wet electrodes [1].

Since the amount of skin hydration is directly connected to the impedance levels, wet electrodes are the most commonly used in the medical field due to low and consistent values of electrode and skin impedances, which produce high-quality recordings. On the opposite end, the dry electrodes, as their name implies, avoid using any kind of gel or moisture, providing a dry and dehydrated environment to record the EEG signals. However their application is simple and easy [1][2].

The wet setup typically includes electrolyte fluids (conductive gels or pastes) and reference electrodes (Ag/AgCl), usually made of silver (Ag) and Silver Chloride (AgCl). This environment is referred to as gel-based electrode. Conductive gels are typically composed of chloride ions (Cl^-) since the electrolyte and electrode must contain the same ion in order to provide a stable environment between the interface electrode and skin, ensuring that the impedance values are below the reference value of 5.0 kΩ[1][2].

Although wet electrodes are the most widely used and considered the best option for good quality signal acquisitions, they have disadvantages. The patient's preparation before initiating the recording itself is time-consuming and involves trained professionals. The application of gels and pastes on the scalp can cause some itchiness, leading to patient discomfort during the exam, and since they dry over time, it is necessary to wash the hair after performing the EEG. Additionally, the abrasive nature of the conductive electrolyte can cause undesired allergic reactions. These drawbacks limit the application of wet electrodes [1][2].

Semi-dry electrodes open the door to a finer but not perfect solution, where the idea is to

combine the setup practicality of the dry electrodes with the high-quality acquisitions of the wet ones [1].

In essence, the ultimate goal is to develop dry electrodes that combine all the previously described advantages in order to achieve a system that is practical, simple, comfortable and performs well during acquisitions [2].

There are several different types of electrodes with different shapes, sizes, and forms available for use when recording an EEG [12].

2.2.4.2 Electrode Positioning

Since EEG signal processing and analysis is a relevant research area with important relevance in the medical field, and in order for researchers to study, compare and discuss the same results, arose the need to regulate and develop a standard procedure to define the location and placement of electrodes at the patient's scalp.

Consequently, the International Federation of Societies for Electroencephalography and Clinical Neurophysiology proposed an electrode topographical placement for 21 electrodes referred to as the 10-20 system in 1958 [47]. The numbers 10 and 20 represent the approximate distances that occur between neighbour electrodes taking into account certain anatomic landmarks, meaning that in this system the distance between the electrodes is either 10% or 20% of the total distance [48] [12].

The 10-20 system, figure 2.16, uses left A1 and right A2 earlobe electrodes as reference, and the remain electrodes are designated according to their location, meaning that F, C, T, P, O correspond, respectively, to the frontal, central (central line of the brain), temporal, parietal and occipital brain regions. Therefore, electrodes that combine various letters are located between these 5 main regions. The odd numbers indicate the left side of the brain and, consequently, the even numbers the right side [48][12].

Afterwards and in order to obtain more spatial resolution the American Clinical Neurophysiology Society and the International Federation of Clinical Neurophysiology proposed the 10-10 system that results from applying specific modifications to the 10-20 standard [48], figure 2.16.

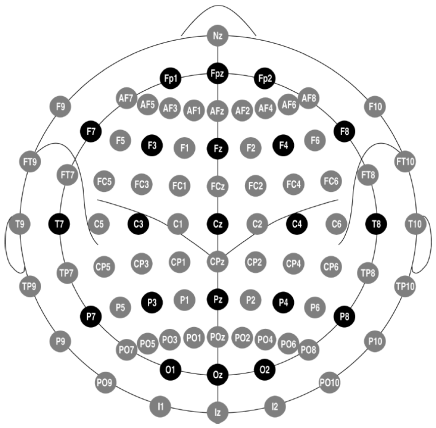

Figure 2.16: Electrode positions and labels. Black circles represent the positions from the 10-20 system and grey circles represent the positions from the 10-10 system (retrieved from [49]).

When comparing both standards, the 10-20 system is better suited for clinical usage and routine exams, providing more efficiency. On the other hand, the 10-10 system is more suitable for studies where more detailed data is required, such as in patients with epileptic seizures, as it allows a higher density of electrodes in the scalp [48].
Although a deviation of the 10-10 system has been proposed in literature, the American Clinical Neurophysiology Society and the International Federation of Clinical Neurophysiology have not recognised the 10-5 system as an official standard [48].

2.2.5 EEG Limitations

Although EEG possesses many advantages and is often used in literature to evaluate brain activity, it also has some drawbacks. Depending on the main focus of the research work and the hypotheses intended to be studied, the EEG recordings may not be the most suitable and insightful method to answer the research questions.
The first limitation lies in the poor spatial resolution provided by this method. EEG is unable to measure with precision the neural activity from deep brain structures, since the electrodes are located on the brain surface, making it difficult to understand the signal origin. Thus, the activity can be either from the cortex or deeper regions [22].

2.3 EEG Signal Processing

Due to the complexity of the EEG signal provided by the high quantity of nonlinear data and the high volume of randomness, it is fundamental to implement advanced tools in order to process the signal and achieve the best possible balance between data and noise. Subsequently, these signal processing techniques allow the identification of brain rhythms [11].
Consequently, to obtain clean data that accurately translates the neural activity of a population of neurons without losing important information, it is essential to apply the correct

and most suitable pre-processing techniques according to the main objectives of the study in development [11].

2.3.1 Analysis Architecture

Analyzing brain activity, identifying brain rhythms, and developing accurate prediction models are powerful tools that can diagnose and improve the neural conditions of individuals with impairments. In various EEG research studies, this process is commonly segmented into 5 stages: signal acquisition, pre-processing, feature extraction, feature selection and classification [11] [50], described in figure 2.17.

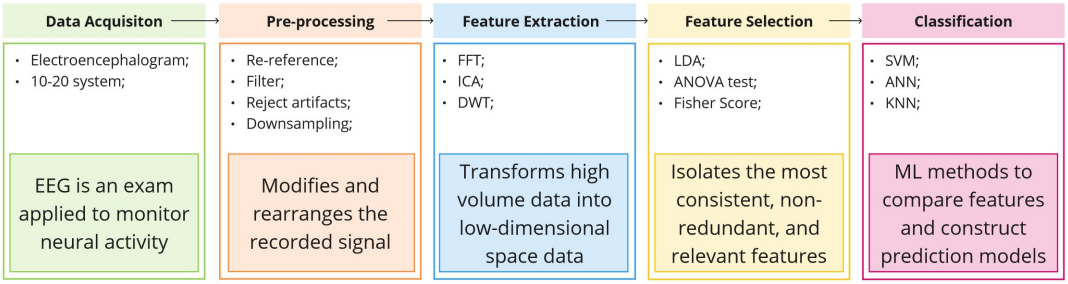

Figure 2.17: EEG signal processing pipeline.

Data acquisition can vary in terms of the selected method (non-invasive or invasive) and in the number of electrodes used to record the signal, which are commonly positioned according to the 10-20 system [11]. Thereafter, pre-processing is crucial to eliminate artifacts from the signal and create epochs that facilitate the analysis. This stage is described in sub-subsection 2.3.2.

The feature extraction step is responsible for transforming the high volume set of EEG data into a low-dimensional space signal. By reducing the size of the data and removing redundant information, this step increases the accuracy and performance of the models while also increasing the learning speed. Creating features allows the preservation of the original signal's key and crucial characteristics, while improving the processing performance [11][51].

The feature selection process chooses the features that are more relevant. Thus, focusing on the most important variables leads to better training and more accurate models that are able to predict and anticipate specific events with precision [51].

Finally, the last step focuses on training machine learning algorithms, with the selected data, in order to develop models that can identify specific neural patterns within the different experimental conditions [11][51].

2.3.2 Pre-processing

Pre-processing is an important step that occurs after data acquisition and right before data analysis, meaning it is responsible for modifying and rearrange the raw signal to facilitate its analysis [51].

The pre-processing stage can be characterised by two different approaches: the first one focuses on simply organising the data for easier observation without changing the signal itself, for example by extracting epochs. The second approach focuses on rejecting and altering bad data that is inevitably interfering with the signal analysis. Thus the main goal is to exclude artifacts and bad electrodes and apply filters while still preserving the vital signal [22].
In general, the ultimate goal is to improve data quality for correct analysis. Upholding the premise that no matter how sophisticated the pre-processing techniques employed are, they are useless if they start with faulty data. In other words, no methodology can substitute good data [22].
This cleaning process is crucial due to the presence of artifacts in the recorded EEG signal that contaminate the information. The main artifacts that interfere with EEG data can be classified into two categories: physiologic and system artifacts [12][51][52].
Physiological artifacts or intrinsic are determined by the patient's behaviour which ultimately interferes with the recorded data set. The noise is related to muscle movements, eye blinking process, breathing, sweating and heartbeat. On other hand, system artifacts or extrinsic are associated with the electronic equipment used to record the signal. Therefore, these interferences occur due to cable or connection faults, impedance variations of the scalp's electrodes, among others. The power supply frequency is also one of the main artifacts, varying between 50 and 60 Hz depending on the country [12][51][52].
According to the literature, there are various different approaches and steps that can be taken in order to achieve a good pre-processing stage to efficiently clean the data from the previously described artifacts. As a result, the figure 2.18 outlines some of the procedures that are frequently used in the literature to ensure an effective signal pre-processing, removing unnecessary data for further coherent analysis [22][51][52].

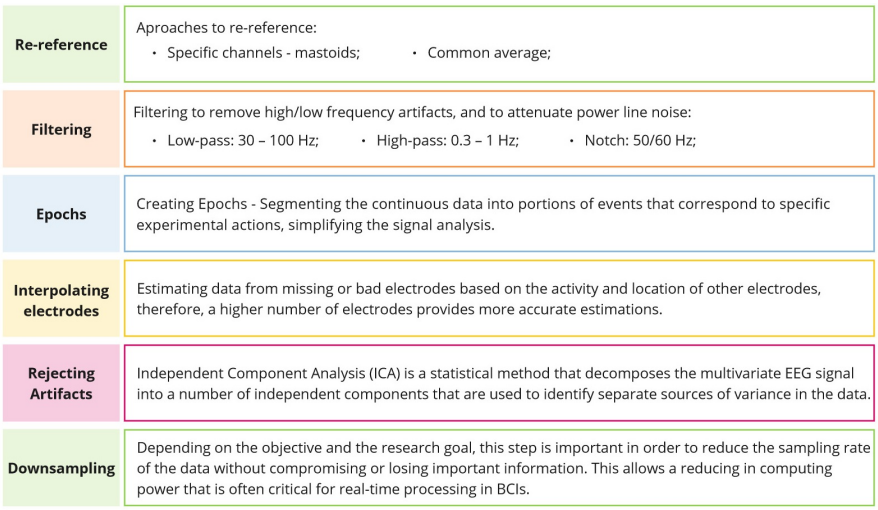

Figure 2.18: Fundamental pre-processing steps.

Re-referencing the data is a common procedure that consists on selecting a reference value that allows all electrodes to be compared to an equal point, therefore eliminating the

common noise of all recorded electrode signals, resulting on a linear transformation of the signal. There are two main approaches to this stage: the re-reference value results from the average of all electrodes, or the re-reference is associated to a specific EEG channel located in the earlobes or the mastoid bone [22][52].

Filtering the data is crucial to remove low- and high-frequency artifacts thtough the application of High-pass Filter (HPF), Low-pass Filter (LPF), band-pass and band-stop filters, as well as notch filters at 50Hz or 60Hz to attenuate the interference from the electrical line noise [22][52], figure 2.19.

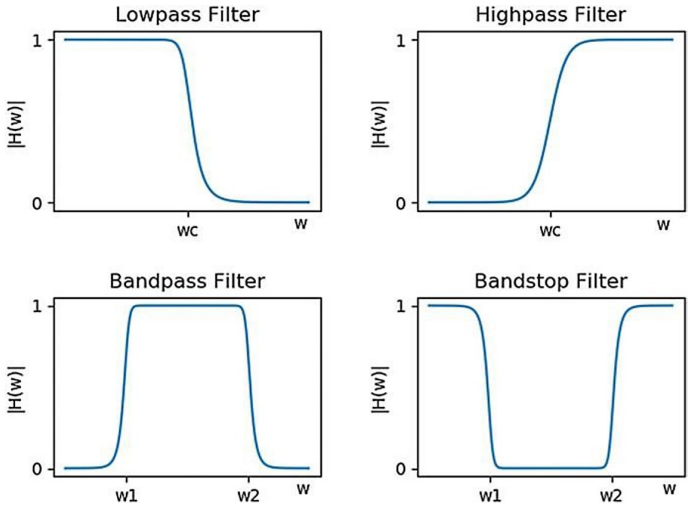

Figure 2.19: Types of filters: low-pass, high-pass, band-pass, and band-stop (retrieved from [52]).

Creating **epochs** designates the process of creating smaller segments of data when compared to the original EEG data, this segmentation is according to specific events that occurred during the experimental activity [22].

When analyzing the signal characteristics, the EEG signal is described as a two-dimensional matrix representing the number of electrodes and the signal over time. After segmenting and creating the epochs, the signal is now represented by a three-dimensional matrix representing electrodes, time, and the number of trials [22].

Interpolating electrodes refers to the process where algorithms are implemented in order to estimate data from bad (noise is substantially higher when compared to the neural signal) or missing (EEG signal is non-existent) electrodes, taking into account the EEG data from the surrounding electrodes. However, since it could affect the analysis, this approach should always be carefully considered. An alternative to this consists of omitting these from the data [22].

Blind Source Separation (BSS) is a widely used method based on the principle that the various signals (image, audio, and electrical) recorded by different channels correspond to a combination of different signals. This BSS technique uses mathematical algorithms to calculate the signal's statistically independent source components, separating a multivariate signal into its individual constituents [53][54][12], figure 2.20.

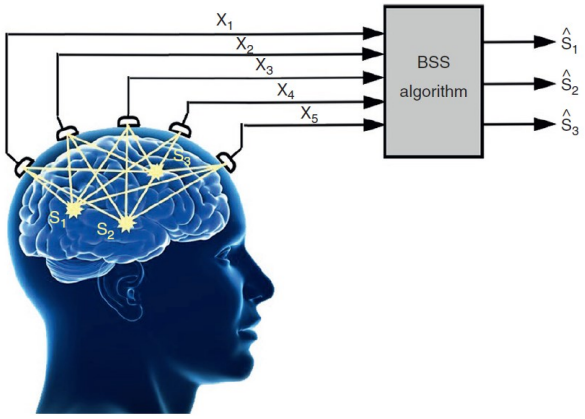

Figure 2.20: BSS basic concept (retrieved from [12]).

The most common algorithm of BSS is Independent Component Analysis (ICA), though in literature, the Principal Component Analysis (PCA) and Canonical Correlation Analysis (CCA) algorithms are also used to, correspondingly, reduce the dimension of the original recorded dataset and find the maximum correlation between two different variables in order to interpret their relationship, for example, the correlation between the EEG signal and visual stimulus [53][54].

ICA is commonly used for **Rejecting Artifacts** since it separates the complex EEG signal into different sources, including either brain activity or extracting the independent components related to artifacts such as muscle movement, eye blinking, heart rate, or external electrical interference. In this method the basic principle considers that components are independent form each other and must be non-Gaussian [53][54][55].

In a more detailed way, figure 2.21 showcases the ICA algorithm. The variable s represents the source signals $(s_1, ..., s_p)$ where p is the number of source signals, A represents the mixing matrix $(a_1 1, ..., a_n p)$ where n is the number of channels, x represents the recorded signals $(x_1, ..., x_n)$ and $\hat{s}$ represents the estimation of the original sources $(\hat{s}_1, ..., \hat{s}_n)$ [55][12].

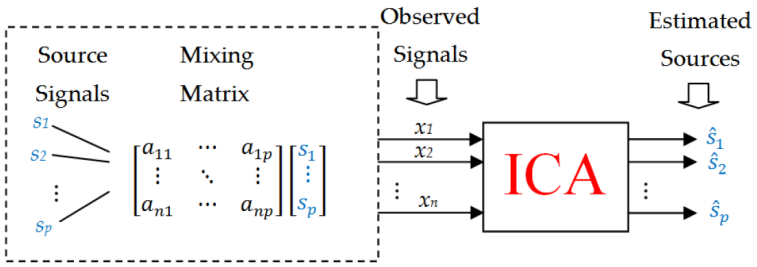

Figure 2.21: Diagram of ICA algorithm (retrieved from [55]).

According to the diagram, the recorded signals assume the form of equation 2.1 [55][12].

$$x = As \quad (2.1)$$

In order to obtain a version of the original sources ($\hat{s}$), ICA multiplies the original data (equation 2.1) by an unmixing matrix (W). Consequently, the signal separation into source versions is performed according to equation 2.2 [55][12].

$$\hat{s} = Wx <=> \hat{s} = WAs \quad (2.2)$$

Overall, ICA has a wide application range being used for data pre-processing stage with artifact rejection and for feature extraction (time-domain)[53].

Downsampling is another pre-processing step that translates the process of decreasing the sample rate of the recorded data without losing critical information. The degree of reduction of the sample size depends on the analysis that is intended to be done. Nevertheless, this step allows a dimensional reduction of data that results in lower computation time and storage space required to process the EEG data [22][51].

2.3.3 Feature extraction & Feature selection

The process of extracting features from the signal provides a vector with the most significant characteristics, which is used as the input to train and develop classification models [56].

In this stage, the EEG signal can be analysed in four different domains: time, frequency, time-frequency and spatial-time-frequency [11][51].

Each domain and, consequently, each feature extraction method has it advantages and disadvantages. Therefore, the suited approach depends on the main objective of the work and the information intended to be analysed [11].

Figure 2.22 shows a scheme with some of the most common feature extraction methods applied in the biomedical field to analyze and classify EEG signals [11][51].

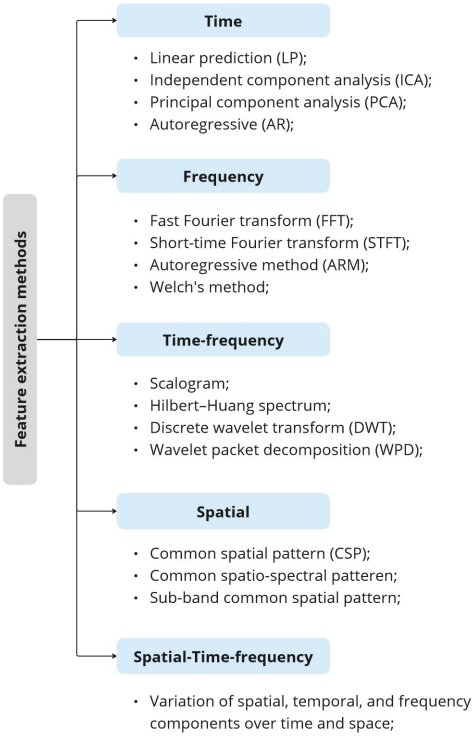

Figure 2.22: Feature extraction methods in different domains.

Features are properties and characteristics retrieved from data in order to study their behaviour. Therefore, these features can be retrieved from the raw signal itself, from the pre-processed signal, or after transforming the signal by applying some of the methods demonstrated in the scheme of figure 2.22 for a more deeper analysis [51].

These features, figure 2.23, can be divided into four different categories: statistical, spectral, non-linear and functional connectivity based [51].

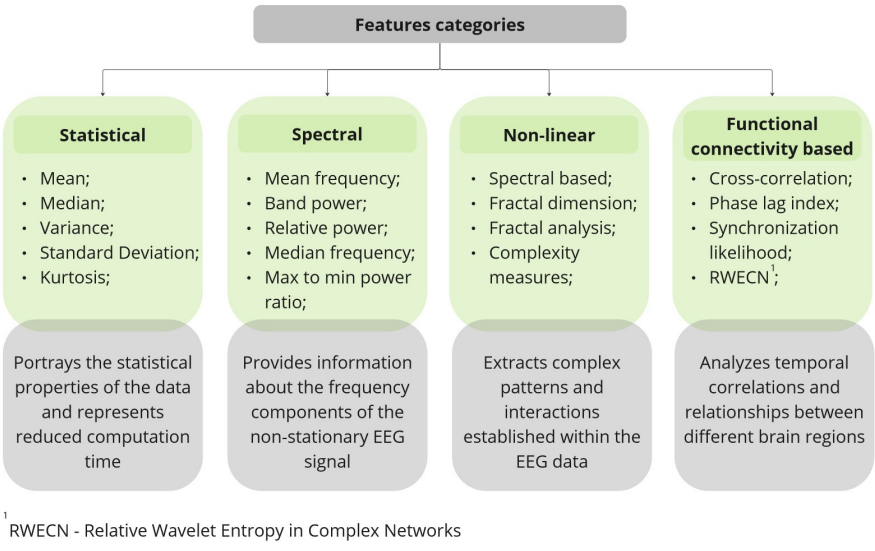

Figure 2.23: Different feature categories.

Feature selection is a relevant stage that allows a reduction of the time required to train the models, since it allows a selection of the most relevant features, optimizing the results. In order to reduce the size of the original feature dataset, various types of methods, such as student t-test, correlation-based method, Analysis of Variance (ANOVA) test, and genetic algorithm, can be selected to perform this stage [51].
Regarding the various feature extracting techniques presented in this section, this work emphasizes the study of the Welch's method (frequency domain) and the Wavelet Transform (WT) (time-frequency domain).

2.3.3.1 Welch's method

Literature showcases several different methods to calculate the Power Spectral Density (PSD) of the EEG signal, and one of the most common approaches is Welch's method. Fast Fourier Transform (FFT) is also another method that is frequently used to estimate the PSD [57].
Firstly, before understanding the Welch algorithm, PSD is a fundamental concept in signal processing, since it offers information about the signal's power distribution in the frequency domain. This is an important step in finding the dominant frequency components and compare the relative power in different frequency bands, such as, theta, delta, alpha, beta and gamma [57].
Welch's method implies the signal division into several overlapping segments, usually with an overlap of 50%. Afterwards, a smooth window function is applied to each data segment. One of the most commonly used is the Hamming window, and this process is crucial since it prevents spectral leakage [57], figure 2.24.

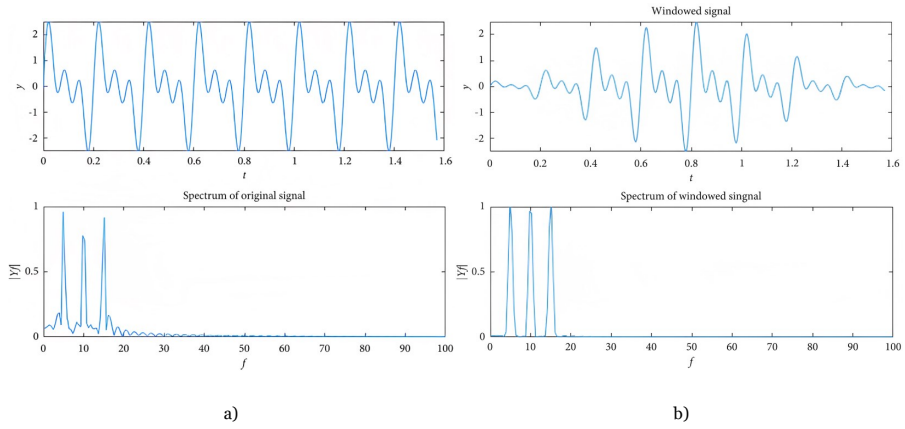

Figure 2.24: Hamming window: a) Original signal and the spectrum leakage; b) windowed signal with reduced spectral leakage (adapted from [57]).

The third step involves applying to each segment the Fourier transform. Afterwards, the fourth step involves computing the periodogram, meaning that for each segment in the frequency domain, the power spectrum is calculated. The power spectrum corresponds

to the squared magnitude of the previously calculated Fourier transform. Finally, the PSD results in averaging the previously calculated periodograms [57].

2.3.3.2 Wavelet Transform

The WT is a widely used time-frequency domain method applied to EEG signals, since it is a suitable approach to decompose the non-stationary data into its frequency components. A wavelet, by definition, is considered a short wave that is capable of representing both time and frequency characteristics of the signal [58][59].

The WT can be applied into two main forms, Continuous Wavelet Transform (CWT) and Discrete Wavelet Transform (DWT). In parallel, there are several different types of wavelets such as daubechies, haar, and symlets, among others [60].

The DWT is used to decompose and extract from the signal the corresponding EEG frequency bands of interest, representing the time-frequency domains according to the approximation coefficients (Ax) and the detail (Dx) coefficients, where the letter x corresponds to the decompose level of the coefficients [59][61].

Implementing a DWT involves applying a HPF and a LPF to the input signal. The first level output from the LPF corresponds to the approximation coefficient A1, and the HPF generates the D1 detailed coefficient. Consequently, the approximation coefficient (A1) can be further decomposed into the level 2 approximation and detail coefficients. Through each level of signal decomposition, the frequency resolution increases due to filtering, while the time resolution decreases given the downsampling by half of the signal due to Nyquist rule [58][59].

By decomposing the signal into different levels, specific wavelet coefficients translate the EEG frequency bands of interest, delta (1-4 Hz), theta (4-8 Hz), alpha (8-115 Hz), beta (15-30 Hz), and gamma (30-60 Hz) [61][58].

2.3.4 Classification

The concept of Machine Learning (ML) describes the ability of certain algorithms to learn and recognize specific patterns in a training set and associate this input with a certain outcome [56].

The methods of ML employed in EEG signal classification are described. In terms of classification, there are four approaches: supervised, unsupervised, deep, and, the less common type, reinforcement learning [11][50], figure 2.25.

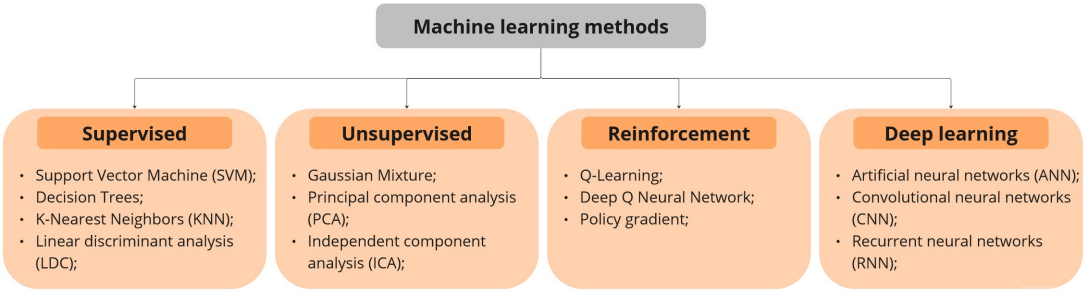

Figure 2.25: Machine learning methods to classify EEG signals.

Deep Learning (DL) is considered a subfield of ML algorithms, since it is focused on the application of Artificial Neural Network (ANN). DL is a specific field associated with higher and more complex datasets. Consequently, in this scenario, literature showcases that ANN provide better performances when compared to other machine learning methods, outperforming them in applications such as, image, video and audio classification [56][11].

Regarding the various different classification techniques presented in this section, this work emphasizes the study of four different classifiers, namely, Support Vector Machine (SVM), K-Nearest Neighbors (KNN),Linear Discriminant Analysis (LDA) and ANN.

2.3.4.1 SVM

SVM is a supervised learning machine method that is used for both regression and classification problems and can be divided into linear and non-linear approaches representing, accordingly, simple models and more complex ones with higher computational costs [54][61].

When training the model, this algorithm creates a separation hyperplane, figure 2.26, to separate the two different input classes into the appropriate category. The data points nearest to the hyperplane are designated by support vectors, and the classification process is based on the mapping of the new input data point, analyzing which side it falls on, meaning that the model evaluates on which side of the hyperplane the value is located, attributing the corresponding class according to the side [54][61].

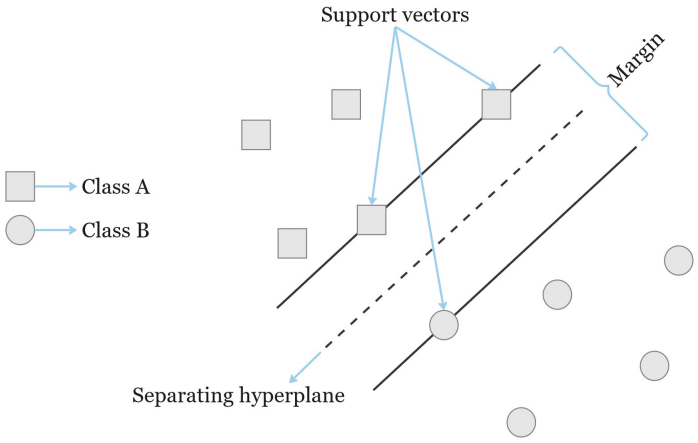

Figure 2.26: SVM architecture.

Although SVM is by default a binary classifier, it can be extended to multiclass problems [61].

2.3.4.2 KNN

KNN is a non-parametric supervised algorithm and is considered a simple machine learning model that classifies different objects based on their k-closest neighbors. Therefore, for a new data point, this model determines the class by calculating the majority of the neighbors class labels, figure 2.27. The letter ”k” identifies the number of chosen neighbors, and consequently, the selected value plays an important part in the model’s performance [62][61].

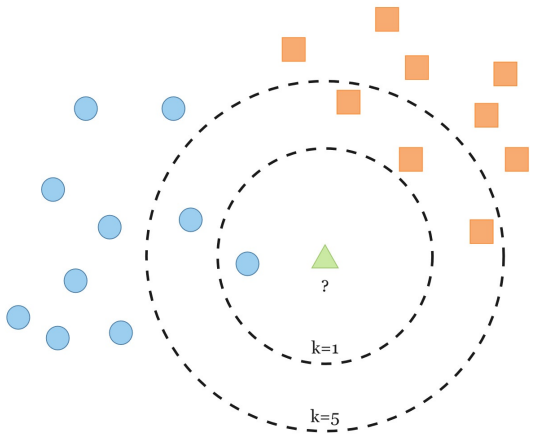

Figure 2.27: KNN model architecture.

Normally, the k is represented by a small positive integer number, and usually odd numbers are selected since they help avoid ties, but it depends on the classification problem. Models with higher accuracy are associated with smaller numbers of k, meaning, if k = 3, the class is attributed based on the three nearest neighbors [62].
A more in-depth analysis about the KNN model and its variants is given in [62].

2.3.4.3 LDA

LDA is classified as a linear technique that uses, like the SVM model, a hyperplane to separate the different classes and classify the input data values. This algorithm is based on the premise that the variance within each class is identical, meaning the covariance of the classes is equal. The main goal of this model is to reduce the input value space while maximizing the separation between classes in the data [61][53].

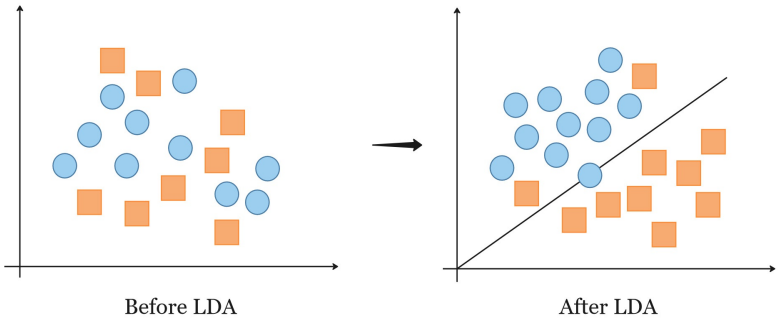

Figure 2.28: LDA model architecture.

One of the advantages of this classifier is its lower computational cost. Although it has been a common approach to classify EEG signal, this technique has some disadvantages, for example, the linear nature of the model used in classification problems of a non-linear signal [53].

2.3.4.4 ANN

ANN, as previously mentioned, is widely used for classification and regression problems which involve large datasets of data. The model itself and the structure is inspired by the functioning of the human brain, more specifically, how the neurons communicate between them [61][54].

Taking a closer look into the deep learning algorithms, there are different architectures in neural networks. For instance, when the information travels in only one direction, these networks are designated as forward neural networks and can be divided into Single-layered Feed-forward Neural Network (SFNN) and Multilayered Feed-forward Neural Network (MFNN). The SFNN is the simplest form of feed-forward networks, and the output layer is fully connected to the input one [54].

In contracts, the MFNN possesses hidden layers between the input and the output. In addition, Recurrent Neural Networks (RNN) have an architecture that allows the output to be connected to the input since it forms a direct cycle that allows the information to persist and establishes a feedback loop between the output and input neurons [54].

The neural network structure is represented by input, hidden, and output layers, figure 2.29. The number of input neurons depends directly on the number of input features (features vector). The hidden layer is composed of neurons and a sigmoid transfer function. Finally, the number of output nodes depends on the number of target classes [61][54][63].

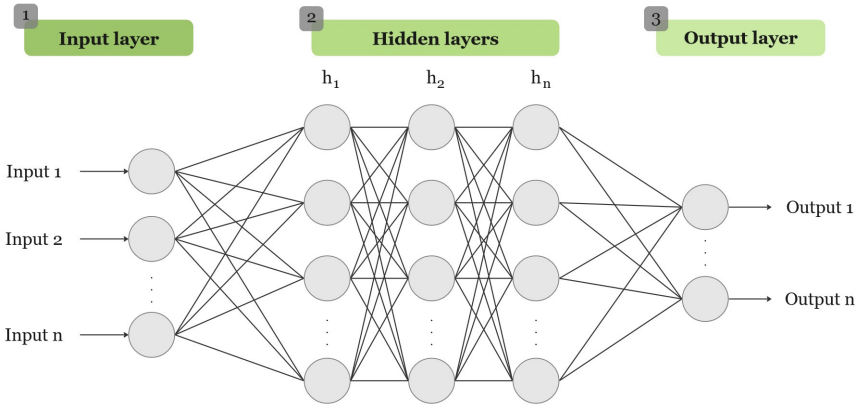

Figure 2.29: ANN architecture.

The basic unit of ANN is the artificial neuron also designated as perceptron (neural network unit). The basic functioning of these units consists on input values that are multiplied by a certain and specific weight. Afterwards, these values are summed and this weighted sum is then passed to an activation function [63].
The activation function, equation 2.3 (where $\sigma(z)$ is the sigmoid function, z is the input, and e is the Euler's number), controls the output since it is responsible for concluding if the weighted sum value is smaller or bigger than the threshold value. Consequently, the output is estimated based on the sum of inputs' weights when compared to the threshold value, for example, in a binary classification if the threshold value is 0.5 and the weighted sum is 0.8 the output is 1 [63].

$$\sigma(z) = \frac{1}{1 + e^{-z}} \quad (2.3)$$

2.4 Studies on exoskeletons, EEG, and tactile discrimination

This section of the essay provides some articles present in the literature that are connected, in certain ways, to the theme proposed in this work. A succinct summary of each article is provided in light of their individual similarities to this theme.

2.4.1 Pavements on Interjoint Coordination

The first selected article studies show healthy individuals, with and without an exoskeleton, coordinate their joints while walking on common ground pavements. Thus, the main goal is to comprehend the main effects of different pavements on interjoint coordination and how it can vary between wearing an exoskeleton and walking without it [64].
The experimental activity described in [64] selects different types of pavement, recruits eight healthy volunteers, and uses an exoskeleton. Consequently, it exhibits certain simi-

larities when compared to the proposed theme in this study.

In order to investigate the knee-ankle and hip-knee coordination, each individual was instructed to walk on five different types of pavements: tiled, carpeted, wooden, concrete, and pebbled, with and without the AIDER exoskeleton [64], as demonstrated by figure 2.30.

According to this study's findings, the pavement's irregularity and the compression capacity have the greatest effects and influences on interjoint coordination. As a result, this article provides more detailed information about joint movement and its kinematics, providing useful knowledge in order to develop more efficient exoskeletons capable of adapting to different pavements aimed at the rehabilitation field [64].

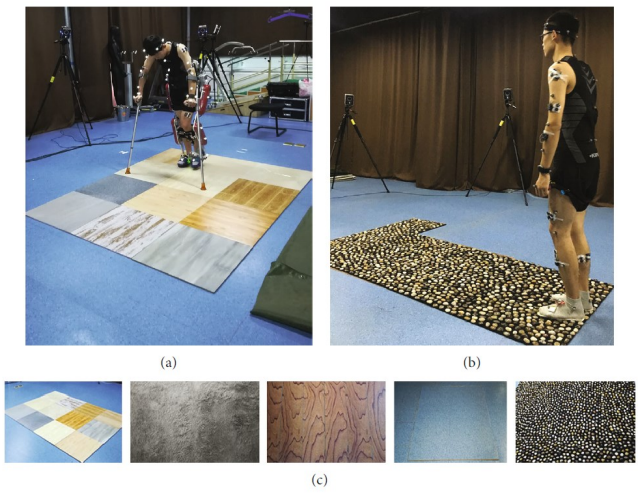

Figure 2.30: Experimental activity: a) Patient walking with exoskeleton on tile floor; b) Patient walking without exoskeleton on pebbled floor; c) 5 experimental pavements (adapted from [64]).

2.4.2 Neuromuscular Plasticity

In [65] the authors also use an exoskeleton, but in this specific case the main goal is to examine the short-term neuromuscular plasticity induced after a training session using the robotic wearable device.

In order to address this hypothesis, the study selected stroke survivors, used the EKSO GT exoskeleton and the brain activity was recorded by EEG, in order to, subsequently comprehend the impact of the device on brain plasticity. In addition, more physiological data was recorded by using EMG[4] sensors and IMUs[5], figure 2.31 [65].

[4]Electromyography (EMG) used to measure muscular activity [65].
[5]Inertial Measurement Unit (IMU) used to record kinematic data [65].

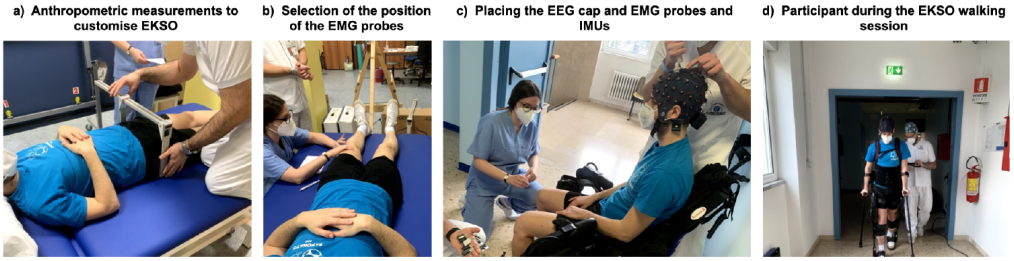

Figure 2.31: Subject experimental preparation: a) anthropometric measurements; b) Position selection for EMG probes c) EEG cap, EMG sensors and IMUs placement; d) EKSO walking session (retrieved from [65]).

After a single training session this article provided evidence of short-term neuromuscular plasticity induced by the wearable robotic device, showcasing the positive impact this type of technology has on the treatment process when compared to conventional types of therapy [65].

Since the article uses EEG to assess neural activity during exoskeleton use, it also has some similarities to the theme of this dissertation.

2.4.3 Surface Roughness Classification

The three studies that follow are relevant to the proposed work in the sense that they analyse the correlation between brain activity and the different surface roughnesses. Although a certain degree of resemblance is encountered, the main goal of the article [66] is to develop and compare machine learning models capable of performing surface roughness classification.

Ultimately, the main objective of [66], is to understand to what extent the brain is able to distinguish with efficiency different degrees of roughness.

The experimental setup consisted on a revolving wheel that contained three surfaces with distinct levels of roughness, from the smoothest to the most rough, as described in figure 2.32. This mechatronic system allowed participants to touch each surface with the index fingers, while recording the brain activity [66].

Consequently, the recorded EEG data was used to develop a model based on convolutional neural networks (CNN) designated by TactileNet, capable of classifying different surface roughness with a 95.67% of accuracy [66].

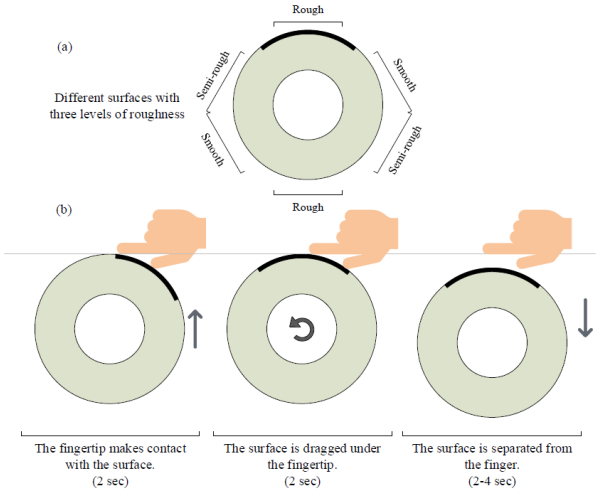

Figure 2.32: Experimental setup: a) Rotating plate with different surfaces; b) Experimental protocol of touching a surface (retrieved from [66]).

The [67] authors applied an identical mechanical system to implement the experimental activity, and the setup is also similar to the previously described study, figure 2.33. Although they possess a certain degree of resemblance, this article focused on comparing four different models to classify surface roughness.

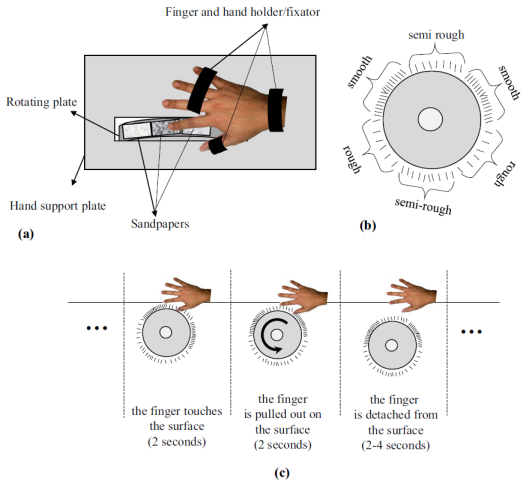

Figure 2.33: Experimental setup: a) Rotating plate and hand fixator; b) Rotating plate with different surfaces; c) Duration of touching a surface (retrieved from [67]).

The selected models were K-nearest neighbors (KNN), support vector machine (SVM), linear discriminant analysis (LDA) and artificial neural network (ANN). This study concluded that the EEG signal varied according to the hand that touched the various surfaces, and by comparing the classifiers performances, the LDA presented the best accuracy, reaching the value of 93% [67].
Additionally, [68] proposed a compact convolutional neural network (CNN) model, EEG-Net which presented an accuracy of 70% in the process of distinguish between three levels

of roughness.
The experimental setup, unlike the two previous articles, included visual stimulus provided by the computer screen located in front of the subject, figure 2.34.

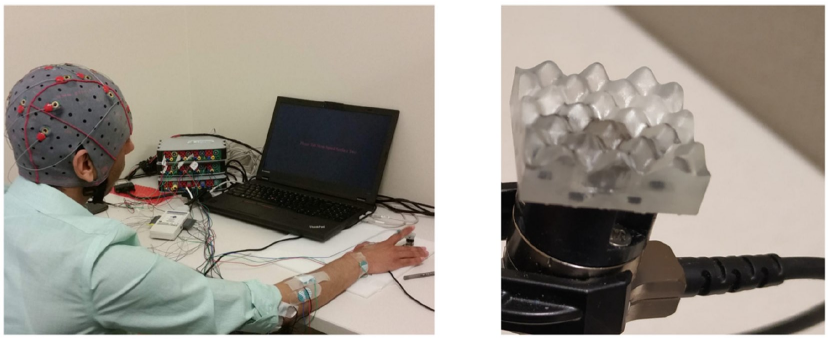

(a) (b)

Figure 2.34: Experimental activity: a) Experimental setup; b) 3D printed surface (retrieved from [68]).

At a global perspective, these three articles [66][67][68] share a common ultimate goal that is related to the proposed work: the development of EEG systems that can provide surface perception. In order to enhance this technology, more knowledge regarding neural activity and its correlation with textured surfaces must be produced.

Chapter 3

Methodology & Processing

This chapter describes the experimental study design conducted in this work. Therefore, the required steps to perform the exoskeleton trial and the EEG signal acquisition are addressed. In section 3.2 the selected approach to perform the EEG signal analysis is presented.
This study is segmented into six main parts as demonstrated in figure 3.1, and each of these steps are described in this chapter.

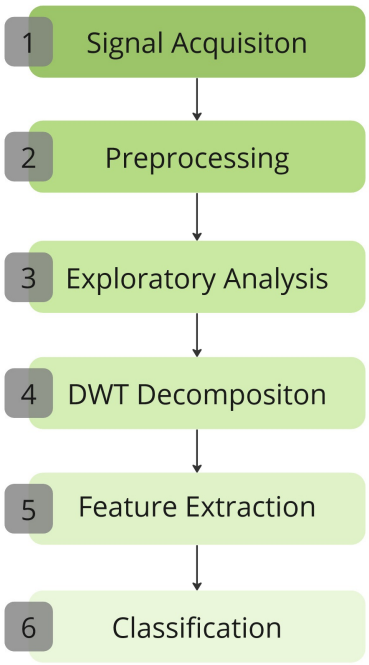

Figure 3.1: Workflow involved in this study.

3.1 Signal Acquisition

This section lists the systematic set of procedures applied in this research in terms of required materials, experimental protocol, and recording environment, in order to obtain the desired signals.

3.1.1 Participants

This study, from a total of six participants, recruited the results from three participants (all females), with ages between 19 and 22 years old. Three of the initial subjects were not included in the study due to problems with the exoskeleton (n = 2) and problems with the

EEG signal (n = 1). The recruited subjects were healthy individuals without any motor impairments, able to wear and support the weight of the exoskeleton, and fit within the manufacturer's measurements specifications related to height and weight, thus fulfilling all the requirements for this study, based on the inclusion and exclusion criteria, detailed in tables 3.1 and 3.2.

Table 3.1: Recruitment - Inclusion guidelines.

Inclusion Criteria (IC)	Description
IC 1	Height: 1.50 - 1.90 meters; Weight: 49 - 102 kg
IC 2	Able to naturally perform the experimental movements
IC 3	Able to support the exoskeleton's weight without pain

Table 3.2: Recruitment - Exclusion guidelines.

Exclusion Criteria (EC)	Description
EC 1	Individuals under 18 years old
EC 2	Individuals with physical impairments

Neural activity was collected at the Catholic University of Portugal in Porto between November 2022 and March 2023 in a total of 4 sessions, which resulted in 3 EEG signals with sufficient quality for subsequent analysis.
All the subjects involved in this study signed a consent form, and the experimental procedure was previously explained in detail. The present study was approved by the committee of the Catholic University of Portugal in Porto (Committee for Health Sciences of the Universidade Católica Portuguesa - 99/2022). Additionally, all the participants included in this study agreed that their image could be used.

3.1.2 Materials

In order to study the neural correlates of pavement textures, this study used a set of four distinct pavements. The selected surfaces were flat, carpet, foam, and rubber circles. These four pavements, figure 3.2, provided distinct touch sensations, to allow studying brain activity and compare the obtained results.

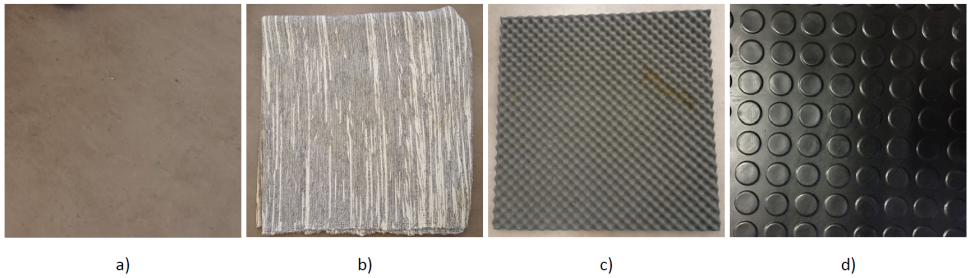

Figure 3.2: Experimental pavements: a) Flat; b) Carpet; c) Foam; d) Rubber circles.

The neural activity generated from the textured surfaces was recorded by a 16 channel EEG cap (actiCAP by Brain Products). The setup, figure 3.3, was composed by the recording system (electrodes, cap, V-Amp 16 and ImpBox), the syringe and the electrolyte gel.

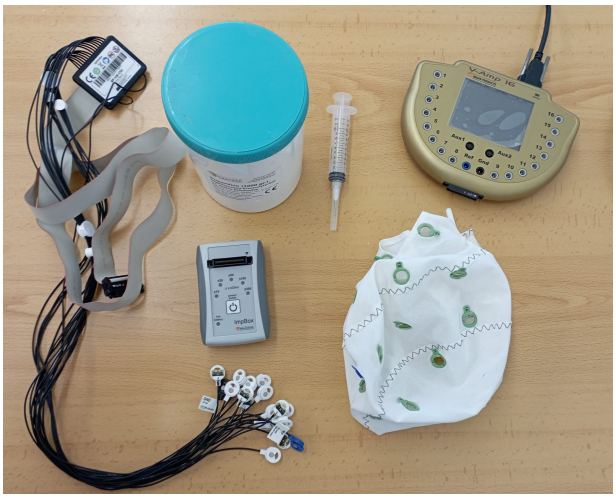

Figure 3.3: EEG recording system, actiCAP by Brain Products.

Finally, in order to analyse the 4 different conditions (4 pavements) during exoskeleton control, this study selected the ExoAtlet I ® exoskeleton.

3.1.2.1 ExoAtlet I ®

ExoAtlet I, figure 3.4, is a lower-limb exoskeleton that weighs up to 36 kg and can be doomed by patients with up to 110 kg. This robotic device was developed to assist patients with SCI, MS, stroke survivors among other neuromuscular diseases and damages [69].

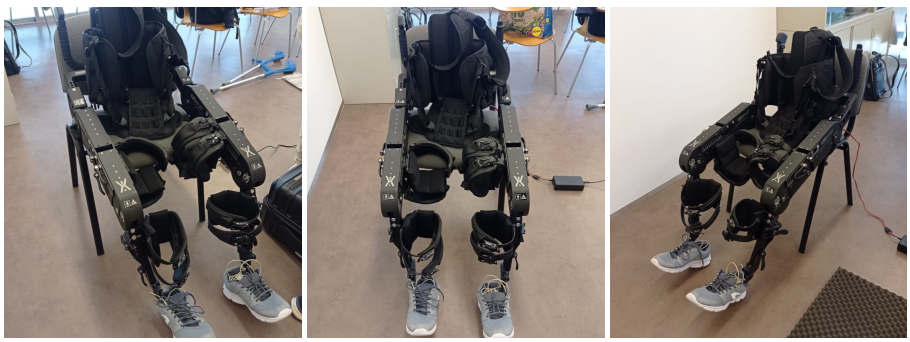

a) b) c)

Figure 3.4: Different perspectives of the ExoAtlet: a) Right view; b) Front view; c) Left view.

The ergonomic handles located in the back of the robotic device can be used by the phys-

iotherapist and guarantee a secure equipment motion. Additionally, each movement is paired with auditory cues and the exoskeleton can be controlled either by a tablet or by the patient itself using specific buttons located in the crutch [69].
This exoskeleton was integrated in recent studies that involve virtual reality, tactile and thermal feedback and also in the development of BCI devices [69].

3.1.3 Experimental protocol

The experimental activity involves 5 crucial steps: subject recruitment, operators, equipment verification, protocol and subject's evaluation. The proposed framework is illustrated in a PRISM schema type, figure 3.5.

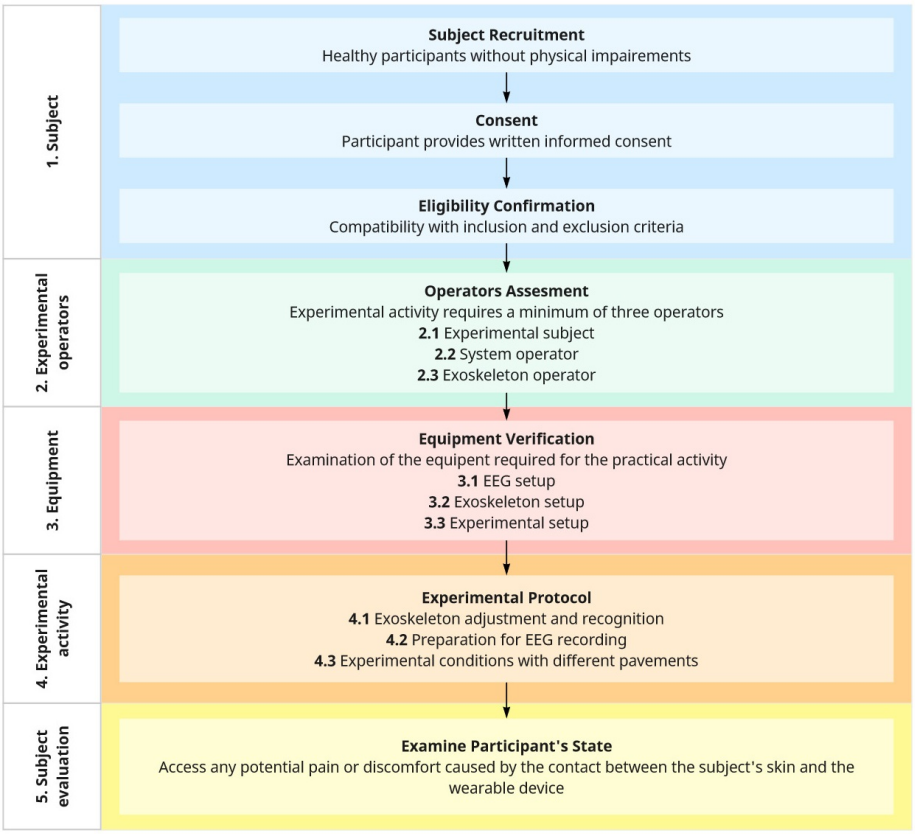

Figure 3.5: PRISM schema.

After selecting the participants according to the previously described criteria and after they signed written consent, the second stage of the protocol ensured that the necessary safety precautions were met, since the experimental activity required a minimum of three individuals: the experimental subject, the system operator and the exoskeleton operator. The **Experimental Subject** was the recruited individual whose EEG signal was being recorded for this study. The **System Operator** was responsible for controlling the computer during signal acquisition, marking the right and left steps, changing the pavements, and ensuring everything was going according to protocol. The **Exoskeleton Operator** ensured the patient's safety throughout the entire experimental activity by controlling ev-

ery movement of the exoskeleton and providing the subject with a sense of safety and comfort.
The third stage consisted on the verification of the three fundamental materials: the exoskeleton, the EEG recording setup, and the pavements. The main goal was to prepare and ensure that the computer and the exoskeleton batteries were fully charged. Then, it was crucial to check the necessary materials for the EEG recording: cap, electrodes, gel, and needle. Additionally, it was also important to test the tablet for the exoskeleton control, verify the sneakers for the data acquisition without the exoskeleton, and confirm the four pavements.
The fourth stage consisted of adjusting the ExoAtlet according to the volunteer's anatomical measurements, figure 3.6.

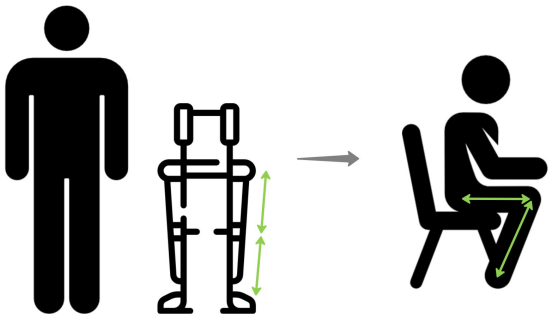

Figure 3.6: Anatomical measurement and exoskeleton adjustment.

Figure 3.7 exemplifies the adjustment of these measurements during the experimental activity.

Figure 3.7: Exoskeleton adjustment during experimental activity.

After confirming the measurements and adjusting the device, the subject was ready to don the exoskeleton, figure 3.8. Consequently, the device changed position from sitting to standing-up and at this stage, the main focus relied on ensuring that the subject was comfortable. Then, the first exercise consisted of transferring weight between the legs so that the patient could become familiar with the new center of gravity. Further, some

simple tests, such as walking in the same place and taking a few steps, were performed, so that subjects could address any possible discomfort so that the problem could be fixed. This approach also allows participants to slowly become acquainted with the exoskeleton's weight and movements, reducing their overall anxiety.

Figure 3.8: Exoskeleton to a sit-to-stand position during the experimental activity.

Once the participant is confident with the robotic device, the 16 electrodes are placed in the subject's scalp while seated in a comfortable position. Then, the system operator confirms that the data is being correctly recorded by performing the three verification tests: masticating (figure 3.9), eye blinking, and closing the eyes. Once everything is confirmed, the eight experimental conditions are recorded.

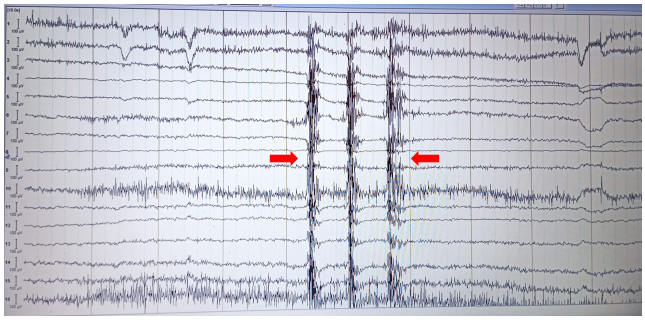

Figure 3.9: Real-time EEG data of the subject chewing three times.

The final stage involves the subject's evaluation to access any pain or injury caused by direct contact between the subject's skin and the wearable device.
More detailed instructions on the procedure for handling the exoskeleton are described in [70].
This study applies a counterbalanced design in order to eliminate the interference of order and sequence effects on the EEG measurements. The systematic variation in the order

in which each subject walks on the pavement improves the validity and reliability of the analysis performed on the recorded data. Therefore, each subject has a different order of pavements to walk on. Table 3.3 showcases the surface order attributed to each volunteer.

Table 3.3: Counterbalanced design.

Subjects (S)	Pavement order
S1_Exo	Flat ⟶ Foam ⟶ Carpet ⟶ Rubber circles
S1_No_Exo	Rubber circles ⟶ Foam ⟶ Carpet ⟶ Flat
S2_Exo	Rubber circles ⟶ Flat ⟶ Foam ⟶ Carpet
S2_No_Exo	Flat ⟶ Carpet ⟶ Rubber circles ⟶ Foam
S3_Exo	Carpet ⟶ Rubber circles ⟶ Flat ⟶ Foam
S3_No_Exo	Foam ⟶ Rubber circles ⟶ Flat ⟶ Carpet

The proposed protocol is presented in figure 3.10.

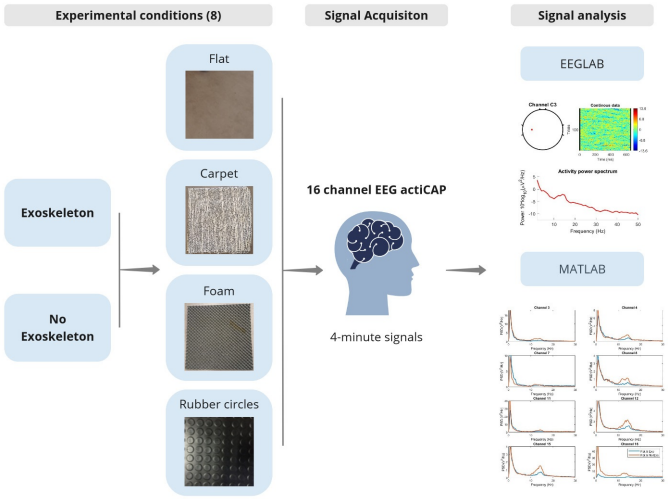

Figure 3.10: Experimental activity flowchart.

After recording the EEG signals for each of the eight experimental conditions, the files are then imported into EEGLAB (MATLAB toolbox), where the signal is processed, analysed and visualised. The signal analysis is described in the following section 3.2.

3.1.4 Signal recording

The EEG measurements were recorded according to the 10-20 system using 16 electrodes positioned on the subject's scalp. Prior to the signal recording, each electrode's impedance value was measured and kept below 50.0 kΩ, figure 3.11.

a) b)

Figure 3.11: Experimental activity: a) EEG cap and electrodes placement; b) Impedance value below 50.0 kΩ.

The signal recordings of the four pavements with exoskeleton were the first experimental conditions to be recorded for all three subjects at a sampling rate of 500 Hz.
Subsequently, the signal recording without exoskeleton was carried out as shown in the figure 3.12, in order to reduce the number of variables and the different stimulus that the experimental subjects are exposed to. When the participant is recording the EEG signal without the exoskeleton there are two important features: i) the type of shoes the subject is wearing, and ii) the fact that the exoskeleton, although it is not being used, it is performing the same movements as the patient.

Figure 3.12: EEG signal acquisition on regular floor, no exoskeleton.

Since the exoskeleton is accompanying the experimental subject, it is providing an auditory stimulus similar and identical to the one the individual is exposed to when using it and is marking the rhythm of each step. Hence, there are approximately the same number of steps in each 4-minute signal recording.

3.2 Signal Pre-Processing

Data was analysed and processed using MATLAB 2019b [71] in addition with the EEGLAB toolbox [72].

3.2.1 EEGLAB

The MATLAB toolbox EEGLAB (available online as a wiki - EEGLAB) is often used in literature to perform the EEG signal processing and is characterised by its interactive graphical user interface, figure 3.13. Another toolbox employed in literature is FieldTrip (available online as a wiki - FieldTrip) [73].

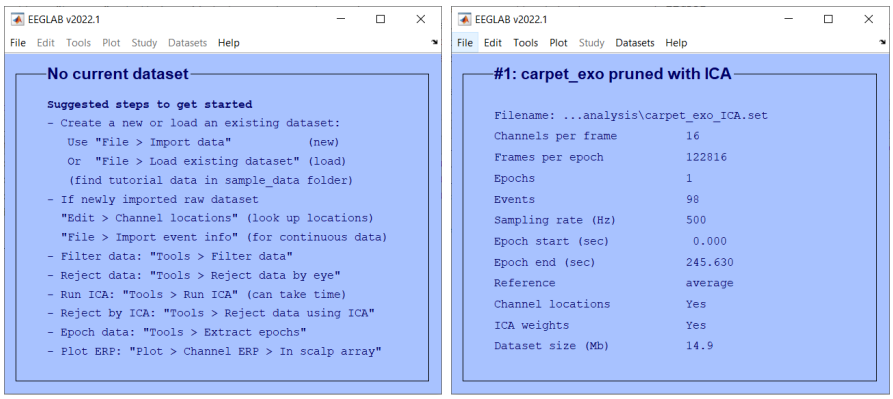

Figure 3.13: EEGLAB user interface: a) Initial interface; b) Interface after importing a dataset from subject 2 (S002) with exoskeleton while walking in place on carpet.

EEGLAB possesses many features and advanced extensions that facilitate the implementation of signal processing steps. Additionally, the extend online documentation, and workshops help navigate through the overwhelming steps and stages of the signal analysis.

3.2.2 Pre-processing pipeline

As mentioned previously, the data was imported into the EEGLAB toolbox in order to pre-process the data. Since 3 subjects were included in this study, and each subject had 8 different experimental conditions, a total of 24 EEG signals were recorded and processed.

1. **Import Data -** the continuous data was imported using the BIOSIG interface provided by the toolbox. To import data, the command *pop_biosig* in EEGLAB was used.

2. **Channel Locations -** to each electrode, the corresponding location was assigned according to the international 10-20 system, figure 3.14. To establish the locations, the command *pop_chanedit* in EEGLAB was used.

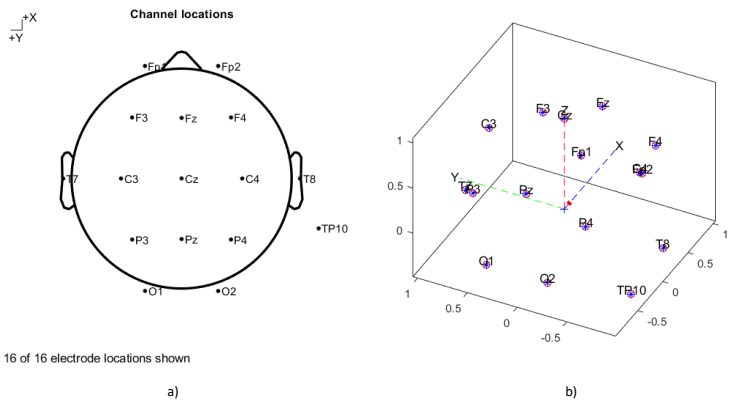

Figure 3.14: Channels locations: a) 2D view; b) 3D view.

3. Filtering - data was filtered with a basic Finite Impulse Response (FIR) filter in order to eliminate artifacts. To filter the data, the command $pop\_eegfiltnew$ in EEGLAB was used.

First a high-pass FIR filter at 1 Hz (lower edge frequency) was applied. Then, a low-pass FIR filter at 50 Hz (higher edge frequency) was applied, figure3.15. The HPF and LPF were applied separately for better results [74].

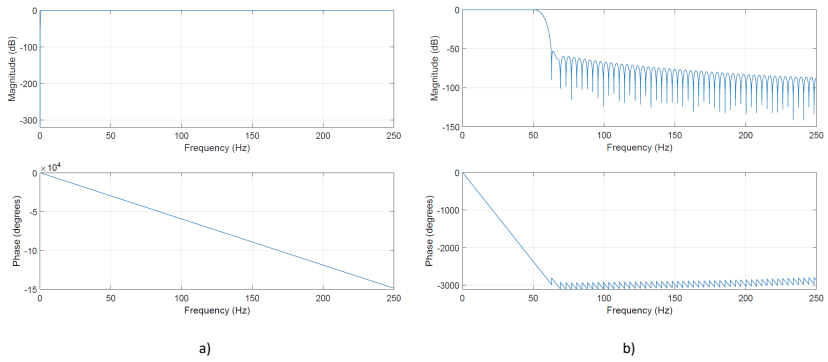

Figure 3.15: FIR filter magnitude and phase response: a) High-pass; b) Low-pass.

This type of FIR filter is commonly applied due to its linearity, stability, and simplicity [75].

Additionally, to remove line noise the Thomas F-statistics implemented in the CleanLine EEGLAB plugin (CleanLine, v.1.04) was also applied to the signal [76][77]. Therefore, as the experiments were carried out in Europe, the plugin was applied to attenuate the 50 Hz electrical interference noise [78], figure 3.16.

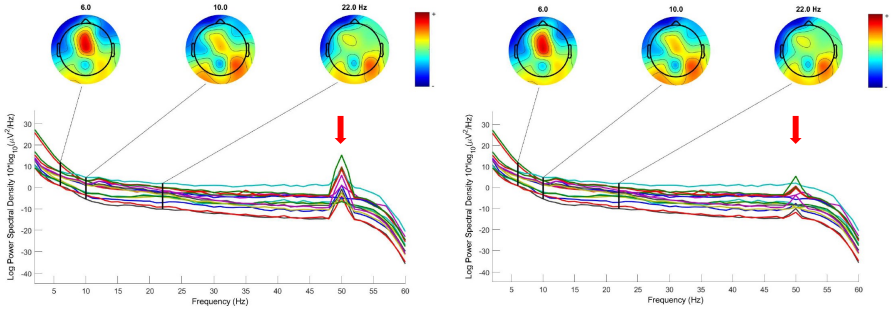

Figure 3.16: Attenuating 50Hz line noise: a) Before CleanLine plugin; b) After CleanLine plugin.

4. Inspect by Eye - inspecting the data and, if necessary, interpolating bad electrodes. To analyse the data, the command *eegplot* in EEGLAB was used.

After analyzing all 3 subjects, subject 1 (S001), unlike the others, presented flat data channels or very noisy ones. Therefore, it was necessary to interpolate those electrodes (EEGLAB command - *pop_interp*). In order to establish a comparison before and after interpolating the electrodes, figure 3.17 exemplifies the results of two specific channels: O1 and O2 (EEGLAB command - *pop_spectopo*).

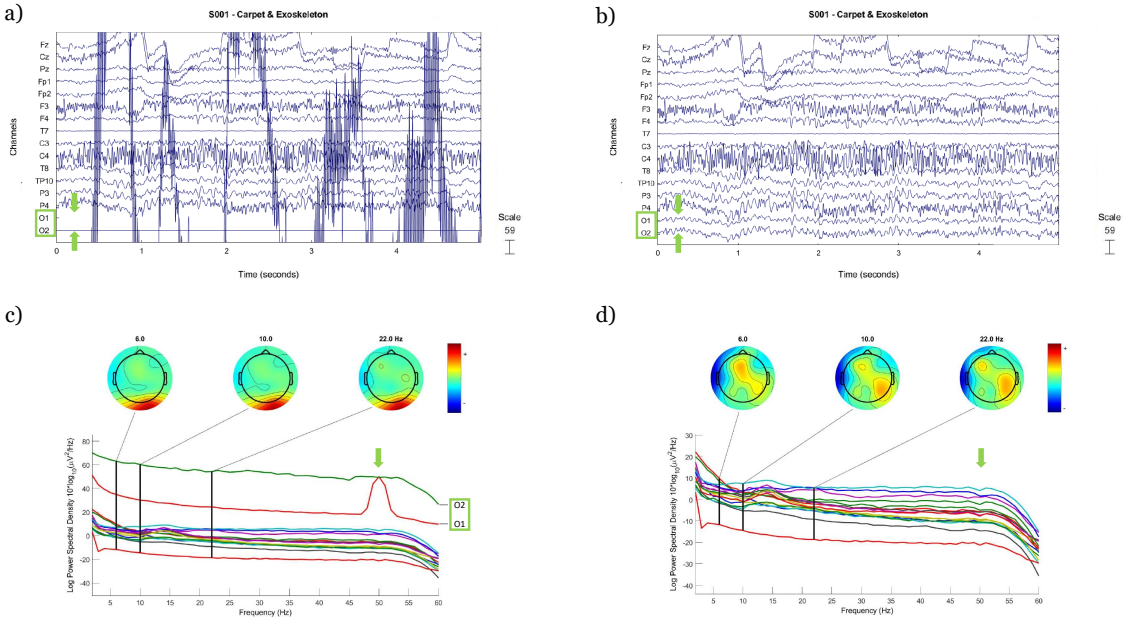

Figure 3.17: Interpolating channels 01 and 02: a) Original channel data analysis; b) Channel data after interpolating; c) Power spectral density and maps analysis; d) Power spectral density and maps after interpolating.

Table 3.4 describes which and how many electrodes were reconstructed.

Table 3.4: S001 - Interpolated electrodes.

Experimental Condition	Electrodes
Flat & Exoskeleton	O1 and O2
Flat & No Exoskeleton	O1
Carpet & Exoskeleton	O1 and O2
Carpet & No Exoskeleton	O1
Foam & Exoskeleton	O1 and O2
Foam & No Exoskeleton	O1
Rubber circles & Exoskeleton	O1 and O2
Rubber circles & No Exoskeleton	O1

5. Re-reference - EEG data was re-referenced to the average value of all 16 channels. Figure 3.18 exemplifies the effect of referencing all channels to a common average signal. To reference the data, the command *pop_reref* in EEGLAB was used.

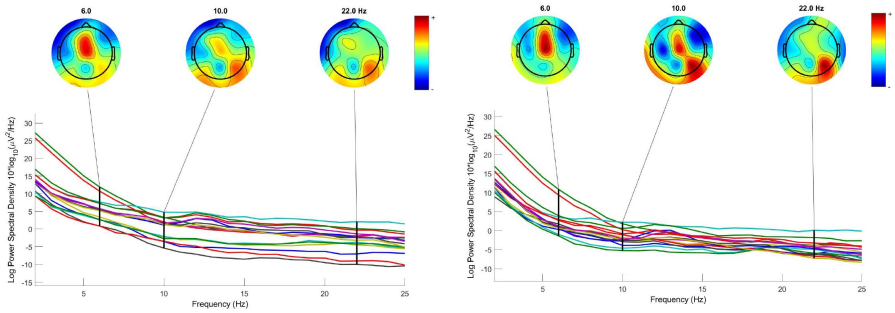

Figure 3.18: Re-reference the data: a) Before; b) After computing the common average.

6. ICA - in order to reject signal artifacts, EEG data was subjected to an ICA in order to reject eye and muscle movement, heart pulse, line noise and channel noise. Therefore, suppressing them from the signal. A high-pass filter of 1 Hz was previously applied, because filtering the data at 1-2 Hz works better for ICA [79].

To perform the ICA, the command *pop_runica* in EEGLAB was used. After running ICA, this statistical method attributes labels to every recorded channel. These labels are attributed according to the component that has a higher percentage, meaning that the main signal source for a particular channel characterizes it. The labels assigned to the channels after decomposing the signal with ICA, are exemplified in figure 3.19 (EEGLAB command - *pop_viewprops*). This study rejected all channels that were labeled as *Muscle*, *Eye*, *Heart*, *Line Noise* and *Channel Noise*. Thus in figure 3.19 b) the components from 3 channels were rejected in order to remove those artifacts from the signal (EEGLAB command - *pop_selectcomps*).

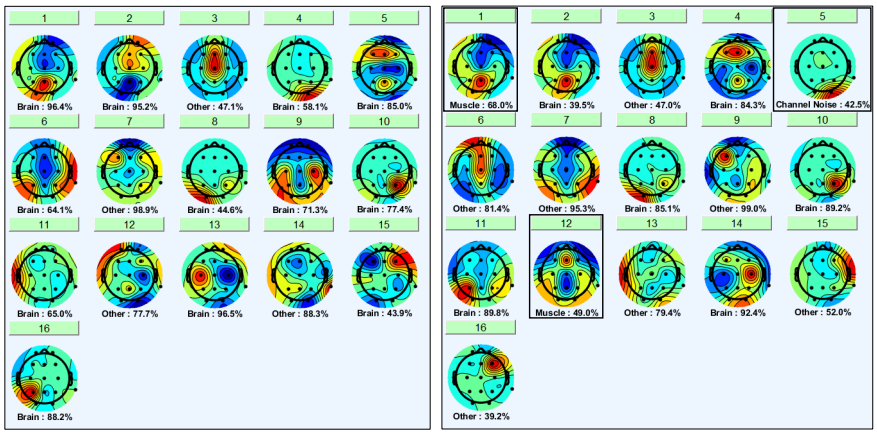

a) b)

Figure 3.19: ICA labels: a) subject 2 walking in rubber circles without an exoskeleton; b) subject 2 walking in rubber circles with an exoskeleton.

After analyzing the channels, the toolbox allows a further deeper and more detailed inspection of each signal, indicating some properties, as exemplified in figure 3.20 (EEGLAB command - *pop_prop_extended*). In this particular experimental activity condition, the muscle movement and channel noise were affecting the EEG signal and the differences in the EEG signal pattern between this two classes is demonstrated in figure 3.20 b).

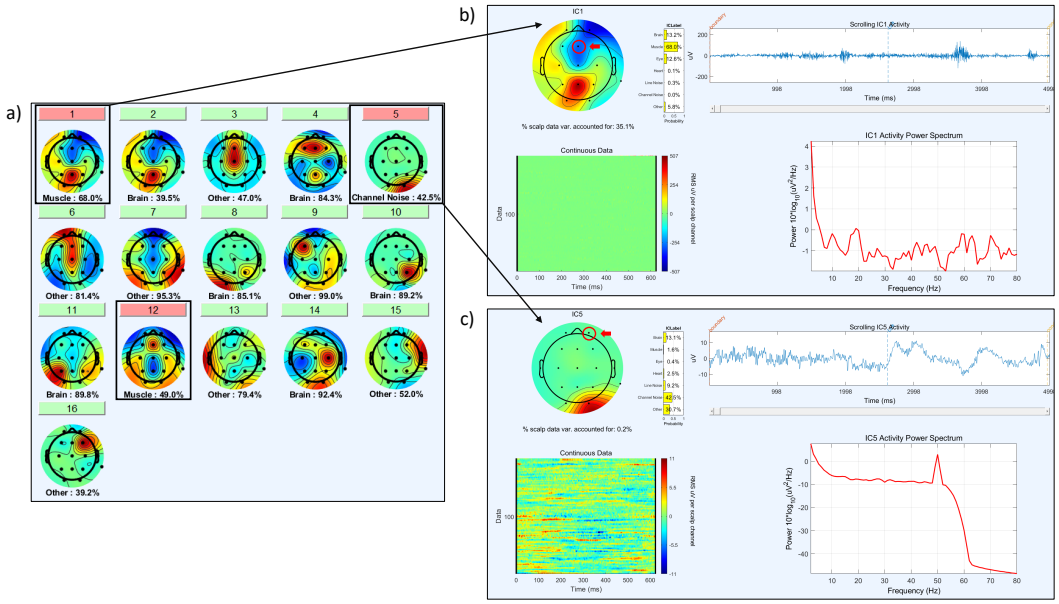

Figure 3.20: ICA channel component rejection: a) rejecting by labels; b) detailed inspection of the rejected channels to recognize the different signal patterns.

7. **Dataset -** the current pre-processed data was then saved as a dataset, that can be then uploaded to the matlab workspace (EEGLAB command - *pop_saveset*).

3.3 Exploratory Analysis

Since the study presents a small number of subjects, initially, an exploratory study of the data was performed.

The main goal of this exploratory analysis is to compare the PSD values across the different experimental conditions to determine whether the data exhibits any patterns or if the power is changed for different pavements. Therefore, this analysis demonstrates whether there is random variability, or whether it is possible to identify certain patterns between conditions.

In order to calculate the PSD, this study applied the pwelch MATLAB function that returns the Welch's power spectral density estimate. The Hamming window was applied to each data segment. Figure 3.21 exemplifies the PSD directly in microvolts squared per Hertz ($\mu V^2/Hz$).

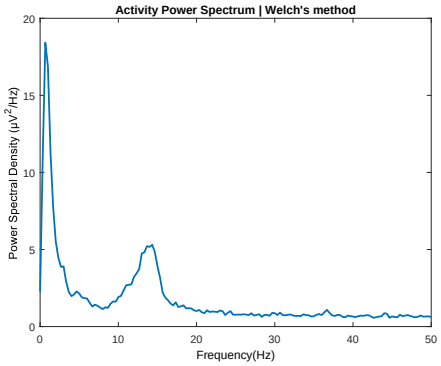

Figure 3.21: PSD for channel 13: S001 walking on carpet pavement without exoskeleton.

In order to validate this approach, this study compared the results obtained with the EEGLAB. Since the MATLAB toolbox represents the PSD in decibels (dB), this work also applied the due logarithm to the previously obtained PSD.

The results are illustrated in figure 3.22. When comparing both signals on the left (figures 3.22 a) and c)) which were obtained with the EEGLAB, with both signals on the right (figures 3.22 b) and d)), which were obtained trough the Welch method, it can be concluded that they are similar.

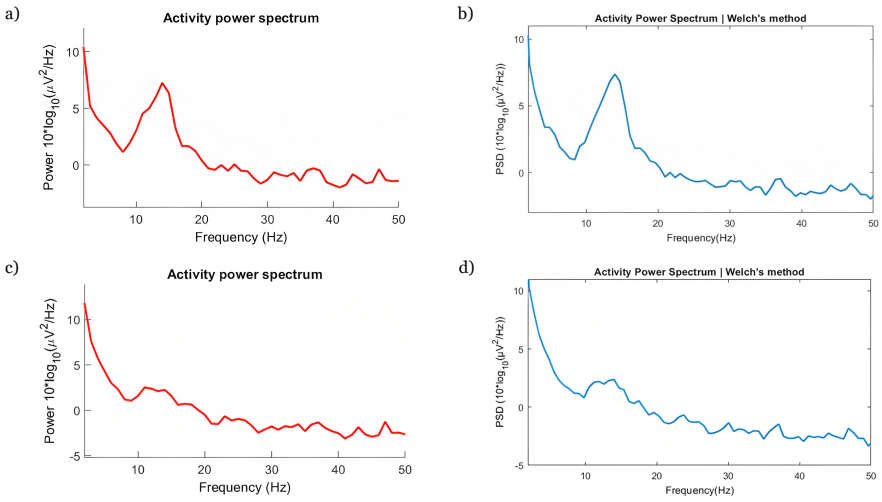

Figure 3.22: Calculus of PSD for carpet pavement without exoskeleton: a) EEGLAB result for channel 13; b) result form this study for channel 13; c) EEGLAB result for channel 10; d) result form this study for channel 10.

After comparing the results, the PSD was computed for all 16 channels across the eight experimental conditions recorded from the three experimental subjects.
Furthermore, to better visualize the differences between the PSD values for each frequency band, the average PSD was calculated for each individual channel.

3.4 DWT Decomposition

In order to extract features from the signal, data was decomposed using the DWT [58].

3.4.1 Epoching EEG data

In order to perform the DWT on the EEG data, firstly the epochs were extracted from the continuous signals. Signals were segmented taking into account the number of steps recorded by the patients in each condition. Therefore, every epoch represents a step taken by the experimental subject. Each epoch as the duration of 2.6 seconds, and it is composed by 1500 data points.
This procedure was performed in EEGLAB, and new datasets were created for wavelet decomposition. More detailed information about the number of epochs is provided in the appendix A.

3.4.2 DWT

This work selected the Daubechies 4 (db4) wavelet as the mother wavelet to decompose the biomedical signal. It is considered the most appropriate and suitable approach to process EEG signals. The LPF applied in this specific wavelet function is a FIR filter with length four, hence the designation db4 [58][75][61][80][81].

The main goal is to decompose the signal into its different frequency bands in order to obtain a discrete signal of the EEG time series sampled at 500 Hz. Therefore, the level of decomposition is based on the Nyquist sampling theorem, that fundamentally indicates that the sampling frequency must be at least twice the maximum frequency element. Consequently, this work's maximum frequency is 250 Hz, and the sampling rate is 500 Hz [81].

Therefore, the amount of decomposition levels directly depends on the five dominant EEG frequency bands required to classify the data, the signal was decomposed at level 6 [58][61][81], figure 3.23.

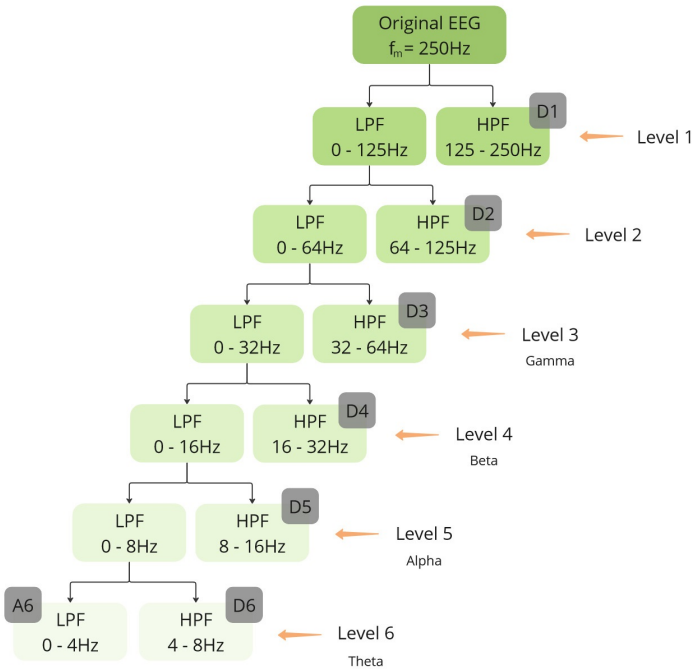

Figure 3.23: Decomposition by DWT of original signal into EEG subbands.

The wavelet coefficients provide information about the 5 frequency bands, delta (0-4Hz), theta (4-8Hz), alpha (8-16Hz), beta(16-32Hz), gamma (32-64Hz), which are represented by their wavelet components, A6, D6, D5, D4, D3, respectively, table 3.5.

Table 3.5: Discrete wavelet transform - signal information.

Wavelet Coefficient	Frequency (Hz)	EEG band
D1	125-250	Noise
D2	64-125	Noise
D3	32-64	Gamma
D4	16-32	Beta
D5	8-16	Alpha
D6	4-8	Theta
A6	0.5-4	Delta

3.5 Feature extraction

After decomposing the signal, this work extracted a total of eight features, figure 3.24, from each of the five frequency bands. These included seven statistical features such as maximum and minimum, mean, median, Standard Deviation (SD), variance [58][59] and Root Mean Square (RMS) [80]. Additionally, it also included one non-linear entropy based feature, which corresponds to the Shannon Entropy (SE) [61].

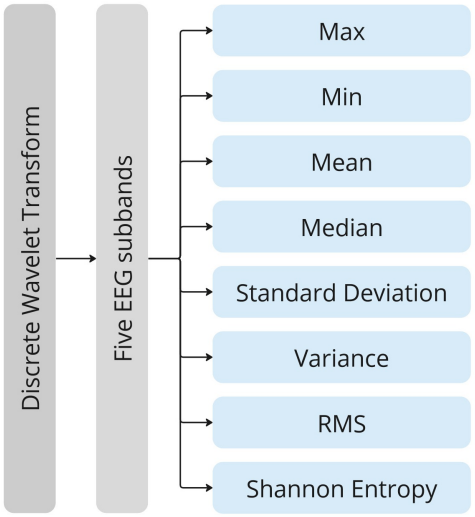

Figure 3.24: Flow diagram of the features.

These are some specifications of the selected features for this study:

1. **Maximum** - Maximum value from the wavelet approximate and coefficients in each sub-band.
2. **Minimum** - Minimum value from the wavelet approximate and coefficients in each sub-band.
3. **Mean** - The average number of all data samples in each sub-band, obtained by the following equation 3.1 [56]:

$$\tilde{x} = \frac{1}{N}\sum_{i=1}^{N} x_i \quad (3.1)$$

4. **Median** - The middle value obtained by sorting the data samples in ascending order (central tendency) in each sub-band, obtained by the following equation 3.2 [56]:

$$Median = \begin{cases} \frac{(N+1)}{2}, & \text{when N is odd} \\ \frac{N}{2} + \frac{(N+1)}{2}, & \text{when N is ever} \end{cases} \quad (3.2)$$

5. **SD** - Measures of the amount of variation in each sub-band, obtained by the following equation 3.3 [56]:

$$S = \sqrt{\frac{1}{N}\sum_{i=1}^{N}(x_i - \tilde{x})^2} \quad (3.3)$$

6. **Variance** - Another measure for the amount of data variance in each sub-band, obtained by the following equation 3.4 [56]:

$$S^2 = \frac{1}{N}\sum_{i=1}^{N}(x_i - \tilde{x})^2 \quad (3.4)$$

7. **RMS** - Represents the square root of the mean value in each sub-band, obtained by the following equation 3.5 [56]:

$$RMS = \sqrt{\frac{1}{N}\sum_{i=1}^{N}x_i^2} \quad (3.5)$$

8. **SE** - Measures the distribution of the data in each sub-band, obtained by the following equation 3.6 [61]:

$$SE = -\sum_{i=1}^{k} p_i log_2 p_i \quad (3.6)$$

3.6 Classification

ML models allow us to discover and recognize complex neural patterns that cannot be inferred from an exploratory study of the signal.
This work selected the most commonly used models to classify the recorded EEG signals, namely, ANN [58][61], KNN[61], SVM [75]; [80]; [81][61], and LDA [61]. The main focus is to study the different models' performance corresponding to their ability to detect the different experimental conditions according to the classification problem.
This work applied the selected classifiers to binary, four-class, and eight-class classification problems. The selected ML algorithms are implemented in MATLAB in addition to the classification learner from the statistics and machine learning toolbox and the neural net pattern recognition from the deep learning toolbox.
For SVM, KNN and LDA models, the dataset was randomly divided into 70% training and 30% testing [75][82] and a 5 cross fold validation [82] was performed. In this work, k

value of the KNN algorithm is equal to 10 for all classification problems.

Regarding the ANN models, the original dataset was randomly divided into 75% training, 15% validation and 15% testing [58].

In terms of architecture, the neural network is a feed-forward network with two hidden layers (*patternnet*). Each hidden layer possesses 10 sigmoid hidden neurons [58] and softmax output neurons [67]. Therefore, in the hidden layers was implemented a logistic activation function (sigmoid) responsible for an output between 0 and 1, and in the output neurons was implemented a softmax activation function suitable for multi-class classification problems, since it converts the inputs into a probability distribution attributing them to a certain class according to the probability value [83]. To train the network, the conjugate gradient backpropagation algorithm was performed (*trainscg*).

The ANN model architecture for binary classification applied in this work is represented in figure 3.25.

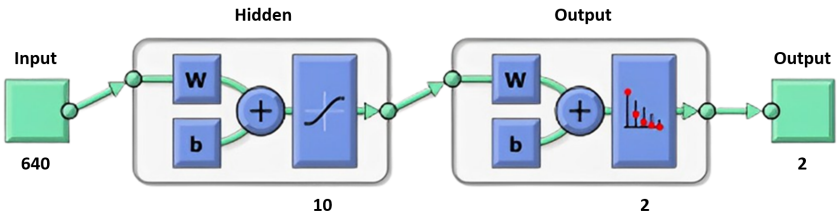

Figure 3.25: Neural network architecture for binary classification.

The ANN model architecture developed in this work for the four-class problem is represented in figure 3.26.

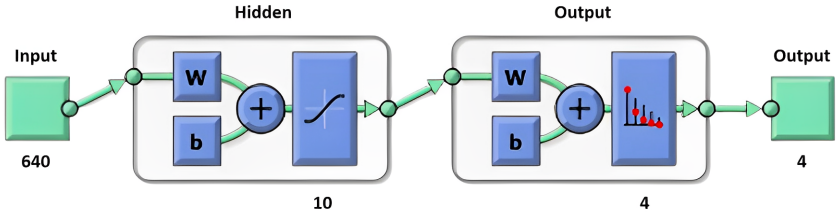

Figure 3.26: Neural network architecture for four-class problem.

Lastly, for the eight-class classification problem, the ANN model architecture is exemplified in figure 3.27.

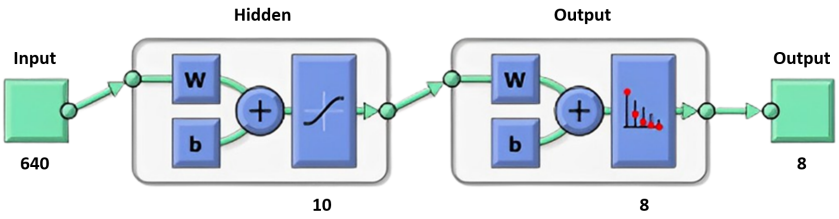

Figure 3.27: Neural network architecture for eight-class problem.

In order to study each classifier and compare their effectiveness in making accurate predictions, a total of 4 metrics based on the confusion matrix were chosen. This matrix provides information about 4 parameters, False Positives (FP), False Negatives (FN), True Negatives (TN) and True Positives (TP) used to calculate the performance metrics: accuracy, recall, precision and F1 score [56].
TP correspond to the correct number of positive cases, TN correspond to the correct number of negative cases, FN correspond to the incorrect prediction of a negative case when the true case was positive, FP correspond to the incorrect prediction of a positive case when the true case was negative [56].
The performance metrics are calculated by the following formulas:

1. **Accuracy**, equation 3.7.

$$Accuracy = \frac{TP + TN}{TP + TN + FP + FN} \quad (3.7)$$

2. **Recall**, equation 3.8

$$Recall = \frac{TP}{TP + FN} \quad (3.8)$$

3. **Precision**, equation 3.9

$$Precision = \frac{TP}{TP + FP} \quad (3.9)$$

4. **F1 score**, equation 3.10

$$F1\ score = \frac{2 * Precision * Recall}{Precision + Recall} \quad (3.10)$$

Chapter 4

Results

This chapter will demonstrate the results obtained from the analysis of the recorded EEG signals.

4.1 Exploratory Analysis

To study the impact of different textures on neural activity, this preliminary analysis of the EEG signal power at each frequency band for the control and exoskeleton conditions was performed for two specific electrodes in the central brain region, C3 and C4 [58], since they are located near the somatosensory cortex that processes sensory and motor information.
Firstly, a few technical details and caveats should be taken into account regarding the results of this exploratory analysis.
Since the recording system used in this work is composed of 16 electrodes, the source of the EEG signals could not be determined [3]. Because of this, the presented results are described in terms of the area where the electrodes were placed, since they may not accurately represent the activity of the brain areas directly beneath them.
This exploratory analysis is based, as previously described, on the PSD values across all the different conditions. Therefore, figure 4.1 demonstrates the results for the first experimental subject walking on flat pavement without an exoskeleton.

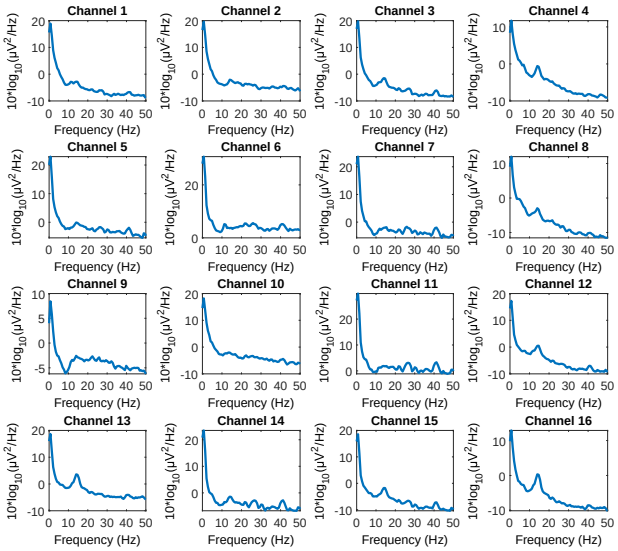

Figure 4.1: PSD for each EEG channel: S001 walking on flat pavement without exoskeleton.

Afterwards, in order to better visualize the differences between the PSD values for each frequency band, the average PSD for each EEG frequency band was calculated for each individual channel, figure 4.2.

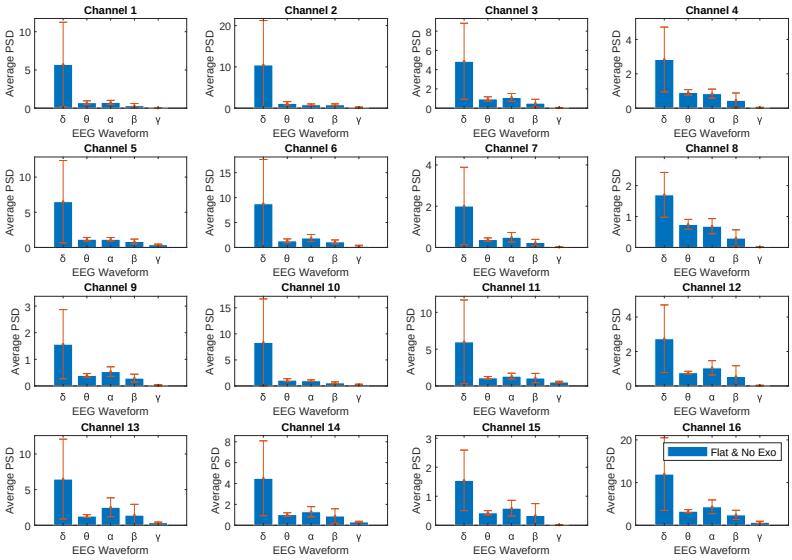

Figure 4.2: Average PSD comparing the power of the different EEG frequency bands.

Lastly, to perform the exploratory analysis and compare values between conditions, this study analyzed the different PSD values according to the graphs shown in the figure 4.3.

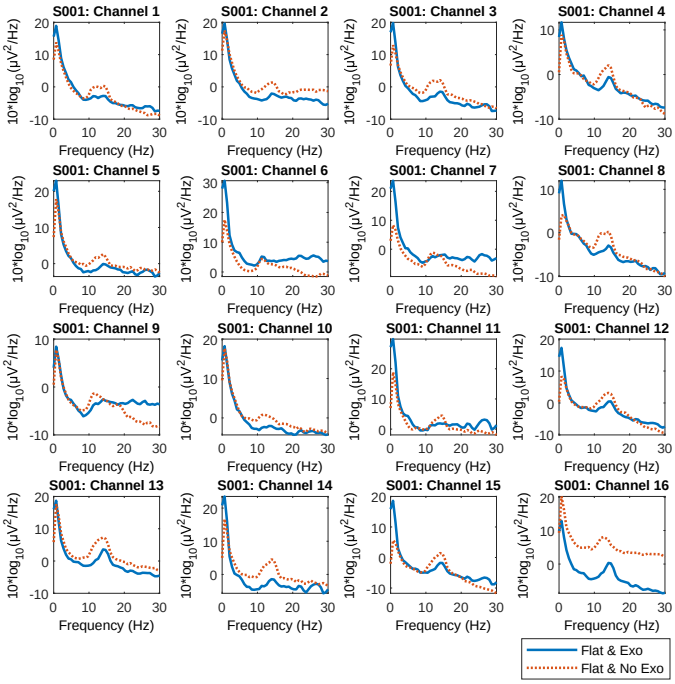

Figure 4.3: Comparing PSD results from control and exo conditions recorded from subject 1 while walking on flat pavement.

4.1.1 Neural activity during exoskeleton control

The initial exploratory analysis was mainly concerned with the identification of major patterns of change between conditions. Therefore, only a qualitative description of these findings is presented, namely as: equal (=), increase (↑), decrease (↓), or nearly similar (≈). Additionally, the tables also present a column designated by "Preferred" that indicates which one of the pavements tested was the subject's favourite, or preferred, to walk on.

By analyzing the PSD of the EEG signal for each electrode, and also by comparing the neural activity during conditions with (Exo) and without exoskeleton (control condition - No exo), revealed that the most prominent signal differences across all subjects and experimental conditions occurred in the delta frequency band, table 4.1.

When analyzing the PSD in the delta frequency band for the C3 electrode, the elevated values occurred in subject 2 (exo carpet: 9.60 $\mu V^2/Hz \pm 3.29$) and subject 3 (exo flat: 3.60 $\mu V^2/Hz \pm 2.88$). Additionally, for the C4 electrode, the increased values occurred in subject 1 (exo foam: 4.50 $\mu V^2/Hz \pm 3.39$), subject 2 (control carpet: 7.24 $\mu V^2/Hz \pm 3.66$), and subject 3 (control foam: 8.02 $\mu V^2/Hz \pm 2.87$ and exo carpet: 10.99 $\mu V^2/Hz \pm 3.11$).

Furthermore, beta (control foam: 3.86 $\mu V^2/Hz \pm 1.64$) and gamma (control foam: 7.57 $\mu V^2/Hz \pm 0.92$) frequency bands also presented elevated values for electrode C4 in subject 1.

As presented in table 4.1 the electrodes C3 and C4 in the exo and control conditions demonstrated that carpet and foam have the highest power values for practically all conditions.

In the remaining texturized pavements, no major differences were found for each of the frequency bands (table 4.1), conditions (electrode C3, subject 2 control; electrode C3, subject 1 exo; electrode C3, subject 3 exo).

Table 4.1: Neural activity during control and exoskeleton conditions.

Electrode	Subject	Condition	Pavement	Delta	Theta	Alpha	Beta	Gamma	Order	Preferred	Note
C3	1	Control	Carpet	≈	=	=	=	=	7	Foam	*
C3	2	Control	Flat	≈	=	=	=	=	5	Foam	
C3	3	Control	Foam	≈	=	≈	=	=	5	Carpet	**
C3	1	Exo	Dot	≈	=	=	=	=	4	Foam	*
C3	2	Exo	Carpet	↑	=	=	=	=	4	Foam	
C3	3	Exo	Flat	↑	≈	≈	≈	≈	3	Carpet	
C4	1	Control	Carpet	≈	=	=	=	=	7	Foam	
C4	2	Control	Carpet	↑	=	=	=	=	6	Foam	
C4	3	Control	Foam	↑	=	=	=	=	5	Carpet	
C4	1	Exo	Foam	↑	=	=	↑	↑	2	Foam	
C4	2	Exo	Foam	≈	=	=	=	=	3	Foam	
C4	3	Exo	Carpet	↑	=	=	=	=	1	Carpet	

↑ - Elevated; ≈ - Identical; = - Equal

* Increase in Alpha [12 and 14Hz] - Peak of condition No Exo is slightly higher;
** Increase in Alpha [12 and 14Hz] - Peak of all conditions;

4.1.2 Neural activity in different pavement textures

By analyzing the PSD of the EEG signal, in the foam pavement, table 4.2, the results indicated that for all subjects, the main power variations occurred in the delta frequency interval and occasionally in all five frequency bands for subjects S001 and S003 in, respectively, C3 and C4.
When comparing C3 and C4 electrodes for exoskeleton and control condition, for both S001 and S002 subjects, the power of the exoskeleton (Exo) signal was higher than the control condition. Contrarily, for the subject S003, the power of the control experimental condition (No exo) was higher (table 4.2).
When analyzing the PSD in the delta frequency band for the C3 electrode, the elevated values occurred in subject 2 (exo foam: 7.15 $\mu V^2/Hz \pm 3.21$), and occurred for the electrode C4 in subject 1 (exo foam : 9.27 $\mu V^2/Hz \pm 3.42$), and subject 2 (exo foam: 6.89 $\mu V^2/Hz \pm 3.49$).
Table 4.2 also showcases that electrode C3 for subject 3 and electrode C4 for subject 1 were related to high powers of, accordingly, no exo and exo conditions across all frequency bands. In the remaining conditions, no major differences were found except in the delta frequency band.

Table 4.2: Neural activity in foam pavement.

Electrode	Subject	Condition	Pavement	Delta	Theta	Alpha	Beta	Gamma	Order	Preferred	Note
C3	1	Exo vs Control	Foam	Exo ≈	=	≈	=	=	2|6	Foam	*
C3	2	Exo vs Control	Foam	Exo ↑	=	=	=	=	3|8	Foam	
C3	3	Exo vs Control	Foam	No Exo ≈	No Exo ↑	No Exo ↑	No Exo ↑	No Exo ↑	4|5	Carpet	
C4	1	Exo vs Control	Foam	Exo ↑	Exo ↑	Exo ↑	Exo ↑	Exo ↑	2|6	Foam	
C4	2	Exo vs Control	Foam	Exo ↑	=	=	=	=	3|8	Foam	
C4	3	Exo vs Control	Foam	No Exo ≈	=	=	=	=	4|5	Carpet	

- Elevated; - Identical; = - Equal

* Increase in Alpha [12 and 14Hz] - Peak of condition "No Exo" is slightly higher;

Comparison of neural activity for the electrodes C3 and C4 in the carpet pavement, table 4.3, demonstrated that the delta frequency band possessed the main signal power variations.
Table 4.3 also showcases that electrode C3 for subject 3 and electrode C4 for subject 3 were related to high powers of exo conditions across all frequency bands. Except in the delta frequency band, no major differences were found in the remaining conditions.
When comparing the foam pavement, table 4.2, with the carpet pavement, table 4.3, the cells highlighted in orange indicate that the power of the exoskeleton condition appears higher for both electrodes for the subject's favourite pavement. That is, for subjects 1 and 2, the preferred pavement was foam, this condition being characterized by a higher signal power with the exoskeleton.
For subject 3, the preferred pavement was the carpet, this condition being characterized by a high power of exoskeleton. When calculating the PSD for these two cases, for electrodes C3 and C4, the obtained values were, accordingly, 3.87 $\mu V^2/Hz \pm 2.24$, and 10.99 $\mu V^2/Hz \pm 3.11$.

Table 4.3: Neural activity in carpet pavement.

Electrode	Subject	Condition	Pavement	Delta	Theta	Alpha	Beta	Gamma	Order	Preferred	Note
C3	1	Exo vs Control	Carpet	No Exo ≈	≈	≈	=	=	3|7	Foam	*
C3	2	Exo vs Control	Carpet	Exo ↑	=	=	=	=	4|6	Foam	
C3	3	Exo vs Control	Carpet	Exo ↑	Exo ≈	Exo ≈	Exo ≈	Exo ≈	1|8	Carpet	
C4	1	Exo vs Control	Carpet	No Exo ↑	=	=	=	=	3|7	Foam	
C4	2	Exo vs Control	Carpet	No Exo ↑	=	=	=	=	4|6	Foam	
C4	3	Exo vs Control	Carpet	Exo ↑	Exo ↑	Exo ↑	Exo ↑	Exo ↑	1|8	Carpet	

- Elevated; - Identical; = - Equal

* Increase in Alpha [12 and 14Hz] - Peak of condition "No Exo" is slightly higher;

When evaluating the neural activity for the electrodes C3 and C4 in the flat pavement, table 4.4, demonstrated that the delta frequency band possessed the main signal power variations. In this case, electrode C3 across all 3 subjects exo conditions possessed the highest power value.
When analyzing the PSD values for the delta frequency band, the elevated values occurred for electrode C3, and the results for subjects 2 and 3 were, accordingly, 6.98 $\mu V^2/Hz \pm$ 2.94, and 3.60 $\mu V^2/Hz \pm$ 2.88.

Table 4.4: Neural activity in flat pavement.

Electrode	Subject	Condition	Pavement	Delta	Theta	Alpha	Beta	Gamma	Order	Preferred	Note
C3	1	Exo vs Control	Flat	Exo ≈	=	No Exo ≈	=	=	1|8	Foam	*
C3	2	Exo vs Control	Flat	Exo ↑	=	=	=	=	2|5	Foam	
C3	3	Exo vs Control	Flat	Exo ↑	=	=	=	=	3|7	Carpet	
C4	1	Exo vs Control	Flat	No Exo ↑	=	=	=	=	1|8	Foam	
C4	2	Exo vs Control	Flat	Exo ≈	=	=	=	=	2|5	Foam	
C4	3	Exo vs Control	Flat	No Exo ≈	=	=	=	=	3|7	Carpet	

- Elevated; - Identical; = - Equal

* Increase in Alpha [12 and 14Hz] - Peak of condition "No Exo" is slightly higher;

When evaluating the neural activity for the electrodes C3 and C4 in the dot pavement, table 4.5, except for the electrode C4 for subject 3, the results demonstrated that the delta frequency band possessed prominent power variations and it was characterized by high power values in the exoskeleton condition. The significantly elevated value occurred in subject 2 for the C4 electrode with a PSD of 6.77 $\mu V^2/Hz \pm$ 3.57.

Table 4.5: Neural activity in dot pavement.

Electrode	Subject	Condition	Pavement	Delta	Theta	Alpha	Beta	Gamma	Order	Preferred	Note
C3	1	Exo vs Control	Dot	Exo ≈	=	=	=	=	4|5	Foam	*
C3	2	Exo vs Control	Dot	Exo ≈	=	=	=	=	1|7	Foam	
C3	3	Exo vs Control	Dot	Exo ≈	=	=	=	=	2|6	Carpet	
C4	1	Exo vs Control	Dot	Exo ≈	=	=	=	=	4|5	Foam	
C4	2	Exo vs Control	Dot	Exo ↑	=	=	=	=	1|7	Foam	
C4	3	Exo vs Control	Dot	No Exo ↑	=	=	=	=	2|6	Carpet	

- Elevated; - Identical; = - Equal

* Increase in Alpha [12 and 14Hz] - Peak of all conditions;

A comparison of neural activity without the exoskeleton in the different pavement textures demonstrated that it only characterized 8 of a total of 24 conditions analyzed (2 electrodes

× 4 pavements × 3 subjects). Meanwhile, the use of the exoskeleton indicated stronger power signals and characterized 16 of the 24 analysed conditions.
In the case of flat and dot pavements, this difference was not very clear, especially for the theta, alpha, beta, and gamma frequency bands (tables 4.4 and 4.5), which showed no difference.
Therefore, after this first analysis, it is necessary to further classify the data in order to infer patterns that go beyond a preliminary analysis. Consequently, by comparing the results provided by the machine learning classifiers with these preliminary findings, there will be more information to conclude whether there is any pattern for identification or not.

4.2 Wavelet Analysis

The results obtained after applying the wavelet decomposition to the neural data are illustrated in figure 4.4.

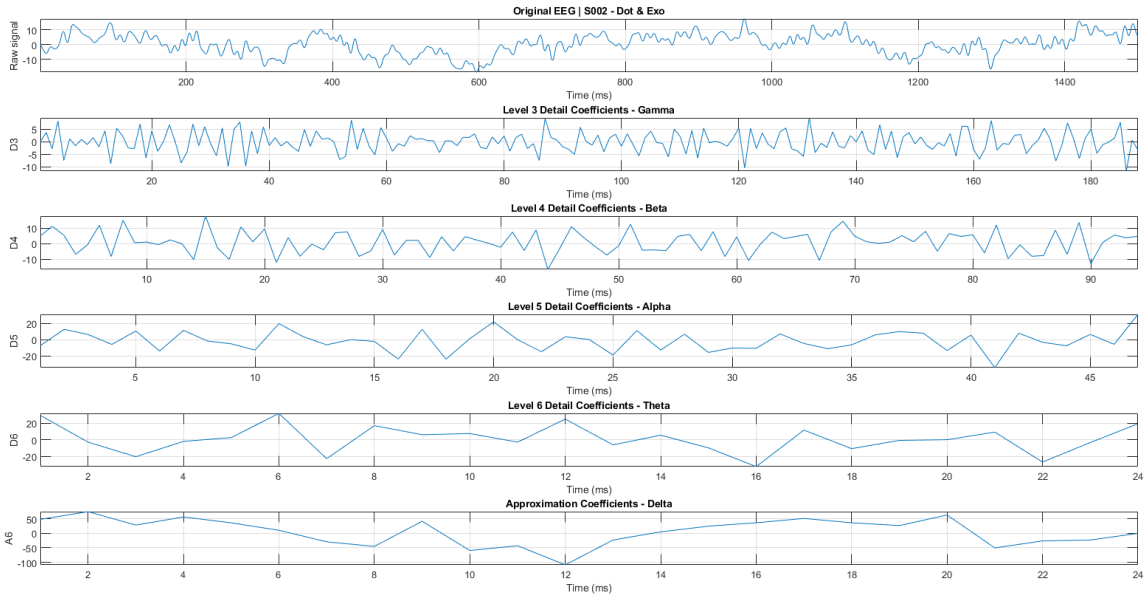

Figure 4.4: Six-layer discrete wavelet decomposition of 1500 epochs for the second experimental subject with exoskeleton walking on rubber circles.

4.3 Feature Extraction

After decomposing the signal, features were extracted from the processed signals for each experimental condition (8) and each experimental subject (3). Therefore, a total of 24 datasets were created, with the features extracted from each epoch in each waveband for all 16 electrodes in the recorded system. Table 4.6 showcases the results obtained for the eight features extracted for channel one, Fz, in each of the five wavebands.

Table 4.6: Extracted features for S002 with exoskeleton walking on carpet.

Features	**Wavelet sub-bands**				
8	Gamma	Beta	Alpha	Theta	Delta
Min	-17.738	-17.619	-29.527	-39.981	-114.405
Max	16.773	32.193	39.809	45.577	121.170
Mean	-0.044	0.340	0.552	-2.840	-7.459
Median	0.443	-0.691	5.608	-6.906	-16.344
Deviation	6.226	10.238	18.274	25.983	54.852
Variance	38.765	104.822	333.938	675.137	3008.766
RMS	6.210	10.189	18.087	25.594	54.213
Entropy	-32370.175	-528.031	-95941.526	-109777.572	-613449.882

Features extracted from the five sub-bands indicate that the delta band frequency is the one with the most discrepant values in relation to the others (table 4.6), sustaining the results previously described in the exploratory analysis.

4.4 Classifying neural activity during exoskeleton control on different pavements

To complement the previous exploratory analysis of the results, neural activity recorded during the different conditions (exo and control) while walking on different pavements (flat, dot, carpet, and foam) was studied using four different classifiers. The algorithms selected by this study were: ANN [58][61][67], KNN[61][67], SVM [75][80][81][61][67], and LDA [61][67].

For each of the three classification problems involved in this study, four different models were created, three of them regarding the individual subjects involved in this work, therefore being designated as subject-dependent classification since the model was trained, validated, and tested with data from the same individual [84].

This work analyzed three different classification problems: the first regarding the control and exo conditions (binary problem), the second concerning the different pavement textures (4-class problem), and the third combining all the experimental conditions (8-class problem).

4.4.1 Binary classification

The main goal of the first classifier was to learn a decision boundary between two possible categories. In this work, the binary classification intends to distinguish between two experimental conditions, the control (No exo) and exoskeleton (Exo). Therefore, the input feature space possessed two different numerical labels as outputs.

4.4.1.1 Individual subjects

The four classifiers have been trained to recognize neural patterns specific to each experimental subject. The performance metrics used to evaluate the model's ability to classify the data are shown in table 4.7.
In table 4.7 and figure 4.5 for subject 1, the SVM and ANN classifiers have achieved perfect performance in terms of accuracy (100%), recall (100%), precision (100%), and F1 score (1), as well as for subject 3, where the SVM, KNN, and ANN have also provided these perfect scores.
Meanwhile, for subject 2 the best performance was provided by the SVM model with an accuracy of 95.714%.

Table 4.7: Subject-dependent classifiers performance for binary problem.

	Accuracy (%)	Recall (%)	Precision (%)	F1 score
S001 | SVM*	**100**	**100**	**100**	**1**
S001 | KNN	98.571	98.684	98.485	0.986
S001 | LDA	98.571	98.684	98.485	0.986
S001 | ANN	**100**	**100**	**100**	**1**
S002 | SVM*	**95.714**	**95.833**	**95.946**	**0.959**
S002 | KNN	90.000	90.543	90.377	0.905
S002 | LDA	88.571	88.862	88.862	0.889
S002 | ANN	95.70	95.70	95.30	0.955
S003 | SVM*	**100**	**100**	**100**	**1**
S003 | KNN	**100**	**100**	**100**	**1**
S003 | LDA	92.857	93.079	92.974	0.930
S003 | ANN	**100**	**100**	**100**	**1**

* Linear SVM;
- Bold rows correspond to higher performance values for each subject;

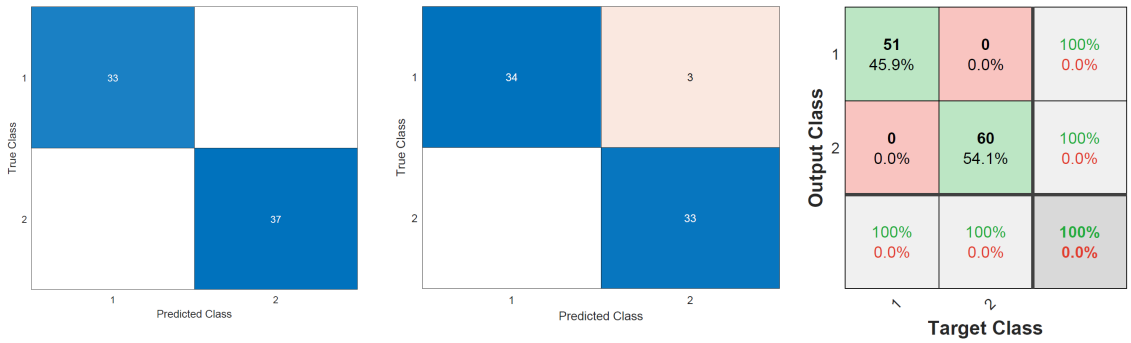

a) b) c)

Figure 4.5: Confusion matrix: a) SVM model for subject 1; b) SVM model for subject 2; c) ANN model for subject 3.

4.4.1.2 All Subjects

This classification involved all three experimental subjects, meaning that the models were trained, validated, and tested with the extracted features from the data. The performance metrics used to evaluate the model's ability to classify the data are shown in table 4.8.
In table 4.8 and figure 4.6, the LDA model has achieved the best performance between the four classifiers, with an accuracy of 98.571%, a recall of 98.387%, a precision of 98.750%, and a F1 score of 0.986.

Table 4.8: All subjects classifiers performance for binary problem.

	Accuracy (%)	Recall (%)	Precision (%)	F1 score
Linear SVM	88.571	88.240	88.750	0.885
KNN	94.286	94.167	94.167	0.942
LDA	**98.571**	**98.387**	**98.750**	**0.986**
ANN	85.10	86.50	83.50	0.850

- Bold row corresponds to higher performance values;

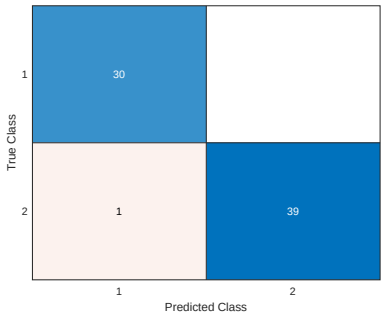

Figure 4.6: Confusion matrix of LDA model for binary classification.

4.4.2 Four-class classification

The second classifier aims to differentiate the four different pavements included in this study: carpet, flat, foam and rubber circles. Therefore, the input feature space possessed four different numerical output labels, distinguishing between each condition.

4.4.2.1 Individual subjects

The four classifiers have been trained to recognize neural patterns specific to each experimental subject. The performance metrics used to evaluate the model's ability to classify the data are shown in table 4.9.
When analyzing table 4.9 and figure 4.7 for subject 1, the SVM model achieved the best performance with an accuracy of 95.714%. For subject 2, the highest accuracy value was

provided by ANN classifier (91.50%). As for the third subject, the KNN was the model that best fit the data from this experimental individual with an accuracy of 98.571%.

Table 4.9: Subject-dependent classifiers performance for four-class problem.

	Accuracy (%)	Recall (%)	Precision (%)	F1 score
S001 | SVM*	**95.714**	**95.685**	**95.417**	**0.956**
S001 | KNN	82.857	82.632	82.500	0.826
S001 | LDA	77.143	77.298	77.500	0.774
S001 | ANN	88.20	87.38	87.95	0.877
S002 | SVM*	88.571	88.012	89.410	0.903
S002 | KNN	75.714	76.651	78.299	0.775
S002 | LDA	81.429	80.625	82.292	0.815
S002 | ANN	**91.50**	**91.45**	**91.85**	**0.917**
S003 | SVM*	97.727	97.727	96.875	0.973
S003 | KNN	**98.571**	**98.529**	**98.438**	**0.985**
S003 | LDA	75.714	75.443	75.347	0.754
S003 | ANN	98.20	98.18	98.38	0.983

* Linear SVM;
- Bold rows correspond to higher performance values for each subject;

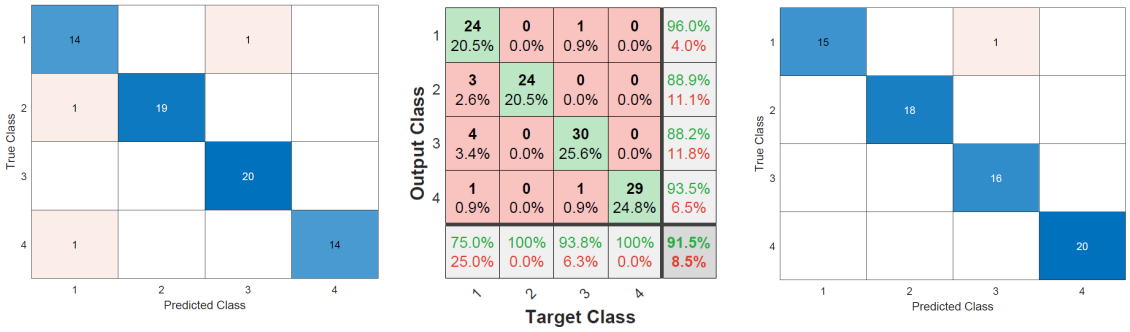

a) b) c)

Figure 4.7: Confusion matrix: a) SVM model for subject 1; b) ANN model for subject 2; c) KNN model for subject 3.

4.4.2.2 All Subjects

By analyzing table 4.8 and figure 4.8, the metrics results indicate that the LDA model's performance was the best out of the four classifiers. The performance was characterized by an accuracy of 88.571%, a recall of 88.160%, a precision of 89.158%, and a F1 score of 0.887.

Table 4.10: All subjects classifiers performance for four-class problem.

	Accuracy (%)	Recall (%)	Precision (%)	F1 score
Linear SVM	87.143	86.890	87.842	0.874
KNN	82.857	82.374	82.613	0.825
LDA	**88.571**	**88.160**	**89.158**	**0.887**
ANN	70.10	70.30	70.10	0.702

- Bold row corresponds to higher performance values;

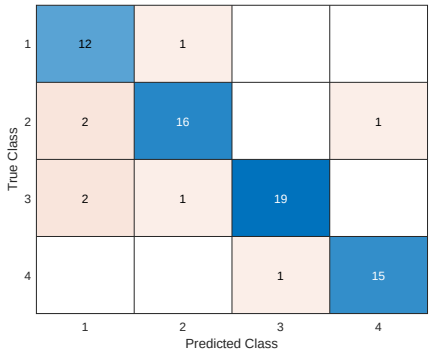

Figure 4.8: Confusion matrix of LDA model for four-class classification.

4.4.3 Eight-class classification

The last classifier combined all experimental conditions. Therefore, the aim was to classify whether the subject was wearing or not the robotic device and on which pavement. Consequently, the input feature space possessed eight different numerical output labels.

4.4.3.1 Individual subjects

The four classifiers have been trained to recognize neural patterns specific to each experimental subject. The performance metrics used to evaluate the model's ability to classify the data are shown in table 4.11.

The metrics results provided by table 4.11 and figure 4.9 indicate that for subjects 1, 2, and 3, the best performance is attributed to the SVM classifier with accuracy of 98.571%, 98.571%, and 100%, respectively. Highlighting, the subject 3 SVM model achieved perfect performance across all metrics: accuracy (100%), recall (100%), precision (100%), and F1 score (1).

Table 4.11: Subject-dependent classifiers performance for eight-class problem.

	Accuracy (%)	Recall (%)	Precision (%)	F1 score
S001 | SVM*	**98.571**	**98.958**	**98.958**	**0.989**
S001 | KNN	82.857	82.971	85.480	0.842
S001 | LDA	92.857	93.655	92.639	0.931
S001 | ANN	84.90	85.84	85.50	0.855
S002 | SVM*	**98.571**	**99.219**	**98.611**	**0.989**
S002 | KNN	75.714	76.517	78.016	0.773
S002 | LDA	92.857	90.923	93.562	0.922
S002 | ANN	98.30	98.13	98.13	0.981
S003 | SVM*	**100**	**100**	**100**	**1**
S003 | KNN	90.000	92.508	92.147	0.923
S003 | LDA	92.857	94.127	92.660	0.934
S003 | ANN	97.30	97.75	97.75	0.978

* Linear SVM;
- Bold rows correspond to higher performance values for each subject;

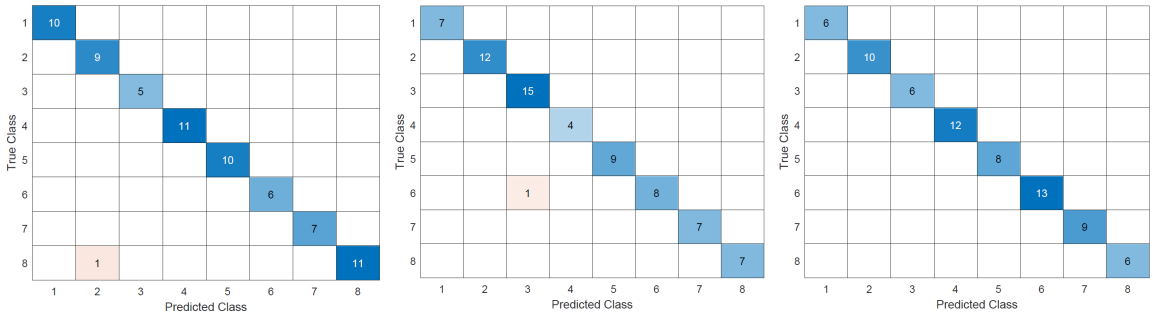

Figure 4.9: Confusion matrix: a) SVM model for subject 1; b) SVM model for subject 2; c) SVM model for subject 3.

4.4.3.2 All Subjects

For this classification, the models were trained, validated, and tested with the extracted features from the three experimental subjects. In this specific case, all the conditions are combined in order to distinguish not only the control from the exoskeleton but also between the four pavements. The performance metrics used to evaluate the model's ability to classify the data are shown in table 4.12.

By analyzing table 4.12 and figure 4.10, the LDA model's performance was the best out of the four classifiers, with an accuracy of 95.714%, a recall of 96.989%, a precision of 93.953%, and a F1 score of 0.955.

Table 4.12: All subjects classifiers performance for eight-class problem.

	Accuracy (%)	Recall (%)	Precision (%)	F1 score
Linear SVM	92.857	91.016	93.669	0.923
KNN	84.286	84.148	82.419	0.833
LDA	**95.714**	**96.989**	**93.953**	**0.955**
ANN	75.00	74.24	74.64	0.744

- Bold row corresponds to higher performance values;

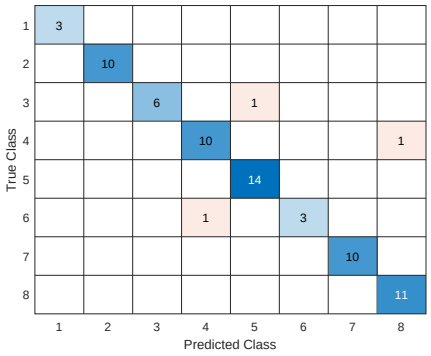

Figure 4.10: Confusion matrix of LDA model for eight-class classification.

Chapter 5

Discussion

In this study we have compared neural activity related to walking in different texturized pavements for subjects wearing an exoskeleton.
Neural activity associated with tactile processing, with and without exo, indicated that the use of the exoskeleton was associated with increased power in the delta frequency band of the C4 electrode. This increase was more prominent in the foam and carpet pavements, specifically for subject 2 (electrode C3), subject 1 (C4 electrode), and subject 3 (C4 electrode).
When subjects used the exoskeleton, neural activity was characterised by an increased power in the delta frequency band, namely in foam and carpet pavements. When analyzing the other pavements, flat and rubber circles (also designated as dot), it was also verified a higher increase in delta frequency for the exoskeleton condition, but not significantly.
Analysis with multiple classifiers, namely, SVM, LDA, KNN, and ANN also indicated that different neural activity was presented when subjects, with and without, the exoskeleton stepped on different pavements.
Namely, SVM presented the best results for single-subject classifications, and LDA presented the best results for group (all three subjects simultaneously) classifications.
Altogether, these results indicated that neural activity encodes both the use of the exoskeleton and the specific textures associated with the different tested pavements.

5.1 Neural activity during exoskeleton control

The use of the exoskeleton was associated with different neural activity.
Analysis of power in the C3 and C4 electrodes revealed that the use of the exoskeleton was associated with an increase in the delta band. This result provided by the Welch method was supported by the analysis with the wavelet transform and the results of the classifiers. Therefore, it can be conclude from this preliminary power analysis of the frequency bands that the exoskeleton and control conditions vary between them. However, no relationship between the control and exo conditions can be determined with just an exploratory analysis of the data. Consequently, additional classification was performed to support these findings.
Although delta frequency band has been previously related to sleep stages, recent research has linked it to attention phenomena in humans [38].
Thus, previous studies have demonstrated that the increase in the delta frequency band

during mental tasks is associated with attention, perception, and decision-making functions [85][86][38].
Consequently, the increase in delta frequency in this study suggests that this may be related to the subjects attention and concentration while using the exoskeleton, as previous studies indicate an increase in delta in task-related phases. Such increase in attention could be explained by the additional cognitive effort required to control the exoskeleton by the participants, when compared to regular walking.
In future studies, it will be important to evaluate if neural activity in the delta frequency band decreases as participants become more used to controlling the exoskeleton.

5.2 Neural activity in different pavement textures

Different neural activity was found when subjects stepped on the different pavements.
The use of foam was associated with the most significant increase in delta frequency in the C3 and C4 electrodes for subjects 1 and 2. Furthermore, the use of carpet was also connected with an increase in power in delta for electrodes C3 and C4 for subject 3.
In addition, the wavelet analysis and the results provided by the classifiers also supported this notion.
Previous studies showcase that tactile processing imply power changes in EEG frequency bands, mostly in alpha and beta, for C3 and C4 electrodes during the response period after tactile stimulation of the index finger [39][87].
The increase in the delta frequency band of the C3 and C4 electrodes when different tactile stimuli are delivered to subjects has been reported previously in [3]. Although the most prominent changes occur in the theta, alpha, and beta frequency bands, this study has shown the presence of power changes in delta and low gamma, although in a less pronounced form [3].
Despite the reduced number of human studies in this particular field, these results support the notion that different tactile stimuli have different neural representations and that these occur even when the subjects are using the exoskeleton.

5.3 Classifying neural activity during exoskeleton control on different pavements

The use of the four different classifiers, revealed that the best performances across all parameters studied (accuracy, recall, precision, and F1 score) were achieved with LDA when performing subject-independent classification. Meaning that the results from the binary, four-class, and eight-class, classification problems involving all subjects were better fitted with the LDA classifier, with accuracy values of 98.6%, 88.6%, and 95.7% accordingly.
LDA has been one of the prime choices in many brain-machine interface studies due to its simplicity and ability to distinguish across different classes, by reducing redundancy while

maximizing the variance between the different classes. Additionally, its performance on binary classification problems makes this model suitable for this type of classification [88][89].

For example, OpenViBE software, which is one of the most widely used open software for the development of brain-machine interfaces, uses LDA as the base algorithm [90].

The overall results were good for all classifiers assessed, despite certain classifiers having slightly poorer performances (accuracy values no lower than 70.1%). This finding further sustains the idea that neural activity varied when subjects were wearing an exoskeleton and stepping on different pavements.

Nevertheless, one interesting finding from the present study is that the neural activity from a single subject (subject-independent) was better classified by SVM model, while the analysis including all subjects (multiple subjects) was better classified by LDA algorithm. Despite not being applicable for two conditions (four-class classification for S002 and S003), the linear SVM demonstrated the best accuracy in the majority of the cases for the individual classifications.

In other words, the results of SVM classifier, in the present study conditions, suggests that it may be better to use this algorithm if a single subject is followed throughout several sessions.

Literature highlights that LDA and SVM are the most popular types of classifiers for BCI applications, but often SVM provides better performance results when compared to other classifiers, outperforming them [9]. However, results from certain studies also indicate that LDA in some cases can perform better than SVM[67][91]. Although there are not many studies for this particular case study, the results obtained by this work are also in line with these previous reviews and studies.

For several reasons, the problem of tactile processing while using an exoskeleton is highly relevant.

Firstly, exoskeletons, present limited operation time and tend to be high power machines capable of generating severe accidents that could result in severe injuries [26][24]. Thus, the ability to deliver tactile information is likely to remain a highly valuable function in the future, not only to make these robotic devices safer but also to enhance patients recovery and improve the rehabilitation process [92].

Furthermore, brain-machine interfaces for neurorehabilitation are increasing the use of tactile feedback. Therefore, describing the details of neural activity associated with tactile processing, as well as the changes induced during exoskeleton control, are likely to be of high relevance when this activity is used to directly control the exoskeleton [92]. In other words, providing tactile feedback to the user when wearing an exoskeleton contributes to a more immersive experience, and to a certain extent, contributes to the way the robotic device interacts with their surroundings. Therefore, describe tactile processing, it is critical to understand to what extent this may affect BCI control.

In future studies, and to further comprehend how different pavements affect neural activity, it will be important to analyze the effect of more uneven and irregular pavement

textures, such as Portuguese sidewalk or gravel, in the delta frequency band.
Regarding the discussed results, a few technical details should be taken into account. Firstly, and as previously mentioned, since EEG signals were recorded with a system of 16 electrodes, the study was unable to accurately represent specific areas of the brain [3]. Additionally, the fact that the "walk in place" movement provided by the exoskeleton was different from the human natural walk, the reduced number of signal recordings (n = 3), and the fact that the subjects considered were all female. These three aspects are also caveats to this study.
In conclusion, research of tactile processing for BCI systems is crucial for a number of reasons, including providing sensory feedback to the user, precise control to minimize accidents, and improving the neurorehabilitation field.

5.4 Limitations

The EEG signal was recorded with an impedance value of 50k Ω, which can directly affect the quality, accuracy and reliability of the signal since it increases the presence of artifacts, making it more difficult to distinguish between the neural information and the electrical noise [1][2].
When addressing the experimental activity, since it was time consuming and the 8 conditions were recorded continuously over time with no breaks, the signal quality may suffer as the gel dries out over time. Therefore, at the middle of the recordings, the impedance values could be monitored and the gel could be reapplied, if needed, to ensure good data.
Lastly, the number of electrodes in the EEG recording system (16 electrodes) prevents this work to study specific brain areas of interest [3].

Chapter 6

Conclusions and Future Work

6.1 Conclusion

Exoskeletons are a cutting-edge technology that has not only gained more visibility in the last few years but has also been demonstrating its enormous potential to humans.
Consequently, it is expected that exoskeletons will improve the quality of life of people who suffer from physical impairments enabling, them to performance simple tasks, while boosting their autonomy.
To our best knowledge, this is the first study to address and classify the neural activity of pavement texture processing while using an exoskeleton.
By analyzing the different EEG signals obtained by the three volunteers, it was found that there were changes associated with the delta frequency band for the C3 and C4 electrodes of the subjects with the exoskeleton according to the robustness of the different surfaces.
Comparing the performances of the different classifiers, it was concluded that LDA showed the best performance on the three classification problems involving all subjects. The best performance, with an accuracy of 98.571%, was obtained by the binary problem.
However, for the subject-dependent classifications (individual data), the results have indicated that the best performance was achieved by the SVM model, which in specific cases achieved perfect performance with accuracy values of 100%.
Consequently, since the models were able to accurately identify and distinguish between the experimental conditions, this suggests that there are not only differences in neural activity between control and exoskeleton conditions but also while walking on different textures.
Ultimately, these results support the hypothesis that, when compared to the control condition, the use of exoskeletons while walking on different textures is correlated with different neural activity patterns.

6.2 Future Work

In terms of future work, one of the main aspects is to increase the number of experimental subjects included in the study in order to build more robust and reliable models and perform statistical analysis. Additionally, as texture perception differs with age, enhancing the variability in terms of age range is also a key point.
Furthermore, the pavements selected for this study were chosen based on the ability to test them in a laboratory environment, therefore, recording EEG signals in outdoor en-

vironments such as Portuguese sidewalk, sand or even gravel, could provide additional information about neural texture coding.
Additionally, increasing the number of electrodes in the EEG recording system will improve spatial resolution, allowing specific areas of the brain to be studied.
Lastly, optimizing the model's performance by addressing and studying the impact of specific parameters, such as the k value for KNN model and the number of hidden layers and neurons for ANN classifier, could result in more reliable models.

Bibliography

[1] G.-L. Li, J.-T. Wu, Y.-H. Xia, Q.-G. He, and H.-G. Jin, "Review of semi-dry electrodes for EEG recording," *Journal of Neural Engineering*, vol. 17, no. 5, p. 051004, 2020. xii, 30, 31, 32, 88

[2] G. Li, S. Wang, and Y. Y. Duan, "Towards conductive-gel-free electrodes: Understanding the wet electrode, semi-dry electrode and dry electrode-skin interface impedance using electrochemical impedance spectroscopy fitting," *Sensors and Actuators B: Chemical*, vol. 277, p. 250–260, Aug 2018. xii, 30, 31, 32, 88

[3] M. Pais-Vieira, P.-V. Carla, A. Mehrab, P. André, P. André, K. Carolina, and O. Manuel, "Neurophysiological correlates of tactile width discrimination in humans," 2022. xii, 25, 71, 86, 88

[4] W. Ding, S. Hu, P. Wang, H. Kang, R. Peng, Y. Dong, and F. Li, "Spinal cord injury: The global incidence, prevalence, and disability from the global burden of disease study 2019," *Spine*, vol. 47, no. 21, p. 1532–1540, Nov 2022. [Online]. Available: https://journals.lww.com/10.1097/BRS.0000000000004417 1, 12, 15

[5] E. Observatory, *Portugal: Country health profile 2021*. OECD Publishing, 2021. [Online]. Available: https://eurohealthobservatory.who.int/publications/m/portugal-country-health-profile-2021 1, 15

[6] C. W. Tsao, A. W. Aday, Z. I. Almarzooq, A. Alonso, A. Z. Beaton, M. S. Bittencourt, A. K. Boehme, A. E. Buxton, A. P. Carson, Y. Commodore-Mensah, M. S. Elkind, K. R. Evenson, C. Eze-Nliam, J. F. Ferguson, G. Generoso, J. E. Ho, R. Kalani, S. S. Khan, B. M. Kissela, K. L. Knutson, D. A. Levine, T. T. Lewis, J. Liu, M. S. Loop, J. Ma, M. E. Mussolino, S. D. Navaneethan, A. M. Perak, R. Poudel, M. Rezk-Hanna, G. A. Roth, E. B. Schroeder, S. H. Shah, E. L. Thacker, L. B. VanWagner, S. S. Virani, J. H. Voecks, N.-Y. Wang, K. Yaffe, S. S. Martin, on behalf of the American Heart Association Council on Epidemiology, P. S. Committee, and S. S. Subcommittee, "Heart disease and stroke statistics—2022 update: A report from the american heart association," *Circulation*, vol. 145, no. 8, Feb 2022. [Online]. Available: https://www.ahajournals.org/doi/10.1161/CIR.0000000000001052 1, 15

[7] M. Al-Quraishi, I. Elamvazuthi, S. Daud, S. Parasuraman, and A. Borboni, "EEG-based control for upper and lower limb exoskeletons and prostheses: A systematic review," *Sensors*, vol. 18, no. 10, p. 3342, Oct 2018. [Online]. Available: http://www.mdpi.com/1424-8220/18/10/3342 2, 15, 17, 18, 19, 20

[8] E. H. Houssein, A. Hammad, and A. A. Ali, "Human emotion recognition from eeg-based brain–computer interface using machine learning: a comprehensive review," *Neural Computing and Applications*, vol. 34, no. 15, p. 12527–12557, Aug 2022. [Online]. Available: https://link.springer.com/10.1007/s00521-022-07292-4 2, 4, 5, 24, 25, 26

[9] F. Lotte, L. Bougrain, A. Cichocki, M. Clerc, M. Congedo, A. Rakotomamonjy, and F. Yger, "A review of classification algorithms for EEG-based brain–computer interfaces: A 10 year update," *Journal of Neural Engineering*, vol. 15, no. 3, p. 031005, 2018. 2, 87

[10] J. Reaves, T. Flavin, B. Mitra, M. K, and V. Nagaraju, "Assessment and application of EEG: A literature review," *Journal of Applied Bioinformatics & Computational Biology*, p. 12, Jul 2021. [Online]. Available: https://www.scitechnol.com/peer-review/an-overview-of-uptake-of-covid19-vaccine-KSlZ.php?article_id=16604 2, 26

[11] M. Luján, M. Jimeno, J. Mateo Sotos, J. Ricarte, and A. Borja, "A survey on EEG signal processing techniques and machine learning: Applications to the neurofeedback of autobiographical memory deficits in schizophrenia," *Electronics*, vol. 10, no. 23, p. 3037, 2021. 2, 33, 34, 38, 41, 42

[12] S. Sanei and J. A. Chambers, *EEG signal processing and machine learning*, second edition ed. Hoboken, NJ: Wiley, 2021. 2, 3, 6, 8, 9, 10, 11, 12, 13, 22, 23, 24, 25, 26, 27, 29, 30, 32, 35, 36, 37, 38

[13] R. Carter, S. Aldridge, M. Page, and S. Parker, *The human brain book*, american edition. revised and updated new edition ed. New York, NY: DK Publishing, 2019. 2, 3, 4, 5, 6, 7, 8, 9, 10

[14] "Central nervous system," [Accessed on 18 November 2022]. [Online]. Available: https://www.britannica.com/science/central-nervous-system 3

[15] P. J. Bazira, "An overview of the nervous system," *Surgery (Oxford)*, vol. 39, no. 8, p. 451–462, Aug 2021. [Online]. Available: https://linkinghub.elsevier.com/retrieve/pii/S0263931921001411 3, 5, 6, 7, 8

[16] Sathyasnkr, "Human brain archives," [Accessed on 18 November 2022]. [Online]. Available: https://edugyanshala.com/tag/human-brain/ 4

[17] "Types of glia," Aug 2022, [Accessed on 18 November 2022]. [Online]. Available: https://qbi.uq.edu.au/brain-basics/brain/brain-physiology/types-glia 7

[18] D. Kuriakose and Z. Xiao, "Pathophysiology and treatment of stroke: Present status and future perspectives," *International Journal of Molecular Sciences*, vol. 21, no. 20, p. 7609, 2020. 11

[19] L. Sutcliffe, H. Lumley, L. Shaw, R. Francis, and C. I. Price, "Surface electroencephalography (eeg) during the acute phase of stroke to assist with diagnosis and prediction of prognosis: A scoping review," *BMC Emergency Medicine*, vol. 22, no. 1, 2022. 11, 12

[20] M. Simis, D. Doruk Camsari, M. Imamura, T. R. Filippo, D. Rubio De Souza, L. R. Battistella, and F. Fregni, "Electroencephalography as a biomarker for functional

recovery in spinal cord injury patients," *Frontiers in Human Neuroscience*, vol. 15, 2021. 12

[21] F. Miraglia, F. Vecchio, C. Pappalettera, L. Nucci, M. Cotelli, E. Judica, F. Ferreri, and P. M. Rossini, "Brain connectivity and graph theory analysis in alzheimer's and parkinson's disease: The contribution of electrophysiological techniques," *Brain Sciences*, vol. 12, no. 3, p. 402, 2022. 12, 13

[22] M. X. Cohen, *Analyzing Neural Time Series Data: Theory and Practice*. The MIT Press, 2014. [Online]. Available: https://direct.mit.edu/books/book/4013/analyzing-neural-time-series-datatheory-and 13, 24, 25, 26, 27, 29, 33, 35, 36, 38

[23] A. Rodríguez-Fernández, J. Lobo-Prat, and J. M. Font-Llagunes, "Systematic review on wearable lower-limb exoskeletons for gait training in neuromuscular impairments," *Journal of NeuroEngineering and Rehabilitation*, vol. 18, no. 1, p. 22, Dec 2021. [Online]. Available: https://jneuroengrehab.biomedcentral.com/articles/10.1186/s12984-021-00815-5 15, 20, 21

[24] H. Lee, P. W. Ferguson, and J. Rosen, *Lower Limb Exoskeleton Systems—Overview*. Elsevier, 2020, p. 207–229. [Online]. Available: https://linkinghub.elsevier.com/retrieve/pii/B9780128146590000114 15, 17, 18, 19, 22, 87

[25] "Apparatus," [Accessed on 22 November 2022]. [Online]. Available: https://dictionary.cambridge.org/dictionary/english/apparatus 16

[26] G. Nikhil, G. Yedukondalu, and S. Rao, "Robotic exoskeletons: a review on development," *International Journal of Mechanical and Production Engineering Research and Development*, vol. 9, no. 4, pp. 529–542, 2019. 16, 17, 18, 19, 22, 87

[27] N. Yagn, "Apparatus for facilitating walking, running, and jumping." Jan 1890, U.S. Patent No. 420,179. 16

[28] B. J. Makinson, "Research and development prototype for machine augmentation of human strength and endurance. hardiman i project," *General Electric Company*, p. 25, May 1971. 17

[29] "Harmony exoskeleton," [Accessed on 23 November 2022]. [Online]. Available: https://reneu.robotics.utexas.edu/harmony-exoskeleton 18

[30] "Keep workers strong, healthy, and efficient," [Accessed on 23 November 2022]. [Online]. Available: https://www.bioservo.com/products/ironhand 18

[31] "Rex technology," Mar 2023, [Accessed on 23 November 2022]. [Online]. Available: https://www.rexbionics.com/product-information/ 18

[32] R. S. Calabrò, A. Naro, M. Russo, P. Bramanti, L. Carioti, T. Balletta, A. Buda, A. Manuli, S. Filoni, and A. Bramanti, "Shaping neuroplasticity by using

powered exoskeletons in patients with stroke: a randomized clinical trial," *Journal of NeuroEngineering and Rehabilitation*, vol. 15, no. 1, p. 35, Dec 2018. [Online]. Available: https://jneuroengrehab.biomedcentral.com/articles/10.1186/s12984-018-0377-8 20

[33] Marketing, "Eksonr," Aug 2022, [Accessed on 23 November 2022]. [Online]. Available: https://eksobionics.com/eksonr/ 20

[34] "Cyberdyne inc." Oct 2021, [Accessed on 23 November 2022]. [Online]. Available: https://www.cyberdyne.com/ 21

[35] "Rewalk robotics - more than walking," May 2022, [Accessed on 23 November 2022]. [Online]. Available: https://rewalk.com/ 21

[36] P. C. P. Panteliadis*, "Historical Overview of Electroencephalography: from Antiquity to the Beginning of the 21st Century," *Journal of Brain and Neurological Disorders*, vol. 3, no. 1, pp. 1–10, Aug. 2021. [Online]. Available: https://doi.org/10.5281/zenodo.5359323 22, 23

[37] A. Coenen, O. Zayachkivska, W. J. Konturek, and W. Pawlik, "Adolf Beck, co-founder of the EEG: An essay in honour on his 150th birthday," 2013. 23

[38] J. A. Barios, S. Ezquerro, A. Bertomeu-Motos, E. Fernandez, M. Nann, S. R. Soekadar, and N. Garcia-Aracil, "Delta-Theta intertrial phase coherence increases during task switching in a BCI paradigm," *Biomedical Applications Based on Natural and Artificial Computing*, p. 96–108, 2017. 25, 85, 86

[39] S. Su, G. Chai, X. Sheng, J. Meng, and X. Zhu, "Contra-lateral desynchronized alpha oscillations linearly correlate with discrimination performance of tactile acuity," *Journal of Neural Engineering*, vol. 17, no. 4, p. 046041, aug 2020. [Online]. Available: https://dx.doi.org/10.1088/1741-2552/aba55f 25, 86

[40] J. H. Lee, H. Kim, J.-Y. Hwang, J. Chung, T.-M. Jang, D. G. Seo, Y. Gao, J. Lee, H. Park, S. Lee, and et al., "3D printed, customizable, and multifunctional smart electronic eyeglasses for wearable healthcare systems and human–machine interfaces," *ACS Applied Materials & Interfaces*, vol. 12, no. 19, p. 21424–21432, 2020. 27

[41] D. Looney, C. Park, P. Kidmose, M. L. Rank, M. Ungstrup, K. Rosenkranz, and D. P. Mandic, "An in-the-ear platform for recording electroencephalogram," *2011 Annual International Conference of the IEEE Engineering in Medicine and Biology Society*, 2011. 27, 28

[42] S. L. Kappel, S. Makeig, and P. Kidmose, "Ear-EEG forward models: Improved head-models for ear-EEG," *Frontiers in Neuroscience*, vol. 13, 2019. 27

[43] L. M. Ferrari, U. Ismailov, J.-M. Badier, F. Greco, and E. Ismailova, "Conducting polymer tattoo electrodes in clinical electro- and magneto-encephalography," *npj Flexible Electronics*, vol. 4, no. 1, 2020. 27, 28, 29

[44] Y. R. Tabar, K. B. Mikkelsen, N. Shenton, S. L. Kappel, A. R. Bertelsen, R. Nikbakht, H. O. Toft, C. H. Henriksen, M. C. Hemmsen, M. L. Rank, and et al., "At-home sleep monitoring using generic ear-eeg," *Frontiers in Neuroscience*, vol. 17, 2023. 28

[45] J. Parvizi and S. Kastner, "Promises and limitations of human intracranial electroencephalography," *Nature Neuroscience*, vol. 21, no. 4, p. 474–483, 2018. 30

[46] N. V. Thakor, "Translating the Brain-Machine Interface," *Science Translational Medicine*, vol. 5, no. 210, 2013. 30

[47] *Electroencephalography and Clinical Neurophysiology*, vol. 10, no. 2, p. 370–375, May 1958. [Online]. Available: https://linkinghub.elsevier.com/retrieve/pii/0013469458900531 32

[48] J. N. Acharya, A. Hani, J. Cheek, P. Thirumala, and T. N. Tsuchida, "American Clinical Neurophysiology Society Guideline 2: Guidelines for Standard Electrode Position Nomenclature," *Journal of Clinical Neurophysiology*, vol. 33, no. 4, pp. 308–311, 2016. 32, 33

[49] R. Oostenveld and P. Praamstra, "The five percent electrode system for high-resolution eeg and erp measurements," *Clinical Neurophysiology*, vol. 112, no. 4, p. 713–719, 2001. 33

[50] M.-P. Hosseini, A. Hosseini, and K. Ahi, "A review on machine learning for EEG signal processing in bioengineering," *IEEE Reviews in Biomedical Engineering*, vol. 14, p. 204–218, 2021. 34, 41

[51] A. Khosla, P. Khandnor, and T. Chand, "A comparative analysis of signal processing and classification methods for different applications based on eeg signals," *Biocybernetics and Biomedical Engineering*, vol. 40, no. 2, p. 649–690, 2020. 34, 35, 38, 39, 40

[52] A. Vajravelu, W. S. Bin, W. Zaki, A. Chandran, and M. A. . L. Shanmugavelu, "An Analysis On The Preprocessing Procedure Of Eeg Signal," *Turkish Journal of Computer and Mathematics Education*, vol. 12, no. 11, pp. 6099–6109, 2021. 35, 36

[53] M. Saeidi, W. Karwowski, F. V. Farahani, K. Fiok, R. Taiar, P. A. Hancock, and A. Al-Juaid, "Neural decoding of EEG signals with machine learning: A systematic review," *Brain Sciences*, vol. 11, no. 11, p. 1525, 2021. 36, 37, 38, 44

[54] Z. Huang and M. Wang, "A review of electroencephalogram signal processing methods for brain-controlled robots," *Cognitive Robotics*, vol. 1, p. 111–124, Jul 2021. 36, 37, 42, 44

[55] D. Mika, G. Budzik, and J. Józwik, "Single Channel Source Separation with ICA-Based Time-Frequency Decomposition," *Sensors*, vol. 20, no. 7, p. 2019, 2020. 37, 38

[56] F. J. Ramírez-Arias, E. E. García-Guerrero, E. Tlelo-Cuautle, J. M. Colores-Vargas, E. García-Canseco, O. R. López-Bonilla, G. M. Galindo-Aldana, and E. Inzunza-González, "Evaluation of machine learning algorithms for classification of EEG signals," *Technologies*, vol. 10, no. 4, p. 79, 2022. 38, 41, 42, 67, 68, 70

[57] Q. Xiong, X. Zhang, W.-F. Wang, and Y. Gu, "A parallel algorithm framework for feature extraction of eeg signals on mpi," *Computational and Mathematical Methods in Medicine*, vol. 2020, p. 1–10, 2020. 40, 41

[58] L. C. Cheong, R. Sudirman, and S. Hussin, "Feature extraction of EEG signal using wavelet transform for autism classification," vol. 10, pp. 8533–8540, 01 2015. 41, 65, 66, 67, 68, 69, 71, 77

[59] A. Hamad, E. H. Houssein, A. E. Hassanien, and A. A. Fahmy, "Feature extraction of epilepsy EEG using discrete wavelet transform," in *2016 12th International Computer Engineering Conference (ICENCO)*, 2016, pp. 190–195. 41, 67

[60] "Choose a Wavelet," [Accessed on 25 April 2023]. [Online]. Available: https://www.mathworks.com/help/wavelet/gs/choose-a-wavelet.html 41

[61] S. Ibrahim, R. Djemal, and A. Alsuwailem, "Electroencephalography (EEG) signal processing for epilepsy and autism spectrum disorder diagnosis," *Biocybernetics and Biomedical Engineering*, vol. 38, no. 1, p. 16–26, Sep 2018. 41, 42, 43, 44, 65, 66, 67, 68, 77

[62] K. Taunk, S. De, S. Verma, and A. Swetapadma, "A brief review of nearest neighbor algorithm for learning and classification," *2019 International Conference on Intelligent Computing and Control Systems (ICCS)*, 2019. 43

[63] A. R. Florea and M. Roman, "Artificial neural networks applied for predicting and explaining the education level of twitter users," *Social Network Analysis and Mining*, vol. 11, no. 1, 2021. 44, 45

[64] J. Wang, J. Qiu, L. Hou, X. Zheng, and S. Yu, "Effect of common pavements on interjoint coordination of walking with and without robotic exoskeleton," *Applied Bionics and Biomechanics*, vol. 2019, p. 1–8, 2019. 45, 46

[65] R. Di Marco, M. Rubega, O. Lennon, E. Formaggio, N. Sutaj, G. Dazzi, C. Venturin, I. Bonini, R. Ortner, H. Cerrel Bazo, and et al., "Experimental protocol to assess neuromuscular plasticity induced by an exoskeleton training session," *Methods and Protocols*, vol. 4, no. 3, p. 48, 2021. 46, 47

[66] A. Amini, K. Faez, and M. Amiri, "Surface roughness classification in dynamic touch using eeg signals," *2022 30th International Conference on Electrical Engineering (ICEE)*, 2022. 47, 48, 49

[67] G. Baghdadi, M. Amiri, E. Falotico, and C. Laschi, "Recurrence quantification analysis of eeg signals for tactile roughness discrimination," *International Journal of Machine Learning and Cybernetics*, vol. 12, no. 4, p. 1115–1136, 2020. 48, 49, 69, 77, 87

[68] O. Özdenizci, S. Eldeeb, A. Demir, D. Erdoğmuş, and M. Akçakaya, "EEG-based texture roughness classification in active tactile exploration with invariant representation learning networks," *Biomedical Signal Processing and Control*, vol. 67, p. 102507, May 2021. 48, 49

[69] "Exoatlet I – product page," Jul 2022, [Accessed on 15 December 2022]. [Online]. Available: https://exoatlet.lu/product-page-exoatlet-i/ 53, 54

[70] C. Pais-Vieira, M. Allahdad, J. Neves-Amado, A. Perrotta, E. Morya, R. Moioli, E. Shapkova, and M. Pais-Vieira, "Method for positioning and rehabilitation training with the ExoAtlet ® powered exoskeleton," *MethodsX*, vol. 7, p. 100849, 2020. 56

[71] *MATLAB version 9.7.0.1247435 (R2019b)*, The Mathworks, Inc., Natick, Massachusetts, USA, 2019. 59

[72] A. Delorme and S. Makeig, "EEGLAB: An open source toolbox for analysis of single-trial EEG dynamics including independent component analysis," *Journal of Neuroscience Methods*, vol. 134, no. 1, p. 9–21, 2004. 59

[73] R. Oostenveld, P. Fries, E. Maris, and J.-M. Schoffelen, "Fieldtrip: Open source software for advanced analysis of meg, eeg, and invasive electrophysiological data," *Computational Intelligence and Neuroscience*, vol. 2011, p. 1–9, 2011. 59

[74] "a. Filtering," [Accessed on 30 January 2023]. [Online]. Available: https://eeglab.org/tutorials/05_Preprocess/Filtering.html 60

[75] P. S. Ghare and A. Paithane, "Human emotion recognition using non linear and non stationary EEG signal," *2016 International Conference on Automatic Control and Dynamic Optimization Techniques (ICACDOT)*, 2016. 60, 65, 68, 77

[76] R. N. Jin, H. Inada, J. Négyesi, D. Ito, and R. Nagatomi, "Carbon dioxide effects on daytime sleepiness and eeg signal: A combinational approach using classical frequentist and bayesian analyses," *Indoor Air*, vol. 32, no. 6, 2022. 60

[77] O. Griffiths, B. N. Jack, D. Pearson, R. Elijah, N. Mifsud, N. Han, S. Libesman, A. Rita Barreiros, L. Turnbull, R. Balzan, and et al., "Disrupted auditory n1, theta power and coherence suppression to willed speech in people with schizophrenia," *NeuroImage: Clinical*, vol. 37, p. 103290, 2023. 60

[78] "NITRC: Cleanline: Tool & Resource info," [Accessed on 30 January 2023]. [Online]. Available: https://www.nitrc.org/projects/cleanline 60

[79] I. Winkler, S. Debener, K.-R. Muller, and M. Tangermann, "On the influence of high-pass filtering on ICA-based artifact reduction in EEG-ERP," *2015 37th Annual International Conference of the IEEE Engineering in Medicine and Biology Society (EMBC)*, 2015. 62

[80] B. Kaur, D. Singh, and P. P. Roy, "Eyes open and eyes close activity recognition using EEG signals," *Communications in Computer and Information Science*, p. 3–9, 2018. 65, 67, 68, 77

[81] J. E. Jacob, G. K. Nair, T. Iype, and A. Cherian, "Diagnosis of encephalopathy based on energies of EEG subbands using discrete wavelet transform and support vector machine," *Neurology Research International*, vol. 2018, p. 1–9, 2018. 65, 66, 68, 77

[82] Q. Wang, D. Zhao, Y. Wang, and X. Hou, "Ensemble learning algorithm based on multi-parameters for sleep staging," *Medical & Biological Engineering & Computing*, vol. 57, no. 8, p. 1693–1707, 2019. 68

[83] "List of deep learning layers," [Accessed on 12 May 2023]. [Online]. Available: https://www.mathworks.com/help/deeplearning/ug/list-of-deep-learning-layers.html 69

[84] D. Nath, Anubhav, M. Singh, D. Sethia, D. Kalra, and S. Indu, "A comparative study of subject-dependent and subject-independent strategies for eeg-based emotion recognition using lstm network," *Proceedings of the 2020 the 4th International Conference on Compute and Data Analysis*, 2020. 77

[85] B. Güntekin and E. Başar, "Review of evoked and event-related delta responses in the human brain," *International Journal of Psychophysiology*, vol. 103, p. 43–52, 2016. 86

[86] T. Harmony, "The functional significance of delta oscillations in cognitive processing," *Frontiers in Integrative Neuroscience*, vol. 7, 2013. 86

[87] S. Eldeeb, D. Weber, J. Ting, A. Demir, D. Erdogmus, and M. Akcakaya, "Eeg-based trial-by-trial texture classification during active touch," *Scientific Reports*, vol. 10, no. 1, 2020. 86

[88] W. He, Y. Zhao, H. Tang, C. Sun, and W. Fu, "A Wireless BCI and BMI System for Wearable Robots," *IEEE Transactions on Systems, Man, and Cybernetics: Systems*, vol. 46, no. 7, p. 936–946, 2016. 87

[89] M.-H. Lee, S. Fazli, J. Mehnert, and S.-W. Lee, "Subject-dependent classification for robust idle state detection using multi-modal neuroimaging and data-fusion techniques in BCI," *Pattern Recognition*, vol. 48, no. 8, p. 2725–2737, 2015. 87

[90] Y. Renard, F. Lotte, G. Gibert, M. Congedo, E. Maby, V. Delannoy, O. Bertrand, and A. Lécuyer, "OpenViBE: An open-source software platform to design, test, and use brain–computer interfaces in real and virtual environments," *Presence: Teleoperators and Virtual Environments*, vol. 19, no. 1, p. 35–53, 2010. 87

[91] M. K. Ishak, "Classification of EEG signal for movement intentions-based brain computer interfaces," *International Journal of Advances in Computer Science and Technology (IJACST)*, vol. 3, no. 11, pp. 07–12, 2014. 87

[92] A. R. Donati, S. Shokur, E. Morya, D. S. Campos, R. C. Moioli, C. M. Gitti, P. B. Augusto, S. Tripodi, C. G. Pires, G. A. Pereira, and et al., "Long-term training with a brain-machine interface-based gait protocol induces partial neurological recovery in paraplegic patients," *Scientific Reports*, vol. 6, no. 1, 2016. 87

Appendix A

Appendix

Document appendix - Presenting extra information.

A.1 Epochs extracted from continous EEG data

Table A.1: EEG epochs - S001.

Epochs | S001		
Exo	Carpet	101
	Flat	100
	Rubber circles	100
	Foam	99
No Exo	Carpet	96
	Flat	104
	Rubber circles	98
	Foam	97

Table A.2: EEG epochs - S002.

Epochs | S002		
Exo	Carpet	96
	Flat	106
	Rubber circles	99
	Foam	93
No Exo	Carpet	97
	Flat	97
	Rubber circles	97
	Foam	97

Table A.3: EEG epochs - S003.

Epochs | S003		
Exo	Carpet	93
	Flat	77
	Rubber circles	95
	Foam	95
No Exo	Carpet	95
	Flat	96
	Rubber circles	95
	Foam	97